Durham E-Theses

Enhancement of polymer light-emitting diode performance through doping and improved charge injection

Higgins, Roger W.T.

How to cite:

Higgins, Roger W.T. (2001) *Enhancement of polymer light-emitting diode performance through doping and improved charge injection*, Durham theses, Durham University. Available at Durham E-Theses Online: http://etheses.dur.ac.uk/3787/

Use policy

Enhancement of polymer light-emitting diode performance through doping and improved charge injection

Roger W.T.Higgins

A thesis submitted to the University of Durham for the degree of Master of Science by Research and Thesis

2 6 APR 2002

Abstract

Research into the performance enhancement of polymer light-emitting diodes, through techniques of doping and improved charge injection, is reported. Initial electroluminescent (EL) characterisation of all host polymers used; in particular poly(2-methoxy-5-(2'-ethyl-hexyloxy)-1,4-phenylene vinylene) (MEH-PPV) and α,ω-Bis[N,N-di(4-methylphenyl)aminophenyl]-poly(9,9-bis(2-ethylhexyl)fluoren-2,7-diyl) (PF2/6am4) in both mono- and bi-layer configuration is presented. For all studies indium tin oxide was used as the primary anode, with either aluminium or calcium as the cathode. The polymers are all soluble and were processed from spin coating to produce films of order 100 namometres in thickness.

A range of protonated polyaniline thin films are characterised for use as hole-transporting layers (HTLs) with MEH-PPV. The HTL fermi level is found to be crucial to its effectiveness in facilitating hole injection.

Following this the published studies of PF2/6am4 doping with highly efficient dopants (Rubrene and three metal-porphyrin derivatives) are presented. Techniques summarised in chapter 3 are used in order to convert the measured light output into optical units of candela per metre squared and lumens per watt. The external quantum efficiency for each configuration fabricated is also calculated. Previously reported studies of the dopants are used in order to aid discussion as to the key properties that make a dopant suitable for use in donor:acceptor systems. It is noted that the dopants' excited state lifetime is directly related to the current density at which peak performance is observed, and it is recommended that in order to avoid dopant saturation the dopants' excited state lifetime should be as small as possible without sacrificing emission efficiency.

Having established the considerable challenges to be overcome for energy transfer systems to be commercially viable, an alternative doping technique is presented: host perturbation. First the effect of doping both MEH-PPV and PF2/6am4 with a range of rare earth lanthanide metal: organic complexes is investigated. The effect on the intersystem crossing is observed to be highly host dependent, with improvements in efficiency only for MEH-PPV. These results are compared with theoretical predictions.

In all studies we draw comparison from similar studies carried out by other groups where possible.

Declaration

All material contained in this thesis is original and is the result of my own work except where explicit reference is made. Material from work of others has been suitably indicated.

This thesis has not been submitted in whole or in part for the award of a degree at this or any other university.

The copyright of this thesis rests with the author. No quotation from it should be published without their prior consent and information derived from it acknowledged.

Acknowledgments

Contents

Figure Index

Table Index

Publications resulting from this work

[1]   Higgins, R. W. T.; Burrows, H. D.; Monkman, A. P. Manipulating the singlet yield in polymer light-emitting diodes with heavy metal dopants. *Physical Review B* **Submitted**.

[2]   Higgins, R. W. T.; Hothofer, H. G.; Scherf, U.; Monkman, A. P. A study of the energy transfer to porphyrin derivatives when used as dopants in polymer light-emitting diodes. *Journal of Applied Physics* **Submitted**.

[3]   Higgins, R. W. T.; Monkman, A. P.; Nothofer, H. G.; Scherf, U. Effects of singlet and triplet energy transfer to molecular dopants in polymer light-emitting diodes and their usefulness in chromaticity tuning. *Applied Physics Letters* **2001**, *79*, 857-859.

[4]   Higgins, R. W. T.; Zaidi, N. A.; Monkman, A. P. A study of emeraldine base polyaniline (PANi) with various counter ions as an alternative to poly(3,4-ethylenedioxythiophene) (PEDT) as a hole-transporting layer in polymer light-emitting diodes. *Advanced Functional Materials* **Submitted**.

[5]   Monkman, A. P.; Palsson, L.-O.; Wang, C.-S.; Bryce, M. R.; Batsanov, A. S.; Howard, J. A. K. Protonation and subsequent intramolecular hydrogen bonding as a method to control chain structure and tune luminescence in heteroatomic conjugated polymers. *Journal of the American Chemical Society* **Submitted**.

Chapter 1 Introduction

When we think of light emitting diodes, thoughts turn to the commonly used inorganic devices based on silicon (amongst others), with its convenient energy gap in the visible spectrum. Light emission from organic materials is less well known, yet there are examples in nature that carry a fascinating elegance. Living creatures, most familiarly fireflies, emit light with amazingly high efficiencies, especially compared to our common-place inorganic materials. This is because of the high quantum efficiency of luminescence shown by a wide range of organic materials when compared to inorganic materials. Over the past 20 years[2], the potential for organic light emitting devices has been accelerated into our awareness through a combination of intensive academic interest and commercial expectation.

The versatility of polymers is already familiar to us, from car bumpers to bullet-proof vests; there are examples of how we can benefit from their flexibility, durability and simple fabrication processes. Another interesting property of some polymers is their ability to conduct electricity and emit light. Initially semiconducting polymers were not considered realistic candidates for electroluminescence due to the high voltages (1000V or greater[3]) required. With the development of thin-film devices in the late 1980s this barrier was removed. Then in 1990 came the first report of electroluminescence in thin films of poly(phenylene vinylene) (PPV)[1]. Nearly 10 years on and the technology is invading the market place. 55 companies are involved in the development and production of polymer light-emitting diode (PLED) applications and TDK and Sony have exhibited prototype full colour displays.

The attraction of semiconducting polymers (and indeed small molecules) as an alternative to current technology (silicon LEDs, liquid crystal displays) is multifaceted. With the global electronic display market worth an estimated $50bn a year, companies are on a constant search for ways to increase their share of the market. Currently displays are relatively complicated to manufacture. Inorganic semiconducting surfaces have to be structured regularly at the atomic level. Any irregularities can lead to device failure via the creation of "non-bonding" orbitals. Devices are fabricated under high pressure, require epitaxial growth and the range of bandgaps attainable is limited even when extending to quaternary compounds. Trying to fabricate new bandgaps can be complicated by insolubility of compound constituents and the need to match the lattice of the layers to the underlying substrate to prevent debilitating defect density levels.

Organic semiconductors are far less sensitive to interface preparation techniques. Unlike inorganic materials, polymer semiconductors are largely covalently bonded, which allows the use of multiple polymer-polymer interfaces in a multilayer system. A Polymer's chain structure does not suffer from lattice defect problems. There are no dangling bonds (unpaired electrons) and so fabrication can be performed under normal atmospheric conditions[9]. Chain length, side groups and constituent elements can all be varied leading to a wide range of attainable band gaps (and hence emission wavelengths).

Liquid crystal display technology is of a high quality, offering large display sizes, but the active viewing angle is poor, and more fundamentally limiting is the fact that the liquid crystals are themselves non-emissive. Instead they function as modulators of light from a primary source; berefringent liquid crystal molecules whose orientation is manipulated by an applied electric field. Organic semiconducting devices have no restriction on viewing angle and are capable of colour tuning and electroluminescence in one.

Already mentioned above was the flexibility of polymers in general. The current 'prime candidates' for active layers (poly(phenylene vinylene) (PPV) for example) are extremely durable once prepared from their precursor (see method of production) and remain stable at temperatures up to 1000K. This compares to current devices favourably. With the usual method of preparation involving soluble materials, there may come a time in the near future when devices are created by printing the layers into a substrate. Indeed this technique is currently being developed[1]. Such a simple fabrication technique would make organic devices appealing. Semiconducting polymers are also competitive in an area that, until the late 1980s, no one could have possibly imagined - operating voltages. Whereas before thin film technology semiconducting polymers were overlooked due to very high drive voltages, in the past few years devices have been constructed to operate at ~5V thanks to film thickness the order of nanometres.

The aim of this work is to investigate two common ways of improving the efficiency of polymer light-emitting diodes: doping the active layer with molecular species and improving electron-hole capture through the use of heterojunctions. It begins with a brief review of the main theoretical considerations, and a discussion of the experimental techniques and assumptions employed. Chapter 4 discusses the effects of architecture modification on poly[2-methoxy-5-(2'-ethylhexyloxy)-1, 4-phenylene vinylene] (MEH-PPV) PLEDs, and goes on to establish the electroluminescent

characteristics of all the active layer polymers used in this study. Chapter 5 deals with undoped active layers of MEH-PPV where the injection of hole-polarons is varied by modifying the composition of the heterolayer sandwiched between the indium tin oxide (ITO) anode and MEH-PPV. These heterolayers are also used with other active layers in order to further aid understanding of the key requirements for a good heterojunction. Chapters 6 and 7 describe the experimental results of doping derivatives of the blue-emitting polymer polyfluorene (PFO) with a range of highly luminescent acceptor molecules, and offers analysis and suggestions for the observed performance. Chapter 8 investigates the doping of MEH-PPV and PFO with dopants that, rather than receive host singlet energy via Forster transfer, perturb the system via heavy atom effects and paramagnetic triplet quenching effects. Finally Chapter 9 draws general inferences from the results for future studies into PLED performance enhancement.

References

[1]   Burroughes, J. H.; Bradley, D. D. C.; Brown, A. R.; Marks, R. N.; Mackay, K.; Friend, R. H.; Burns, P. L.; Holmes, A. B. *Nature* **1990**, *347*, 539-541.

[2]   Friend, R.; Burroughes, J.; Shimoda, T. *Physics World* **1999**, *12*, 35-40.

[3]   Kido, J. *Polymers for Advanced Technologies* **1997**, *8*, 379-379.

2.1 DEFINITION OF CONJUGATED POLYMER

Polymers are long chains of atoms built up from sub-units or monomers. There are few elements that can bond to form long chain structures; those occupying groups IV and VI of the periodic table, of which Carbon (group IV) is most familiar as the building block of organic life on the planet.

Carbon appears in a vast multitude of compounds due to its bonding with the other elements. A member of Group 4 in the periodic table it has four valence electrons in the configuration $2s^2 2p^2$ which can be hybridised to form two, three or four bonding lobes in the sp^3, sp^2 or sp configuration respectively, as shown in Figure 2-1
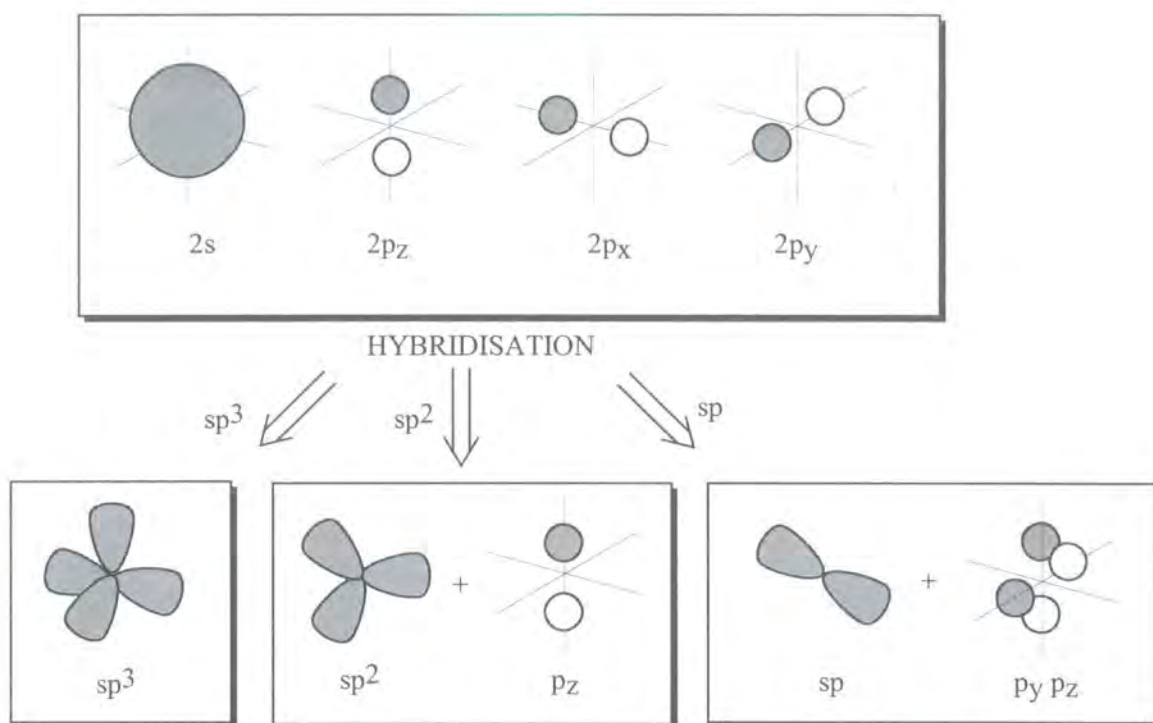
Figure 2-1 (Adapted from the literature[74]) Hybridisation states of the carbon atom. The different phases of orbitals are indicated by shading.

In conjugated polymers the carbon atoms along the backbone of the polymer are sp^2 hybridised, allowing them to form three sigma bonds with neighbouring atoms. The remaining $2p_y$ orbital uninvolved in the hybridisation process contains a lone unpaired electron. The separation of two sp^2 hybridised Carbon atoms bonded by a σ-bond is such that their $2p_y$ lobes can overlap, resulting in a delocalised electron density normal to the sp^2 hybridisation plane. This delocalisation is thermodynamically favourable and hence a weak bond (relative to a σ-bond) is formed, known as a π-bond. The π-bond

has bonding (π) and antibonding (π^*) phases with a corresponding energy difference. Whilst these *unsaturated* double bonds are also found in molecules such as ethene (Figure 2-2), multiple π-bonds in the same structure can lead on to conjugation.
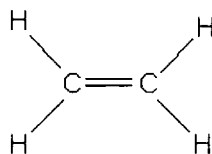
Figure 2-2 Chemical structure of ethene

For a polymer with alternating single and double Carbon-Carbon bonds along its backbone the overlap of neighbouring π-electron densities is such that further delocalisation is observed along several monomer units. These delocalised electrons are only loosely bonded to their parent atoms and can be easily polarised, giving rise to electrical and optical properties. The simplest conjugated polymer, polyacetylene, shown below, bears a resemblance to its molecular counterpart.
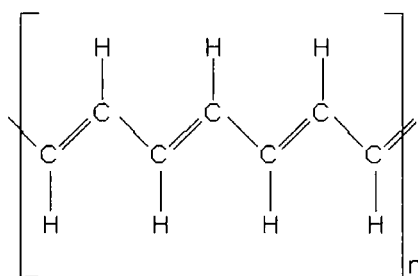
Figure 2-3 Chemical structure of polyacetylene

The length of delocalisation is often referred to as the conjugation length. The conjugation length is limited by twists in the chain and impurities present in the polymer[65,38]: accidental doping being unavoidable when synthesising polymers.

In the idealised case with no defects or twists breaking the conjugation the overlapping orbitals give rise to a half filled band of allowed states. This band is a superposition of valence (full π bonding) and conduction (empty π^* antibonding) bands. With no band gap the polymer behaves as a metal, essentially in one dimension due to its highly anisotropic nature.

This delocalised structure in polymers turns out to be susceptible to a distortion; the polymer dimerising into a pattern of alternating single and double bonds. This is known as the Peierls' distortion[61]. A dimersied polymer yields a bandgap. The dimerised structure has two phases, notionally the two directions in which the double

bonds can point. If the two phases are equivalent in energy then the polymer has ground state degeneracy. Alternatively, asymmetry in the backbone can mean that one phase has a higher associated energy than the other. In both cases a band gap is formed between the occupied π-bonding valence band and the empty π-bonding conduction band. The polymer now behaves as a semiconductor, with an optically excitable bandgap that is the origin of photoexcitation features of the conjugated polymers commonly used in light-emitting diodes (PLEDs).

The next section provides an overview of the two main theories of excitations in conjugated polymers: the band model presented by Su, Schrieffer and Heeger (SSH theory) [39] and the exciton model supported by Bassler[12] amongst others. The former models conduction in a doped system using a modified Hubbard potential[1] and describes conjugated polymers analogously to inorganic semiconductors with free charge carriers dominating conduction whilst the latter describes tighter bound charge pairs in a system with similarities to the Exciton model of small molecules and organic crystals.

The fact neither has comprehensively explained all the experimental results published illustrates the complex task of describing a large disordered system that demonstrates characteristics from both related fields.

2.2 THEORIES OF EXCITATIONS IN CONJUGATED POLYMERS

2.21 The Semiconductor Model - SSH Theory

Polymers exhibit periodicity over a long range in similarity to the metal lattice structure of inorganic semiconductors, the difference being that whilst in metallic bonding this periodicity extends to three dimensions, in polymers it is highly anisotropic due to the large difference in strength of intra- and inter- chain interactions. SSH theory[39] uses the inherit periodicity of conjugated polymers to describe conduction/excitations therein in terms of transitions across a semiconductor band gap, allowing for the 1-D anisotropy.

SSH theory examines the behaviour of poly(acetylene) $(CH)_n$ and was born from the need to explain spin resonance observed from neutral pseudo particles, named solitons in the polymer.

Poly(acetylene) occurs in two isomeric arrangements, cis-$(CH)_n$ and trans-$(CH)_n$, shown below in Figure 2-4.
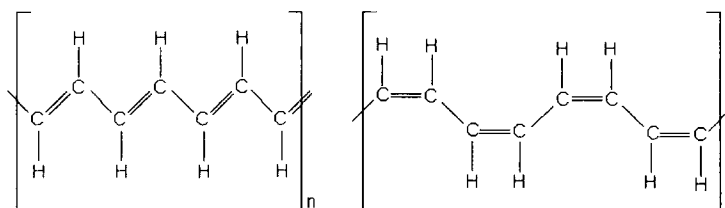
Figure 2-4 Chemical Structure of poly(acetylene). cis-$(CH)_n$ (left) and trans-$(CH)_n$ (right)

Due to the Peierls' distortion the delocalised backbone is more stable with a pattern of alternating single and double bonds and hence there are two phases for each isomer. For trans-$(CH)_n$ the energy of phases A and B (illustrated in Figure 2-5) are the same and hence trans-$(CH)_n$ has a degenerate ground state. Peierls showed[60] that in a state of equilibrium the double bonds are shorter than the single bonds, which increases the elastic energy of the lattice (distortion energy) but lowers the electronic energy by a greater amount. This change splits the half full π band into an effective fully occupied valence band, the upper edge being defined by the highest occupied molecular orbital (HOMO) and an empty conducion band, which has a lower edge defined by the lowest unoccupied molecular orbital (LUMO). This gives the polymer a band gap or HOMO-LUMO gap.
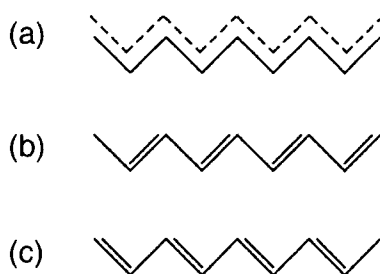
Figure 2-5 Phases of trans-$(CH_3)_n$ (a)Undimerised (b)Phase A (c)Phase B

The resulting energy curve is displayed in Figure 2-6
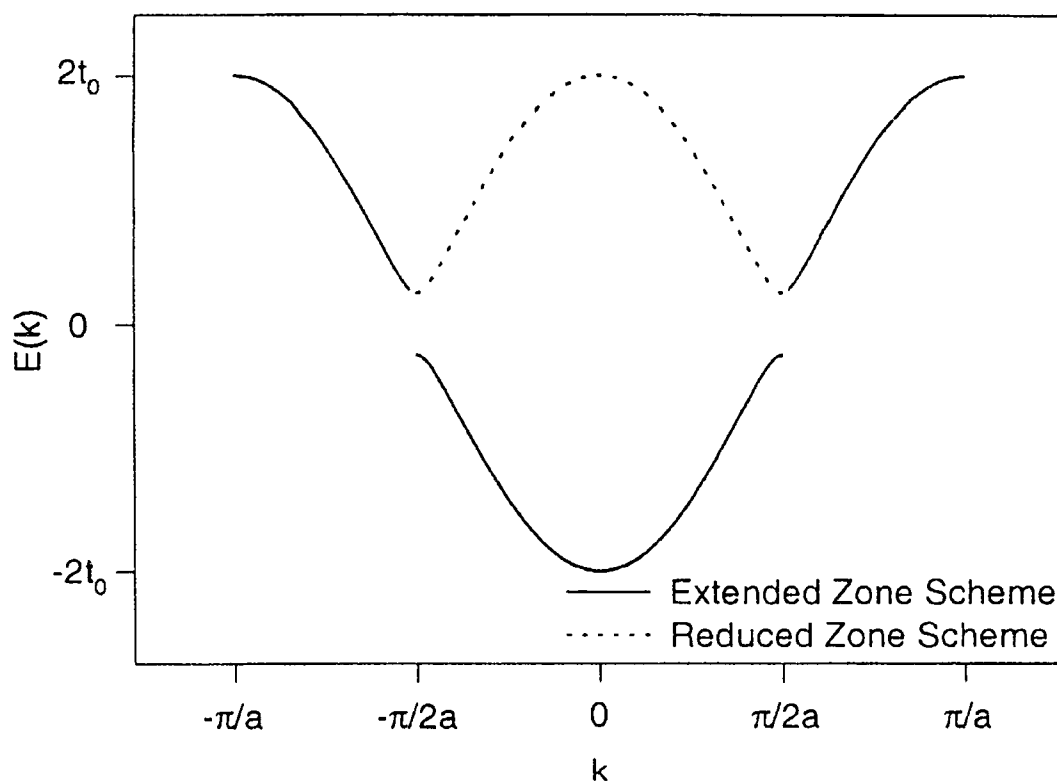
Figure 2-6 Energy as a function of wavelength (E-k) for a perfectly dimersied trans-$(CH_3)_n$ chain (taken from the literature)[24]

In order to describe the electronic structure SSH theory makes two assumptions; that only nearest neighbour interactions contribute and that electron-electron interactions are negligible. Starting from a treatment where the σ-bonds are considered to be constrained oscillators described using a first order Hooke's Law summation over all atoms, and π electrons are treated in a tight-binding Huckel framework separately from the σ-electrons, the SSH Hamiltonian can be constructed by summation of both these

9

contributions and the displacement energy of the chain atoms over the length of the chain:

$$H_{SSH} = \frac{1}{2}\sum_n K(u_{n+1} - u_n)^2 - \sum_{ns} t_{n+1,n}(c'_{n+1,s}c_{ns} + c'_{ns}c_{n+1,s}) + \frac{1}{2}\sum_n M\ddot{u}_n^2 \qquad \textbf{Equation 2-1}$$

where K is the σ-bond force constant, u_n a configuration coordinate for displacment of the nth C atom, $t_{n+1,n}$ is the hopping integral, c'_{ns} creates and c_{ns} destroys π electrons of spin s on the nth atom and M is the mass of a CH group. From this potential one can mathematically demonstrate the energy gap induced by the Peierls' distortion, as well as explaining the existence of solitons (Section 2.51).

SSH theory can also be used to describe non-degenerate ground state polymers such as poly(p-phenylene vinylene) (PPV) coomonly used in this study.

Original SSH theory can now be labelled an oversimplification for the very assumptions that allowed the authors to produce results that explained many of the observed properties of conjugated polymers. Neglecting the electron-electron interaction, in particular, has lead to many discrepancies between observed and predicted results[54]. There have been proposed modifications involving additional terms in the SSH Hamiltonian[55,75], but discrepancies still arise. SSH theory explains the existence of conducting species of conjugated polymers and is used in section 2.3, but for optical phenomena the exciton model currently predicts results closer to the experimental values.

2.22 The Correlated or Exciton Model

The basis of SSH theory is the periodicity of the polymer chain and the assumed lack of correlation between charge pairs. The Exciton model allows for impurities and breaks in periodicity. These impurities limit the conjugation length to the order of 10 repeat units. This means that the conduction path of charge pairs is far from uniform along a chain, and it also raises the significance of interchain interactions and the multidimensionally of conduction routes in a number of closely associated chains.

With the delocalisation in small segments of each chain an optical excitation results in a correlated electron-hole pair or exciton, not two free or loosely bound charge pairs in a valence and conduction band. This system is closer to that successfully used to describe molecular crystals and from this field nomenclature has been adopted to describe the different degrees of exciton correlation.
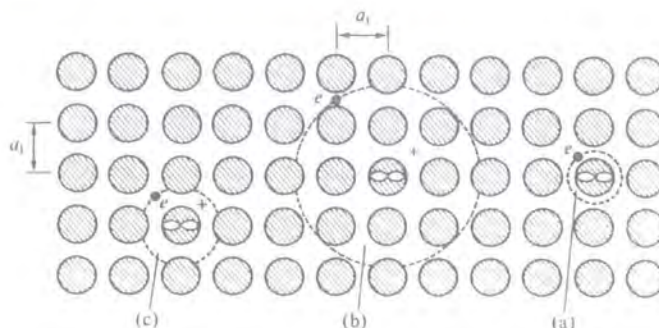
Figure 2-7 (From Pope and Swenberg[62]) (a)Frenkel (b)Mott-Wannier and (c)Charge transfer excitons in a periodic lattice

A **Frenkel** exciton in molecular crystals has both electron and hole on the same molecular unit, with a radius <5Å. Electron and hole are closely correlated and move together through the sample as a unit. The separation is small enough that the Freknel exciton has no permanent dipole moment. In polymers this exciton would be expected to have hole and electron in the same conjugation region. The recombination of the Frenkel exciton is believed to be the source of prompt fluorescence observed in photoexcited conjugated polymers.

A molecular crystal **charge transfer** (CT) exciton is formed when the excitation is sufficient to transfer either hole or electron to a neighbouring molecule; in polymers a neighbouring chain. The electron and hole components of the excitation are on separate chains[62] and they can be mobile or trapped, carrying with them a permanent dipole moment. Intermediates between Frenkel and Mott-Warnier excitons, CT excitons remain strongly correlated. Recently they have been proposed as the source of delayed fluorescence in photoexcitation experiments[64,41], due to the applied electric field dependence of this fluorescence. This issue is still under consideration, however, with the possibility that the delayed fluorescence is the result of radiative triplet-triplet annihilation.

A **Mott-Warnier** (MW) exciton is weakly correlated, with a radius of ~40-100 Å in molecular crystals. This is the closest analogy to the free carrier band model, with the coulombic attraction very weak. Like the Frenkel exciton there is no permanent dipole moment. MW excitons may be stable due to the coulombic attraction being shielded by the polymer medium at large separation. In PLEDs, where the injection initially results in MW excitons, the large electric field applied introduces an extra exciton-influencing factor.

Key to determining which model is a more accurate description of excitations in conjugated polymers is the magnitude of the exciton binding energy E_e, obtained by integrating the coulombic attraction of hole and electron from separation radius to infinity, as it tells us which of the three classes of excitons described above are prevalent. Loosely bound electron hole pairs would favour the band model approach whilst higher exciton would mean that correlation effects are significant as for molecular crystals.

Proponents of both models have developed several methods in order to measure E_e and thus validate themselves. Originally used commonly for this, PPV produced a wide variation in results and left the issue unclear[4,9,73,40,51,53,23]. More recently, several results with other polymers including ladder type poly(para-phenylene) (MeL-PPP) have produced results that favour the exciton model, with $E_e \sim 0.3$-0.4eV. A summary of these results and comparison of theoretical predictions with experimental results can be found in the literature[77,71,70,11,9,10].

2.3 ABSORPTION AND LUMINESCENCE SPECTROSCOPY

Light incident on a material will induce atomic excitations and as a result the intensity of light will fall due to absorption of photons to form excited states. Observing the variation in absorption with incident energy is thus an excellent way in which to probe the various energy levels within the material (for allowed transitions, see below). Similarly fluorescence of a material is useful as it contains information about the migration of excited species within the material[16]. Both are essential to determining whether a candidate is suitable for use in PLEDs.

2.31 Allowed Transitions

The strength of absorption of light of frequency ν in a material depends on the overlap of excited and ground state wavefunctions at that frequency. The Beer Lambert Law describes the drop in intensity at a thickness x within the sample

$$I(x) = I(0)\exp(-\alpha x) \qquad \textbf{Equation 2-2}$$

where I(x) and I(0) are the intensities at thickness x and zero respectively and α is the absorption coefficent, which is frequency dependant. The absorption can vary greatly with frequency because the electronic transitions corresponding to the absorption bands have different probabilities of occurrence[81]. A strong band is associated with an *allowed* transition whilst a weak band is associated with a *forbidden* transition. A way of measuring the absorption strength of a band is to integrate the absorption coefficient across the frequency range of the band

$$f = 6.25\times10^{20} \int_{E_1}^{E_2} \alpha(E)dE \qquad \textbf{Equation 2-3}$$

where E_2 and E_1 delimit the band and f is known as the oscillator strength, which is dimensionless. For allowed transitions f is close to unity whilst forbidden transitions have much smaller values. Generally allowed transitions are strong due to good overlap of excited and ground state wavefunctions, but also due to obeying the selection rules for optical transitions. These can be summarised by redefining f as a product of probabilities

$$f = P_s P_o P_p P_m f_a \qquad \textbf{Equation 2-4}$$

where P_s, P_o, P_p, P_m are probabilities for changes in electron spin, orbital symmetry, parity and momentum respectively and f_a is the oscillator strength of a fully allowed $\pi \rightarrow \pi^*$ transition (i.e. ≈ 1).

- A change in spin is not allowed and hence transitions from singlet to triplet states (and vice versa) have $P_s \sim 10^{-5[81]}$. This selection rule breaks down in the presence of heavy atoms and paramagnets, as they perturb the system's wavefunction and enhance S$\rightarrow$T and T$\rightarrow$S intersystem crossing.

- Without spatial overlap of initial and final wavefunctions the probability of transition will be space or orbital forbidden, with a correspondingly low P_o.

- Most conjugated polymers exhibit some molecular symmetry and so do their orbitals. A wavefunction that changes its sign on reflection through a point of symmetry is said to have odd parity, else it has even parity. Allowed transitions in conjugated polymers involve a change in parity. Even parity transitions tend to have a lower P_p of $\sim 10^{-1}$. An example of even and odd parity orbitals are the π^* and π orbitals of ethylene.

- Transitions resulting in large changes in linear or angular momentum are forbidden, with $p_m \sim 10^{-3}$.

For a semiconducor-type material one expects an onset in absorption at a photon energy corresponding the energy gap. Disorder due to defects or dopants in conjugated polymers leads to breaks in the conjugation as previously mentioned. This results in a distribution of conjugation lengths and hence the absorption spectra of these materials are typically very broad due to a range of effective absorbing species (higher and lower energy segments on the chains). An example absorption spectrum is shown in Figure 2-8, made on a sample of poly[2-methoxy-5- (2-ethylhexyloxy)-1,4-phenylene vinylene] (MEH-PPV).
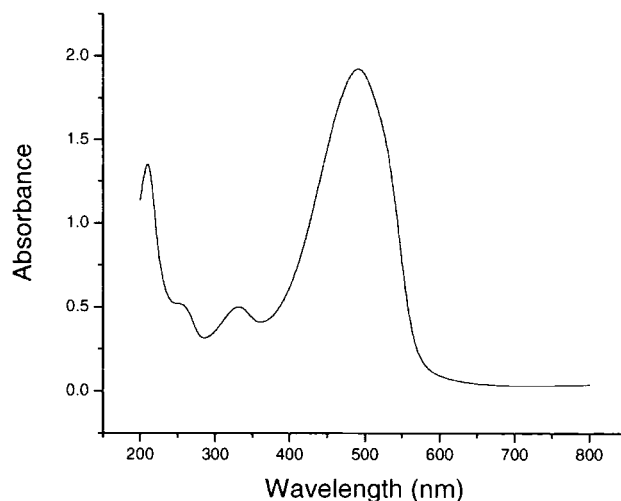
Figure 2-8 Absorption Spectrum of MEH-PPV, courtesy of Mr.C.Sitch

2.32 The Franck Condon Principle

Absorption takes place obeying the Franck-Condon principle, which states that transitions are vertical(see for example Figure 2-9). No nuclear conformation readjustment takes place until after the event. Electrons are transferred from the $v=0$ vibrational sub-level of the electronic ground state for the various vibrational sub-levels of the excited state. These can then undergo radiationless internal conversion, and then the polymer can radiatively emit to repopulate the vibrational sub-levels of the ground state. This scheme is depicted below in Figure 2-9. For a system with symmetric vibrational levels a mirror image relationship can be seen. The observed Stoke's Shift between the $v=0$ and $v'=0$ position is due to the relaxation of excited states to chain segments of lower energy.

Thus, detail in absorption spectra gives information about the structure of the excited state levels and luminescence spectra give information about the structure of the ground state. More information can also be found from photoconductivity measurements: the current measured from an illuminated sample under applied bias. This method is commonly used to measure the value of the exciton binding energy, which as mentioned above is crucial to our understanding of conjugated polymer excitation mechanisms.
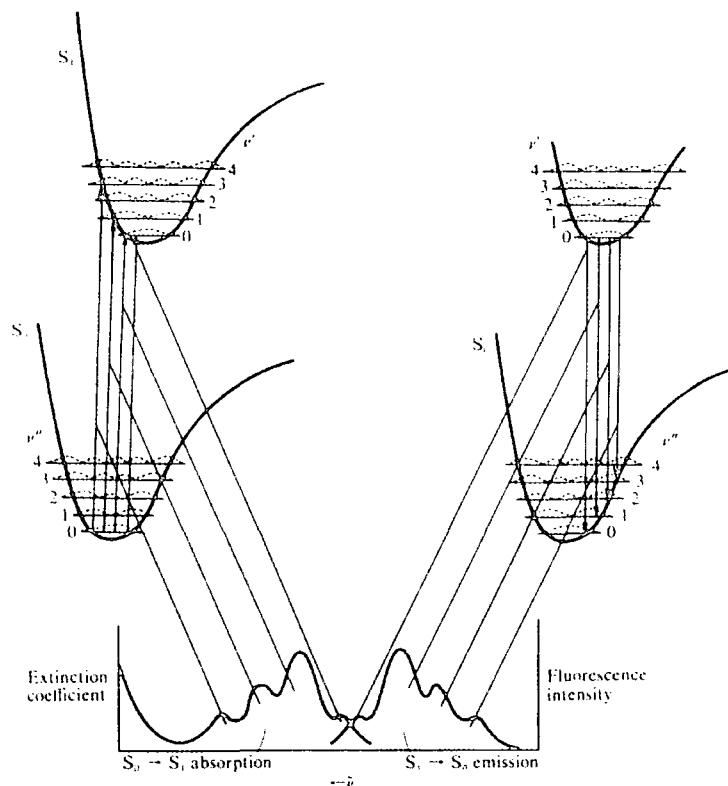
Figure 2-9 Schematic of the contribution in the luminescence and absorption spectra due to vibrational sub-levels

Phosphorescence is observed when the overlap between triplet and singlet excited states is such that on relaxation from higher vibrational excited states the excitation crossing over into the triplet manifold. As already mentioned these transitions are forbidden, or weak, and require spin perturbation. Examples of such perturbations are phonon scattering and spin-orbit coupling.
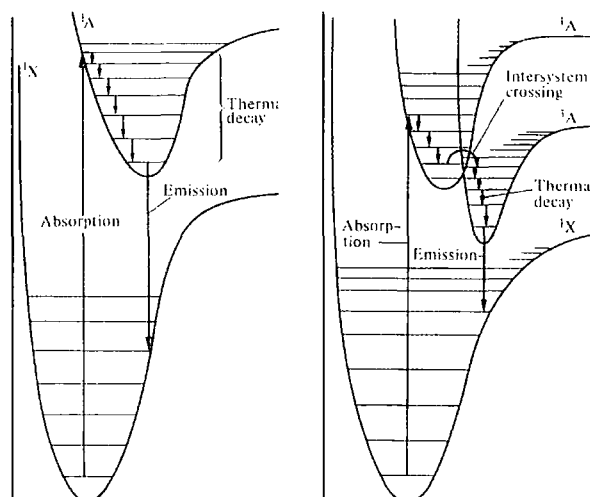
Figure 2-10 Schematic of fluorescence (left) and phosphorescence (right). Illustration taken from the literature[5]

16

2.33 Intermolecular Interactions

The discussion so far has ignored the possibility of interactions between conjugation lengths in close physical proximity. When in solution this maybe an appropriate approximation, but on spin casting thin films of conjugated polymers one introduces combinational effects that contribute significantly to light output following excitation. This is due to the overlap of neighbouring conjugation segments' wavefunctions, either between excited and relaxed chains (aggregates) or between excited chains (excimers).

Aggregates, such as those observed in polyfluorene, appear as broad featureless features red-shifted from normal singlet emission in luminescence spectra. They also appear in absorption spectra due to overlap of their ground state wavefunctions. Aggregation is concentration dependant for both solution and film.

Excimers only appear in luminescence spectra, as they have repulsive ground states that do not overlap. There has been considerable work invested towards understanding excimer emission as it is believed to be less efficient than singlet emission as well as being a potential quenching source for singlet excitons[76,20,83,21]. Results presented in this work, however, show a dependence of excimer emission on triplet concentration, suggesting triplets have a role to play in the formation of the excimer attributed features[42].
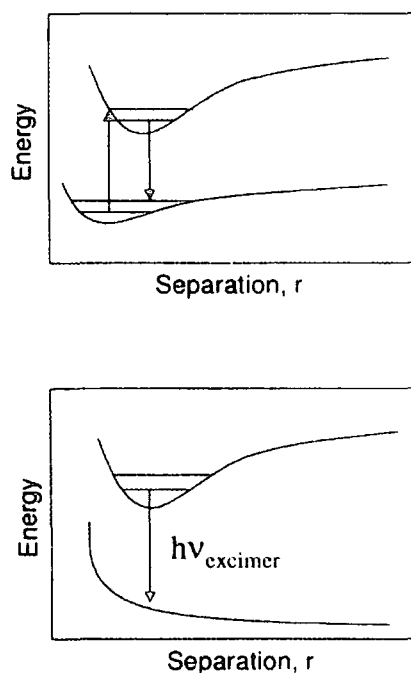
Figure 2-11 Absorption and emission in an aggregated system (top) and emission into the repulsive ground excimer state (bottom)[69]

2.4 DEVICE PHYSICS FOR A POLYMER LIGHT-EMITTING DIODE

2.41 Electroluminescence

Electroluminescence is the phenomena of radiative recombination of externally introduced charge carriers. Electrons and holes are injected into the material by an applied electric field, under which they then migrate in opposite directions and hence have a chance to meet.

I have already touched on the matter of charge injection above. In a basic model electrons and holes are injected into the LUMO and HOMO of the polymer respectively. A more realistic approach is to say injection occurs into the polaron levels[28,22]. Once inside the polymer the charges migrate across the sample as polarons (bipolarons being less mobile), and if negative and positive polarons pass within a capture radius there is a probability of exciton formation. The spin of the polarons is randomly distributed between ±1/2 and hence there will be formation of both singlets and triplets on recombination. Triplet excitons are statistically more likely to form as there are three triplet exciton states and only one singlet excited state.

$$\text{singlet} = \frac{1}{\sqrt{2}}\left[(\uparrow\downarrow)-(\downarrow\uparrow)\right]$$

$$\text{triplet} = (\uparrow\uparrow)$$

$$= \frac{1}{\sqrt{2}}\left[(\uparrow\downarrow)+(\downarrow\uparrow)\right]$$

$$= (\downarrow\downarrow)$$

Equation 2-5

This lead groups to propose that only 25% of recombinations would result in singlets[17,33-35]. More recently this assumption of spin independent recombination has been theoretically[45,25,32] and experimentally[82] questioned. The argument is that overlap between singlet exciton and loosely correlated electron-hole pair wavefunctions is greater than for triplet exciton and electron-hole pair wavefunctions. The singlet is higher in energy than the triplet: pictorially this can be envisaged as the singlet exciton has a greater radius and hence more ionic character similar to the ionic loosely bound pair. Transitions from the first capture state to the tightly bound singlet and triplet excitons may also involve intersystem crossing during the relaxation, with one or both the polarons gaining the energy required to change spin from phonons.
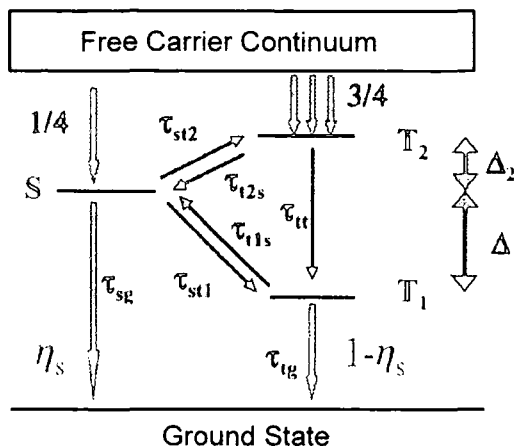
Figure 2-12 Transitions between excited states following initial loose capture, where Δ and Δ_2 are the exchange energies (i.e. difference between singlet and triplet(s) states), S is first excited singlet level, T_1 and T_2 the first two excited triplet levels and τ_{mn} is the lifetime of a transition from state m to n.

Figure 2-12 is reproduced from work by T.M.Hong and H.F,Meng[45] . They propose that initial loose capture (i.e. long distance correlation between the electron- and hole-polarons following injection) is spin independent due to the exchange energy only being important when the two charges in the pair are on the same unit cell[56].

Whatever the nature of the recombination it is known that a considerable fraction of products will be triplets. With transitions between the triplet manifold and the singlet ground state being forbidden, this means that these triplet excitons are long-lived, and their presence is detrimental to performance due to non-radiative singlet-triplet (S-T) quenching. This has lead several groups to dope PLEDs active layers with phosphorescent triplet harvesting molecules, which may utilise triplet energy in light emission or at least remove them from the system and hence reduce S-T annihilation [3,79,8,7,6,57,2].

The electroluminescence and photoluminescence bear a striking reslemblence to each other, and the excited species are believed to be the same for both, with levels populated by charge injection and photon induced transition respectively (Figure 2-13).
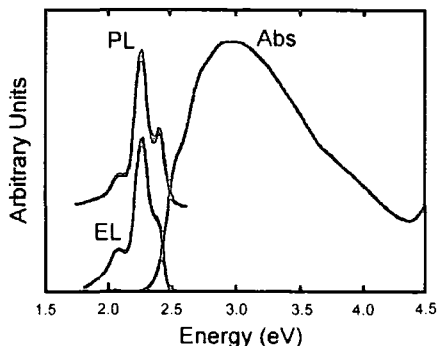
Figure 2-13 The electroluminescence (EL), photoluminescence (PL) and absorption (Abs) spectra of a PPV EL device with Ca and ITO electrodes.

2.42 Device Operation

The efficiency of emission from a PLED is dependent on five key factors[35]

$$\frac{N_p}{N_{ch}} = \Phi_{Capture}\Phi_{Spin}\Phi_{Rad}\Phi_{Escape} \qquad \textbf{Equation 2-6}$$

where N_p is the number of photons escaping the device, N_{ch} is the number of injected charge pairs and their ratio is defined as the External Quantum Efficiency. The injected polarons will not all meet up with oppositely charged counterparts. Some will merely migrate to the opposite electrode and contribute to the dark current (i.e. current that does not contribute to light emission). The efficiency of capture is given as $\Phi_{Capture}$. A hole-electron pair will only radiatively decay from a singlet exciton intermediate, hence Φ_{Spin} is the ratio of singlet to triplet excitons formed by capture. Of the singlets formed some may encounter non-radiative quenching centres before radiatively decaying; the efficiency of decay is given as Φ_{Rad}. Finally any photons fomed within the active layer must escape the device. Possible quenching effects are absorption at the cathode or self-absorption. This is measured by probability Φ_{Escape}.

In addition to this the power efficiency will be enhanced if the barriers to charge injection are minimised. This is a key factor for electron injection; electrons being the minority carriers in most conjugated polymers.
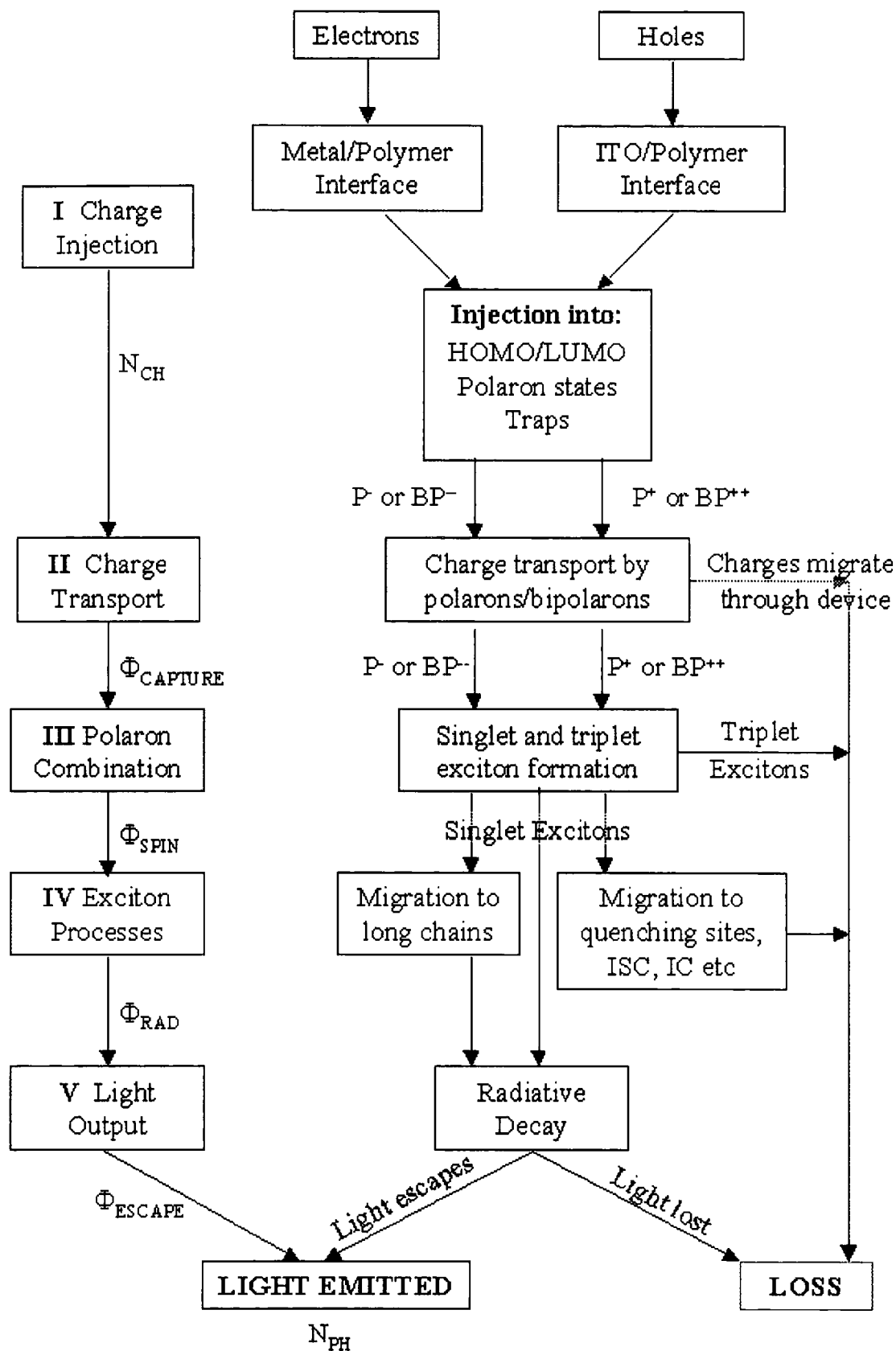
Figure 2-14 Flow chart of the steps to light output in PLEDs, taken from the literature[24].

2.42 Charge Injection

Barriers to injection are formed due to the energy offset between the injecting materials' workfunction and the HOMO (LUMO)[1] of the polymer for hole (electron) injection. For hole injection a low workfunction is required. Due to the need for one of the two electrodes to be transparent in order to let light out Indium Tin Oxide (ITO) has been used for this purpose. Frequently a conducting polymer layer such poly(3,4-ethplenedioxythiophene) doped with poly(4-styrene sulfonate) (PEDT:PSS) is spin-cast inbetween the ITO and the active layer. This aids injection by further band alignment but also helps to balance electron and hole injection by introducing an offset to hole injection referred to as a heterojunction which impedes the hole current. Electrons being the mimority carriers this insertion helps to balance charge flow, which is believed to aid performance by raising $\Phi_{Capture}$. Other options for ITO treatment include plasma etching the ITO to leave a pristine layer[49,50,46]. ITO has a high surface roughness and both this technique and the use of a hole-transporting layer (HTL) helps to minimise short circuits in the device.

Electron injection is complicated by the fact that most low workfunction metals are highly reactive. In this study Aluminium (Al) and Calcium (Ca) are used as cathodes. Both form interfacial regions with the active layer. Al deposition results in the region of reduced conjugation 20-30Å thick. This reduces mobility and adds to injection blocking[14]. Ca:polymer interfaces vary greatly with the evaporation pressure used. 'Pristine' Ca ($<10^{-7}$mbar) results in large Ca^{2+} diffusion into the polymer, forming an altered region ~20-30Å thick. On applying an electric field the ions move further and device breakdown is observed. 'Dirty' Ca ($>10^{-6}$mbar) results in formation of an oxide at the interface, which protects the polymer from ion diffusion. Coincidently this is the pressure region in which most commercial diffusion pumps operate. For a fuller discussion of these effects, as well as improved systems using hybrid interfaces, the author recommends the following articles.[14,67,29,36].
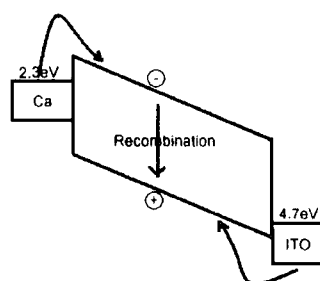
Figure 2-15 Schematic of injection barriers for a single layer PLED. For PPV the barriers when using ITO and Ca are ~0.1ev and 0.2eV for holes and electrons respectively

---

[1] Or polaron levels, as stated above.

2.43 Charge Transport and Mobility

Blom and Vissenberg[15] have produced a good theoretical-experimental comparison for charge transport PPV PLEDs based on time of flight measurements.

In common with earlier work they found that the mobilities of electron and hole polarons are highly field dependent. The current is bulk limited rather than injection limited. Hole polarons move through the bulk by hopping from site to site whilst electrons move through field assisted detrapping from defect states. This is the reason that electron mobility is much lower than hole mobility for most conjugated polymers. Mobilities are also highly dependent on temperature, in particular for electrons, where thermal de-trapping is a key factor in mobility.

2.44 Polaron Recombination

Due to the difference in hole and electron mobilities recombination takes place closer to the cathode than the anode. This yields a further benefit from using heterojunctions, as one can manipulate the position of the recombination zone and hence reduce cathode quenching of excitons.

In a 1998 correspondence Dyakonov[25] describes how recombination leads to prompt and delayed fluorescence components in the photoluminescence of PPV. He ascribes the delayed fluorescence to the radiative annihilation of triplet-triplet (T-T) pairs, and provides experimental evidence. An alternative explanation is given by Bassler[41,70], who suggests that delayed fluorescence is due to the recombination of germinate CT pairs formed on excitation, and shows that a high applied electric field reduces the delayed signel, suggesting dissociation of charged pairs.

In EL experiments the possible contribution of T-T pairs to the optical output by delayed fluorescence is not a major consideration. Statistically only one in nine annihilations will lead to excited singlet formation. The majority contribute to heating effects, whilst a large number of triplets annihilate singlet excitons before they can decay radiatively. This is the difficulty in applying the finding of photoexcitation experiments to EL theory: there are so many differences between the two scenarios. Triplets in photoexcited polymers are the minority excited states whilst in EL studies they dominate. They can be seen as a loss that needs to be minimised, either by introducing a route for them to contribute to optical output (Section 2.55), or removing from the system (Section 2.57).

2.45 Magnetic Field Effects

The introduction of a magnetic field can influence the ratio of singlets to triplets formed by perturbing the intersystem crossing. This effect takes place when the lifetime of the pairs is shorter than spin-lattice relaxation time (a measure of the rate of spin flipping)[25]. Spin evolution takes place due to hyperfine interactions of a polaron spin with magnetic nuclei, which causes mixing, or periodic transitions, between singlet and triplet states. An applied magnetic field lifts the triplet manifold degeneracy (Zeeman effect) leaving only mixing of the singlet and T_0-substate.

Whether this effect enhances or reduces singlet yield is highly dependent on the backbone twist angle and the exchange energy. Modelling by other groups has proposed conditions for singlet enhancement, illustrated in Figure 2-16 and summarised in Chapter 8. It should be noted that the scientific community has yet to respond to this study in a critical way at the time of publication.
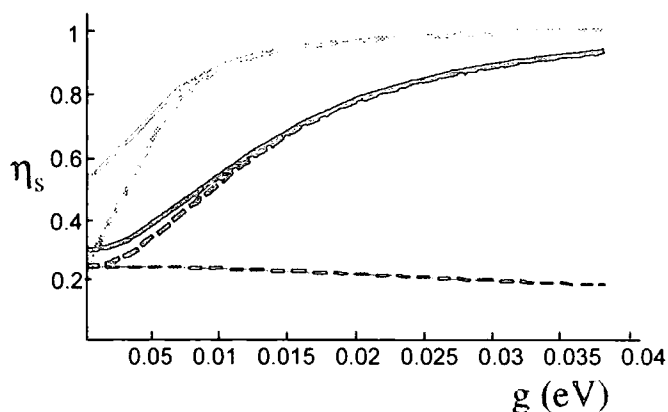
Figure 2-16 Singlet Yield η_s as a function of impurity spin-flip coupling (a measure of the magnetic field strength). Modelling was for two twist angles $\theta=1^0$ (dashed lines) and $\theta=7^0$ (solid lines), each of which were allowed three different exchange energies, $\Delta=0.3$eV (grey lines), 0.5eV (thin lines) and 0.9eV (thick lines). Figure is taken from Hong and Meng[45]

2.45 Exciton Migration

Having formed within the polymer, singlet excitons are susceptible to quenching by numerous routes, many of which are compounded by the migration of singlets and triplets once formed.

Frenkel singlet excitons decay on a timescale of ~300ps has been reported for a PPV derivative[48]. In this time they may migrate along chains, as evidenced by the variation in PLED efficiency with heterolayer thickness[13]. The diffusion range for these singlet excitons is of the order of a few nanometers. In this distance they may move to longer conjugation lengths (i.e.lower energy sites), hence the broad emission spectra. They are believed to migrate via hopping akin to their electron and hole constituents; equations for the jump rates proposed by Richert among others[63].

$$V_{ij} = A(r_{ij})^* \exp\left[-\left(e_j - e_i\right)K_B^* T\right] \qquad e_j > e_i$$
$$V_{ij} = A(r_{ij}) \qquad\qquad\qquad\qquad e_j < e_i$$

Equation 2-7

where V_{ij} is the hopping rate from state i to state j, r_{ij} is the spatial separation of the two sites, e_j and e_i the energy of the two states, T is the temperature in Kelvin and K_B is the Boltzmann Constant.

Triplet excitons are long-lived, with $\tau_T > 300ms$[66]. This means that there mean free path through the polymer is much longer than for singlets, allowing them to be involved in several reactions with either other triplets or singlets. The fact that singlet-triplet annihilation generates more triplets means that triplet population as a percentage of excitons increases with current density (see Equation 2-11).

2.46 Energy Transfer to Dopants

The negative effect of singlet-triplet annihilation as well as the low fluorescence efficiency of some conjugated polymers (~0.3 for PPV) has lead many groups to dope polymers with molecular compounds[44,43,58,19,52]. The majority of studies involved transfer of excited energy to a luminescent dopant with high emission efficiency. This generally has to involve a red-shift in emission relative to host emission in order to obtain overlap between host emission and dopant absorption, which is necessary for resonant energy transfer. This results in a downhill step in energy on transfer from host to dopant. There are two advantages to transferring energy to the dopant: potential reduction in singlet-triplet annihilation and an enhanced efficiency of radiative decay.

If the dopant is phosphorescent then there is the possibility of utilising the triplet yield η_T, "side stepping the selection rules"[68].

2.461 Forster (Resonant) Transfer

There are two types of transfer in addition to reabsorption of host emission, one a sub-definition of the other. *Resonant* or Forster transfer requires an overlap between absorption spectrum of the dopant and the fluorescence spectrum of the host.
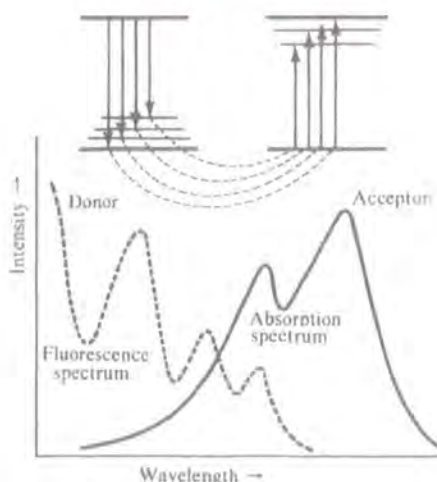
Figure 2-17 Overlap of host emission and dopant absorption that is essential for Forster-type transfer[62].

Forster built on work by the Perrins, who proposed a mechanism of transfer that required coherence and was mediated by the dipole-dipole interaction. This predicted transfer rates that seemed too great compared to results. Forster realised that the assumption of coherence was wrong due to the relaxation of the excitation transfer to vibrational sub-levels of the dopant introducing irreversibility to the process. Coherence is impossible if the vibronic width of the acceptor, ΔE, is much greater than the interaction strength of host and dopant, J.

In the limit where J is much greater than the width of a single vibronic transition, Perrin and Perrin's result holds. For the majority of cases, however, $\Delta E > J$ and the transfer rate has a $1/R^6$ dependence.

$$K_{D \to A} = \frac{1}{\tau_D} \frac{1}{R^6} \left(\frac{3}{4\pi} \right) \int \frac{c^4}{\omega^4 n_o^4} F_D(\omega) \sigma_A(\omega) d\omega \qquad \textbf{Equation 2-8}$$

where $F_D(\omega)$ is the normalised fluorescence emission spectrum, $\sigma_A(\omega)$ the normalised dopant absorption cross section, n_o is the refraction index, c is the speed of light, τ_D is the dopant excited state lifetime and the integration is over all frequencies. Note that the rate $K_{D \to A}$ is zero for no overlap of host emission and dopant absorption. A critical radius, R_0 (the Forster radius), can be defined at which the energy transfer from host to dopant equals the hosts' radiative decay rate:

$$K_{D \to A} = \frac{1}{\tau_D} \left(\frac{R_0}{R} \right)^6 \qquad \textbf{Equation 2-9}$$

where R_0 is typically of the order of 10Å[62] In his classic talk[31] submitted to the 10th Spiers memorial Lecture Forster defines the characteristics of this type of transfer that allow us to distinguish it from other transfer mechanisms:

	Forster transfer	reabsorption	complexing	encounter
Dependence on volume	none	increase	none	none
Dependence on viscosity	none	none	none	decrease
Host Lifetime	decreased	unchanged	unchanged	decreased
Host fluorescence spectrum	unchanged	changed	unchanged	unchanged
Absorption apectra	unchanged	unchanged	changed	unchanged

Table 2-1 Forster defined characteristics of transfer mechanisms

The key characteristic of Forster transfer is the observed reduction in the host's excited singlet state lifetime. In the systems discussed later in this thesis there are usually two possible transfer processes: Forster and Radiative transfer. Radiative transfer does not affect the hosts' excited singlet state lifetime hence measuring it will allow us to distinguigh between the two cases.

Due to Forster transfer being a dipole-dipole interaction it is also valid between states of single multiplicity. Thus one can only have a dopant singlet exciton from a host singlet exciton.

2.462 Dexter Transfer

Dexter extended the theory of resonant transfer to deal with dipole-forbidden transitions involving higher multiplicity states. He expressed the transfer rate for triplet-triplet transfer as

$$K_{D \to A} = \frac{2\pi}{\hbar} |\beta_{DA}|^2 \int F_D(E) F_A(E) dE \qquad \textbf{Equation 2-10}$$

where $\beta_{D \to A}$ is the exchange energy interaction between molecules, $F_D(E)$ is the alised phosphorescence spectrum of the host and $F_A(E)$ the normalised absorption of the dopant, with the integration dE over all energies. Note again that the transfer is dependent on the overlap of host emission and dopant absorption. However, Dexter transfer requires a much smaller separation of D and A and is harder to achieve in polymer systems. It has been shown to be a slow process between polymers and dopants and expected to lead to biexpoential decay[27,37].

2.463 Charge Trapping on Dopant Sites

Several groups have found that on doping polymers with luminescent molecules, efficient energy transfer has been observed, but that the power efficiency has been poor due to the increase in the required drive voltage[58,18,78,79,44,43]. This has been ascribed to charge trapping at the dopant sites[58,44,43]. It occurs when either (or both) the electron affinity of the host is less than that of the dopant or the ionisation potential is greater. This means that on injection the charged polarons are likely to become trapped on the dopant sites. This build up in space-charge within the device results in a redistribution of the electric field, resulting in a higher drive voltage for a given current density over an undoped device. An example of a charge-trapping system is shown below in Figure 2-18.
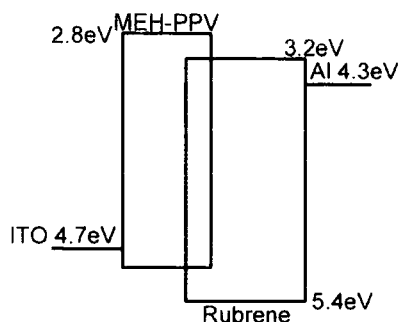
Figure 2-18 The energy bands for a MEH-PPV monolayer PLED doped with Rubrene. In this case Rubrene acts as a trap for positive polarons due to its lower ionisation energy

This charge harvesting is expected to result in excitons formed directly on the dopants as well as those formed by resonant transfer. Thus the depth of these charge traps must be considered when evaluating the performance of a dopant.

This loss in power efficiency has so far been overlooked in the race for high internal quantum efficiencies. It is something this thesis attempts to address by using heavy metal dopants that do not harvest polymer charges.

2.47 Loss or Quenching Mechanisms

We have already discussed the effects of several loss mechanisms in PLEDs above. The losses are significant to such a system: photoluminescence quantum yield (PLQY) measurements give very high values for some polymers (~0.6 for polyfluorene), yet the highest external quantum efficiency for an undoped polymer in this study (for example) is only 1.2%. Understanding this difference is the first step to addressing possible improvements. Only the mechanisms understood to have the main influence on performance are discussed here.

2.471 Singlet-triplet Annihilation

Many authors proposed the quenching of singlet intra-chain excitons by triplet intra-chain or trapped excitons. The high density of triplets due to their favoured formation from recombination, coupled with the increase in triplet numbers on singlet annihilation, makes this route significant to non-radiative quenching. The reaction can be described by Equation 2-11:

$$S_1 + T_1 \rightarrow T_n + S_0$$
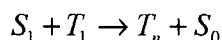
Equation 2-11 Reaction mechanism for triplet-singlet annihilation

where in order to conserve spin one of the products is necessarily of high multiplicity. This high energy triplet T_n can then thermalise down to the T_1 level, thus increasing triplet density.

2.472 Singlet-Polaron Annihilation

"With the number of charged polarons moving through the bulk at high velocity I find it amazing that electroluminescence was ever observed in polymer light-emitting diodes" *A.P.Monkman 2001*.

There is experimental verification of polarons encountering/annihilating singlet intra-chain excitons, be they free polarons predicted by SSH theory or coupled in pairs[26,25,32]. Taken from these works are equations describing the rate of annihilation via collision:

$$\frac{dD}{dt} = gN_0 - (k_r + k_{nr} + k_q p)D$$

$$\frac{dp}{dt} = \eta g N_0 - k_f p$$

Equation 2-12

where D is the density of intra-chain excitations $^1D^*$, polarons p, gN_0 the generation rate of $^1D^*$, η is a polaron generation quantum yield, K_q is the quenching rate constant, and polaron density p can be changed by decreased by some other mechanism represented by rate constant k_f.

It should be noted with caution that Dyakanov is able to draw two conclusions from this experiment. The alternative to singlet annihilation is that polarons merely occupy sites otherwise available for singlet excitons.

2.473 Singlet-singlet Annihilation

Unlike singlet-triplet annihilation there is no need for a triplet product in order to conserve spin. Instead for non-radiative processes the excess energy can be absorbed by the surroundings in terms of a phonon.

$$S_1 + S_1 \rightarrow S_0 + \Omega\big(E = 2(S_1 - S_0)\big) \qquad \textbf{Equation 2-13}$$
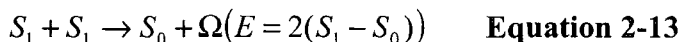
2.474 Cathode Quenching

In additional to collisional quenching by other mobile species, the mismatch in hole- and electron-polaron mobility means that excitons can easily migrate to the metallic cathode within their lifetime. Once there they are efficiently quenched. Friend and co-workers report a diffusion length of ~60nm for intra-chain singlet excitons in PPV[13,80]. PLED active layers in this study are typically 100nm thick. Transfer of excited energy to the modified metal:polymer region formed via metallic ion diffusion are discounted as no change in the emission profile is observed.

2.475 Cathode Mirror Effects

In the same papers consideration is given to interference effects where the cathode acts as a metallic mirror. Photons may be reflected back into the active layer, increasing the chance of reabsorption and thus lowering the efficiency. Standing waves can also be set up, as shown by the variation in PL efficiency when a spacer layer of silicon dioxide (SiO_2) is sandwiched between the polymer and cathode (Figure 2-19).
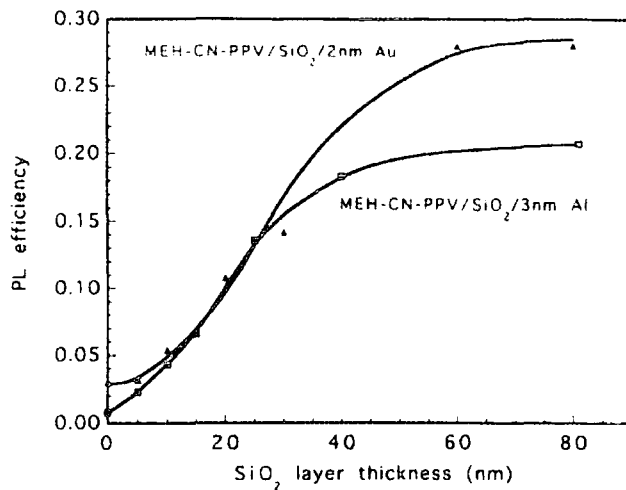
Figure 2-19 Variation in PL quantum efficiency of a 15nm thick MEH-CN-PPV (cyano derivative of PPV) film on a SiO₂ spacer layer on 2nm of gold or 3nm of aluminium as a function of SiO₂ thickness (from the literature[13]).

2.5 CURRENT MODELS OF POLYMER LIGHT-EMITTING DIODE OPERATION

There are many models emerging that can describe individual polymer systems[15,77,47] but fail to provide an accurate model for the entire PLED family. This thesis does not utilise any modelling of electronic properties in its analysis, hence only a brief overview of some classic models is presented.

2.51 Conduction Mediators in Conjugated Polymers

One of the advantages of SSH theory is that it explains the presence of conduction mediators or pseudo particles in conjugated polymers. For a degenerate ground state polymer the energy equivalence of dimerised phases (see for example trans-$(CH)_n$ in Figure 2-5) means that a defect or boundary between opposite phases is stable, and mobile with virtually no cost in energy.

Phase A   Phase B
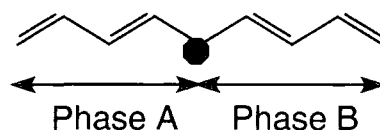
Figure 2-20 The neutral boundary particle S^0

A neutral soliton, S^0, is such a boundary state in the absence of any excess charge. If the soliton was formed due to removal or addition of charge (with a resulting lattice distortion) then one has a negative (electron addition) soliton (S^-) or positive (electron removal) soliton (S^+). These charged solitons are understood to be responsible for conduction in degenerate ground state polymers.

For non-degenerate ground state polymers such as cis-$(CH_3)_n$ and PPV the difference energy between dimerised phases means that solitons are thermodynamically unstable. Instead they exist as spatially confined pairs, and depending on the soliton combination are known as polarons or bipolarons. A positive(negative) soliton combined with neutral anti-soliton (or vice versa) is known as a positive(negative) polaron, whilst a positive(negative) soliton combined with a positive/negative anti-soliton is known as a positive(negative) bipolaron.
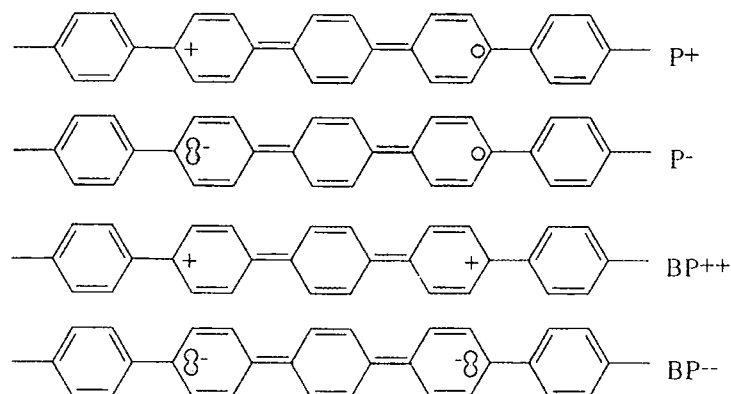
Figure 2-21 Postive and negative polarons(P^+,P^-) and bipolarons (BP^{++},BP^-) in poly(p-phenylene) (PPP)

This gives rise to two sets of energy levels, the polaron energy levels close to the valence and conduction band and the bipolaron levels, which lie closer to the midgap soliton states. As any disruption to the chain by a soliton is now cancelled out by its accompanying anti-soliton, polarons and bipolarons are mobile and contribute to conduction. Polarons are believed to be the main conducting pseudo particles in non-degenerate ground state polymers[28,22], and it is the recombination of oppositely charged polarons formed by charge injection (as opposed to the HUMO and LUMO) that leads to electroluminescence in polymer light-emitting diodes[30]. Bipolaron formation tends to occur at higher current densities and is the reason for lower operating efficiencies under said conditions[15], the recombination of bipolarons not contributing towards the electroluminescence due to the difference in energy of the species involved.

The Exciton model also allows for polarons and bipolarons, formed either due to injection or optical excitation. The excess charge forms a lattice distortion around it. The electron/hole has an effective mass different to that of a free electron due to this distortion. For optical excitation the excitation produces both electrons and holes, which may remain correlated after absorption, resulting product is referred to as a germinate pair.

2.52 Schottky Barrier Diodes

When a metal and a semiconductor are brought into physical contact a Schottky barrier is formed[72]. The imbalance in electron affinities results in migration of charges across the interface and hence a large electric field in induced which depletes the junction of charge; hence the term 'depletion zone'. The Fermi levels of the metal and semiconductor are 'bent' into alignment, as illustrated in Figure 2-22 below.
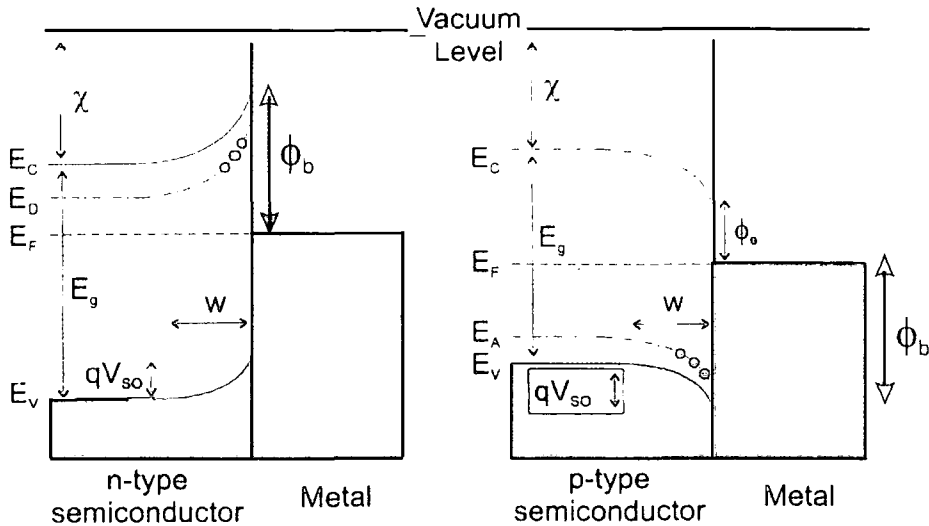
Figure 2-22 Schottky barriers in n- and p-type semiconductors[72]

Where E_C is the conduction band, E_V the valence band, E_g is the band gap, E_D and E_A are the donor and acceptor levels, ϕ_b is the Schottky barrier height, ϕ_e the barrier to electron injection, w the width of the depletion zone, V_{SO} is the built-in voltage and electron affinity of the semiconductor is χ.

This model allows one to derive equations for the current density in the semiconductor, the width of the depletion zone and the capacitance of the interface. However for large applied fields and high barriers to injection as present in PLEDs Fowler-Nordheim (F-N) tunnelling may be a better description.

2.53 Fowler-Nordheim Tunelling

F-N theory describes injection as tunnelling through triangular barriers. Instead of band bending the applied field 'tilts' the polymer bands, thus reducing the barrier thickness as illustrated in
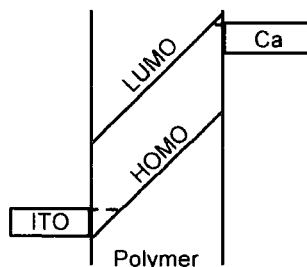
Figure 2-23 F-N tunnelling for an ITO:polymer:Ca device[24]

Again this produces an equation for the current-field dependence. F-N theory predicts that a plot of Ln(current/Field^2) verses 1/F will produce a straight line: a way of comparing results to this theory[59].

References

[1]   *The Hubbard Potential*, 1st ed.; World Scientific: Singapore, 1992.

[2]   Adachi, C.; Baldo, M. A.; Forrest, S. R.; Lamansky, S.; Thompson, M. E.; Kwong, R. C. *Applied Physics Letters* **2001**, *78*, 1622-1624.

[3]   Adachi, C.; Baldo, M. A.; Forrest, S. R.; Thompson, M. E. *Applied Physics Letters* **2000**, *77*, 904-906.

[4]   Alvarado, S. F.; Seidler, P. F.; Lidzey, D. G.; Bradley, D. D. C. *Physical Review Letters* **1998**, *81*, 1082-1085.

[5]   Atkins, P. W. *molecular Quantum Mechanics*, 2nd ed.; Oxford University Press: New York, 1983.

[6]   Baldo, M. A.; Lamansky, S.; Burrows, P. E.; Thompson, M. E.; Forrest, S. R. *Applied Physics Letters* **1999**, *75*, 4-6.

[7]   Baldo, M. A.; O'Brien, D. F.; You, Y.; Shoustikov, A.; Sibley, S.; Thompson, M. E.; Forrest, S. R. *Nature* **1998**, *395*, 151-154.

[8]   Baldo, M. A.; Thompson, M. E.; Forrest, S. R. *Nature* **2000**, *403*, 750-753.

[9]   Barth, S.; Bassler, H. *Physical Review Letters* **1997**, *79*, 4445-4448.

[10] Barth, S.; Deussen, M.; Bassler, H. *Philosophical Transactions of the Royal Society of London Series a-Mathematical Physical and Engineering Sciences* **1997**, *355*, 749-761.

[11] Barth, S.; Hertel, D.; Tak, Y. H.; Bassler, H.; Horhold, H. H. *Chemical Physics Letters* **1997**, *274*, 165-170.

[12] Bassler, H.; Gailberger, M.; Mahrt, R. F.; Oberski, J. M.; Weiser, G. *Synthetic Metals* **1992**, *49*, 341-352.

[13] Becker, H.; Burns, S. E.; Friend, R. H. *Physical Review B-Condensed Matter* **1997**, *56*, 1893-1905.

[14] Birgerson, J.; Fahlman, M.; Broms, P.; Salaneck, W. R. *Synthetic Metals* **1996**, *80*, 125-130.

[15] Blom, P. W. M.; Vissenberg, M. C. J. M. *Material Science and Engineering* **2000**, *27*, 53-94.

[16] Brunner, K.; Tortschanoff, A.; Warmuth, C.; Bassler, H.; Kauffmann, H. F. *Journal of Physical Chemistry B* **2000**, *104*, 3781-3790.

[17] Burroughes, J. H.; Bradley, D. D. C.; Brown, A. R.; Marks, R. N.; Mackay, K.; Friend, R. H.; Burns, P. L.; Holmes, A. B. *Nature* **1990**, *347*, 539-541.

[18] Cerullo, G.; Stagira, S.; Zavelani-Rossi, M.; De Silvestri, S.; Virgili, T.; Lidzey, D. G.; Bradley, D. D. C. *Chemical Physics Letters* **2001**, *335*, 27-33.

[19] Chang, H. H.; Wu, C. C.; Yang, C. C.; Chen, C. W.; Lee, C. C. *Applied Physics Letters* **2001**, *78*, 574-576.

[20] Conwell, E. M. *Physical Review B* **1998**, *57*, 14200-14202.

[21] Conwell, E. M.; Mizes, H. A. *Physical Review B* **1995**, *51*, 6953-6958.

[22] Conwell, E. M.; Wu, M. W. *Applied Physics Letters* **1997**, *70*, 1867-1869.

[23] Dacosta, P. G.; Conwell, E. M. *Physical Review B* **1993**, *48*, 1993-1996.

[24] Dailey, S. A Study of conjugated Polymers and their Applications in Light-Emitting Diodes. Doctorate, University of Durham, 1998.

[25] Dyakonov, V.; Frankevich, E. *Chemical Physics* **1998**, *227*, 203-217.

[26] Dyakonov, V.; Rosler, G.; Schwoerer, M.; Frankevich, E. L. *Physical Review B-Condensed Matter* **1997**, *56*, 3852-3862.

[27] El-ghayoury, A.; Harriman, A.; Khatyr, A.; Ziessel, R. *Journal of Physical Chemistry A* **2000**, *104*, 1512-1523.

[28] Epstein, A. J.; Wang, Y. Z.; Jessen, S. W.; Blatchford, J. W.; Gebler, D. D.; Lin, L. B.; Gustafson, T. L.; Swager, T. M.; MacDiarmid, A. G. *Macromolecular Symposia* **1997**, *116*, 27-38.

[29]   Fahlman, M.; Bredas, J. L.; Salaneck, W. R. *Synthetic Metals* **1996**, *78*, 237-246.

[30]   Fesser, K.; Bishop, A. R.; Campbell, D. K. *Physical Review B* **1983**, *27*, 4804-4825.

[31]   Forster, T. H. "Transfer mechanisms of electronic excitation"; 10th Spiers Memorial Lecture, 1959.

[32]   Frankevich, E.; Ishii, H.; Hamanaka, Y.; Yokoyama, T.; Fuji, A.; Li, S.; Yoskino, K.; Nakamura, A.; Seki, K. *Physical Review B* **2000**, *62*, 2505-2515.

[33]   Friend, R.; Bradley, D.; Holmes, A. *Physics World* **1992**, *5*, 42-46.

[34]   Friend, R.; Burroughes, J.; Shimoda, T. *Physics World* **1999**, *12*, 35-40.

[35]   Friend, R. H.; Gymer, R. W.; Holmes, A. B.; Burroughes, J. H.; Marks, R. N.; Taliani, C.; Bradley, D. D. C.; Dos Santos, D. A.; Bredas, J. L.; Logdlund, M.; Salaneck, W. R. *Nature* **1999**, *397*, 121-128.

[36]   Greczynski, G.; Salaneck, W. R.; Fahlman, M. *Synthetic Metals* **2001**, *121*, 1625-1628.

[37]   Harriman, A.; Romero, F. M.; Ziessel, R.; Benniston, A. C. *Journal of Physical Chemistry A* **1999**, *103*, 5399-5408.

[38]   Harrison, N. T.; Hayes, G. R.; Phillips, R. T.; Friend, R. H. *Physical Review Letters* **1996**, *77*, 1881-1884.

[39]   Heeger, A. J.; Kivelson, S.; Schrieffer, J. R.; Su, W. P. *Reviews of Modern Physics* **1988**, *60*, 781-850.

[40]   Heller, C. M.; Campbell, I. H.; Laurich, B. K.; Smith, D. L.; Bradley, D. D. C.; Burn, P. L.; Ferraris, J. P.; Mullen, K. *Physical Review B* **1996**, *54*, 5516-5522.

[41]   Hertel, D.; Romanovskii, Y. V.; Schweitzer, B.; Scherf, U.; Bassler, H. *Synthetic Metals* **2001**, *116*, 139-143.

[42]   Higgins, R. W. T.; Burrows, H. D.; Monkman, A. P. *Physical Review B* **Submitted**.

[43]   Higgins, R. W. T.; Hothofer, H. G.; Scherf, U.; Monkman, A. P. *Applied Physics Letters* **2001**, *79*, 857-859.

[44]   Higgins, R. W. T.; Hothofer, H. G.; Scherf, U.; Monkman, A. P. *Journal of Applied Physics* **Submitted**.

[45]   Hong, T. M.; Meng, H. F. *Physical Review B* **2001**, *6307*, 5206-+.

[46]   Kim, J. S.; Granstrom, M.; Friend, R. H.; Johansson, N.; Salaneck, W. R.; Daik, R.; Feast, W. J.; Cacialli, F. *Journal of Applied Physics* **1998**, *84*, 6859-6870.

[47]   Koehler, M.; da Luz, M. G. E.; Hummelgen, I. A. *Journal of Physics D-Applied Physics* **2000**, *33*, 2096-2107.

[48]   Kraabel, B.; McBranch, D. W. *Chemical Physics Letters* **2000**, *330*, 403-409.

[49]   Kugler, T.; Salaneck, W. R. *Comptes Rendus De L Academie Des Sciences Serie Iv Physique Astrophysique* **2000**, *1*, 409-423.

[50]   Kugler, T.; Salaneck, W. R.; Rost, H.; Holmes, A. B. *Chemical Physics Letters* **1999**, *310*, 391-396.

[51]   Lee, C. H.; Yu, G.; Moses, D.; Heeger, A. J. *Physical Review B* **1994**, *49*, 2396-2407.

[52]   Lee, C. L.; Lee, K. B.; Kim, J. J. *Applied Physics Letters* **2000**, *77*, 2280-2282.

[53]   Leng, J. M.; Jeglinski, S.; Wei, X.; Benner, R. E.; Vardeny, Z. V.; Guo, F.; Mazumdar, S. *Physical Review Letters* **1994**, *72*, 156-159.

[54]   Liu, J. N.; Sun, X.; Fu, R. T.; Nasu, K. *Physical Review B* **1992**, *46*, 1710-1714.

[55]   Lu, Y. *Solitons and polarons in conducting polymers*, 1st ed.; World Scientific: Singapore, 1988.

[56]   Nakajima, S.; Toyozawa, Y.; Abe, R. *The Physics of Elementary Excitations*; Springer: Berlin, 1978.

[57]   O'Brien, D. F.; Baldo, M. A.; Thompson, M. E.; Forrest, S. R. *Applied Physics Letters* **1999**, *74*, 442-444.

[58]   O'Brien, D. F.; Giebeler, C.; Fletcher, R. B.; Cadby, A. J.; Palilis, L. C.; Lidzey, D. G.; Lane, P. A.; Bradley, D. D. C.; Blau, W. *Synthetic Metals* **2001**, *116*, 379-383.

[59]   Parker, I. D. *Journal of Applied Physics* **1994**, *75*, 1656-1666.

[60]   Peierls, S. R. *Quantum Theory of Solids*, 1955.

[61]   Peierls, S. R. *More Surprises in Theoretical Physics*, 1st ed.; Princeton University Press: Princeton, 1991.

[62]   Pope, M.; Swenberg, C. E. *Electronic Processes in Organic Crystals and Polymers*, 2nd ed.; Oxford Science Publications: Oxford, 1999.

[63]   Richert, R.; Bassler, H. *Journal of Chemical Physics* **1986**, *84*, 3567.

[64]   Romanovskii, Y. V.; Gerhard, A.; Schweitzer, B.; Scherf, U.; Personov, R. I.; Bassler, H. *Physical Review Letters* **2000**, *84*, 1027-1030.

[65]   Rothberg, L. J.; Yan, M.; Papadimitrakopoulos, F.; Galvin, M. E.; Kwock, E. W.; Miller, T. M. *Synthetic Metals* **1996**, *80*, 41-58.

[66]   Rothe, C.; Monkman, A. P. *Physics Review Letters* **Submitted**.

[67]   Salaneck, W. R.; Logdlund, M.; Birgersson, J.; Barta, P.; Lazzaroni, R.; Bredas, J. L. *Synthetic Metals* **1997**, *85*, 1219-1220.

[68]   Samuel, I. D. W.; Beeby, A. *Nature* **2000**, *403*, 710-711.

[69]   Samuel, I. D. W.; Rumbles, G.; Friend, R. H. Primary Photoexcitations in Conjugated Polymers: Molecular Exciton verses Semiconductor Band Model; Sariciftci, N. S., Ed.; World Scientific: New York, 1997.

[70]   Schweitzer, B.; Arkhipov, V. I.; Scherf, U.; Bassler, H. *Chemical Physics Letters* **1999**, *313*, 57-62.

[71]   Schweitzer, B.; Bassler, H. *Synthetic Metals* **2000**, *109*, 1-6.

[72]   Sharma, B. L. E. *Metal-semiconductor Schottky barrier junctions and their applications*; Plenum: New York, 1984.

[73]   Shuai, Z.; Pati, S. K.; Su, W. P.; Bredas, J. L.; Ramasesha, S. *Physical Review B* **1997**, *55*, 15368-15371.

[74]   Solomons, T. W. G. *Organic Chemistry*, 5th ed.; John Wiley and Sons, Inc.: New York, 1992.

[75]   Su, W. P. In *Handbook of Conducting Polymers*; Skotheim, T. A., Ed.; Mark Dekker, Inc.: New York, 1986; Vol. 2nd; pp p.757-794.

[76]   Tretiak, S.; Saxena, A.; Martin, R. L.; Bishop, A. R. *Journal of Physical Chemistry B* **2000**, *104*, 7029-7037.

[77]   van der Horst, J. W.; Bobbert, P. A.; Michels, M. A. J.; Bassler, H. *Journal of Chemical Physics* **2001**, *114*, 6950-6957.

[78]   Virgili, T.; Lidzey, D. G.; Bradley, D. D. C. *Advanced Materials* **2000**, *12*, 58-+.

[79]   Virgili, T.; Lidzey, D. G.; Bradley, D. D. C. *Synthetic Metals* **2000**, *111*, 203-206.

[80]   Wan, W. M. V.; Friend, R. H.; Greenham, N. C. *Thin Solid Films* **2000**, *363*, 310-313.

[81]   Wells, C. H. J. *Introduction to Molecular Chemistry*; Chapman and Hall: New York, 1978.

[82]   Wohlgenannt, M.; Tandon, K.; Mazumdar, S.; Ramasesha, S.; Vardeny, Z. V. *Nature* **2001**, *409*, 494-497.

[83]   Wu, M. W.; Conwell, E. M. *Physical Review B* **1997**, *56*, 10060-10062.

3.1 DEVICE FABRICATION

3.11 Polymer Structure and Synthesis

The main polymers used in this study as active layers are poly(2-methoxy, 5-(2'ethyl-hexyloxy)-*p*-phenylene vinylene) (MEH-PPV), poly(9,9-bis(2-ethylhexyl)fluorene-2,7-diyl) (PFO), PFO's amino-endcapped variant α,ω-Bis[N,N-di(4-methylphenyl)aminophenyl]-poly(9,9-bis(2-ethylhexyl)fluoren-2,7-diyl) (PF2/6am4), ladder-type methyl-poly(p-phenylene) (Mel-PPP) and CSW-78. Their chemical structures are depicted below in Figure 3-1.
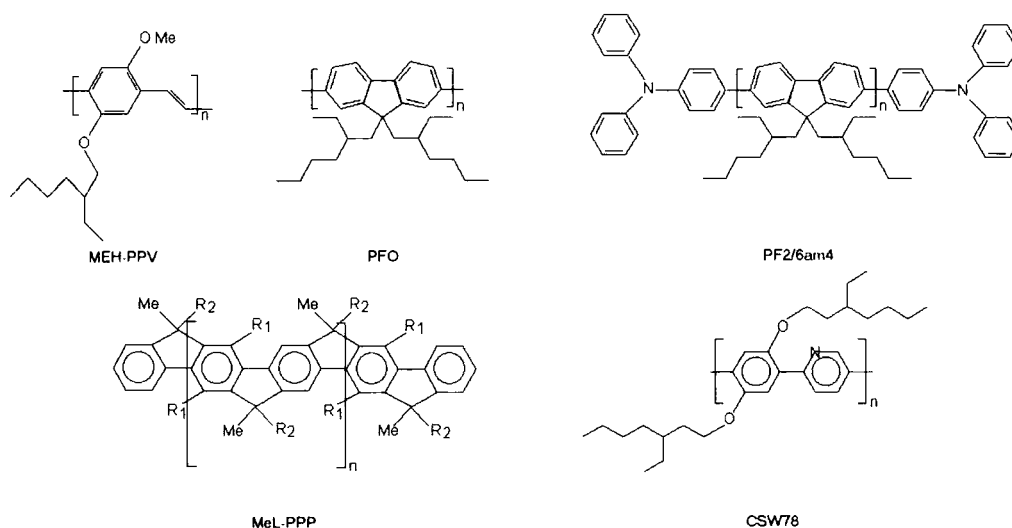
Figure 3-1 Active layer polymers used in this study: MEH-PPV, PFO, PF2/6am4, Mel-PPP and CSW78 (R_1=*n*-C_6H_{13} and R_2=1,4-(C_6H_4)-*n*C_{10}-H_{21})

MEH-PPV was obtained from Covion Chemicals in solid form. PFO, PF2/6am4 and MeL-PPP were supplied by the Max Plank Institute for polymer research; their synthesis routes are described in the literature[5,6]. CSW78 was synthesised by Dr.C.S.Wang (of Durham University Chemistry Department).

This study also uses a variety of polymers for charge –transporting layers sandwiched between either cathode or anode for electron-transporting layers (ETL) or hole-transporting layers (HTL) respectively. These include poly(3,4-ethylenedioxythiophene) (PEDT) doped with polystyrene sulphonated acid (PSSA), emeraldine base polyaniline (PANI) protonated with camphor sulfonic acid (CSA), 2-acrylamido-2-methyl-1-propanesulphonic acid (AMPSA) or polystyrene sulphonated

acid (PSS), and poly(2,5-pyridinediyl) (PPY). These polymers are depicted alongside their protonating ions in Figure 3-1.

Emeraldine Base PANI

PEDT   PPY   CSA   AMPSA

PSS
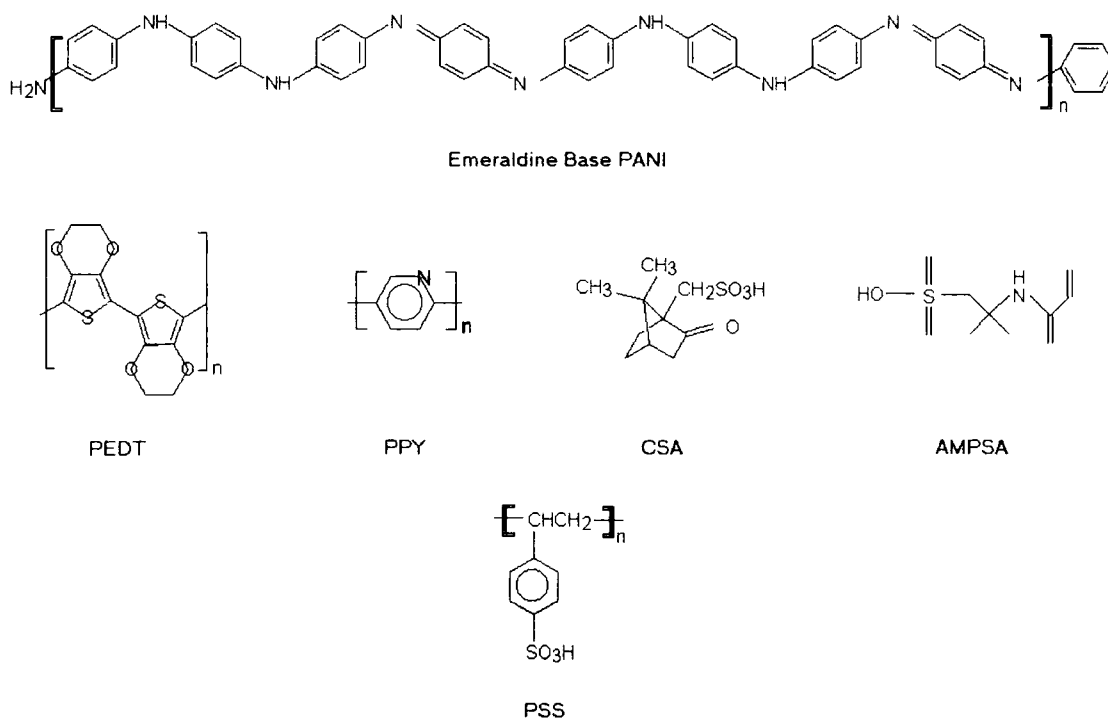
Figure 3-2 Charge transporting layers used in this study: emeraldine base PANI, PEDT and PPY together with relevant counter-ions CSA, AMPSA and PSS

PANI:counter-ion solutions were synthesised by Dr.N.A.Zaidi as previously reported[1], PEDT was obtained commercially from Bayer-AG Chemicals of Germany (Baytron-P Batch K0014 Trial No: A14083); its synthesis is expected to follow the route previously reported by research groups elsewhere[7]. PPY was prepared by Dr L.E. Horsburgh by dehalogenation polycondensation of 2,5-dibromopyridine with a tetrakakis(triphenylphosphine) nickel(0) catalyst following a modified Yamamoto route.

3.12 Substrate Preparation

3.121 Overview

Polymer light-emitting diodes (PLEDs) were fabricated on Indium Tin Oxide (ITO) coated glass measuring 10x15mm in area. The ITO was patterned using a combination of photoresist and acid etching to create the anodic region. On top of this patterned ITO was spin-cast polymer layer(s) directly from solution. For multiple layer PLEDs subsequent layers were spin-coated directly on top of the previous layer, generally after

the primary layer had undergone thermal treatment (see below). The devices were completed by the evaporation of eight individual metal cathodes, resulting in a device that could be tested eight times in order to obtain a realistic result.

3.122 ITO Etching

PLEDs must have one semi-transparent electrode in order for the light generated by radiative recombination within the active layer to escape and reach the observer. Evaporation of semi-transparent metal cathodes is difficult to perform, especially if one wishes to protect a reactive cathode such as calcium from atmospheric bleaching by subsequent capping layers of less reactive metals. Hence the anode is usually chosen as the semi-transparent electrode, and ITO is a popular choice due to its good conductivity, an effective workfunction of ~4.8eV close to the HOMO of most electroluminescent conjugated polymers and high optical tranmission over the range of the visible spectrum (Figure 3-3).
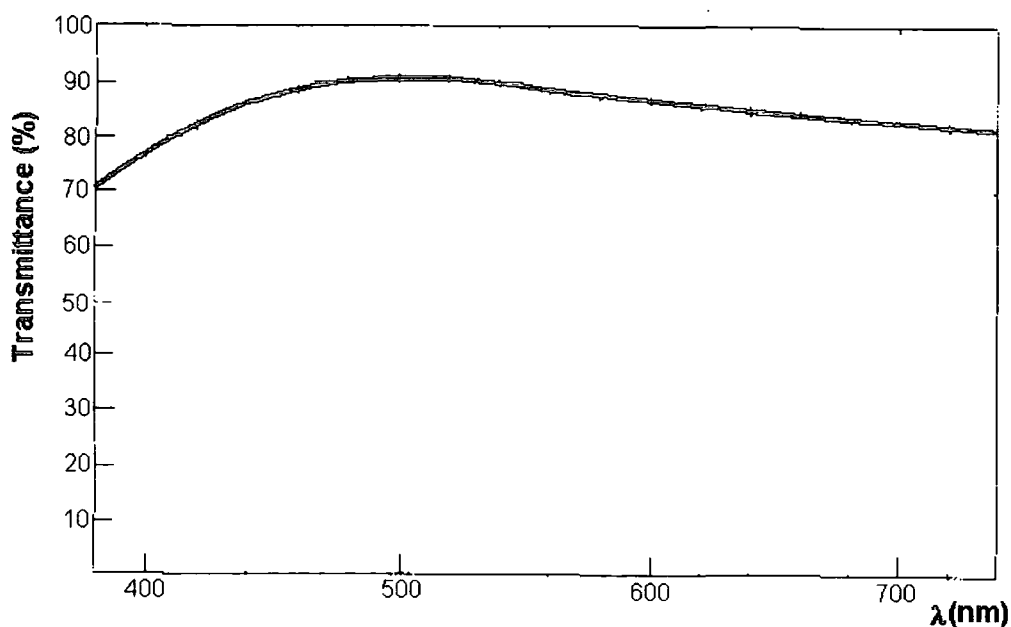
Figure 3-3 Transmission-Wavelength plot for Balzers ITO coated glass (taken from the Balzers Product Catalogue)

The ITO coated glass used in this study was obtained commercially from Balzers. The ITO layer measured 125nm, and had a sheat resistance of 13Ω/ . The large area 600x600mm ITO coated sheets as received from Balzers were cut into tiles measuring 15x10mm using a water-cooled diamond saw. Any rough edges were sanded off, and then a central, vertical stripe of width 7mm was marked out on each tile using a positive photoresist pen. The tiles were left to dry overnight and then the application

44

was repeated. Dry tiles were then placed in an ultrasonic bath at room temperature in concentrated hydrochloric acid, which removes all non-protected ITO. Following 4 minutes of etching any remaining acid on the tiles and the photoresist stripe were neutralised by a series of 5 minute ultrasonic baths in detergent, acetone and finally propan-2-ol (IPA). This process is summarised in the schematic below:
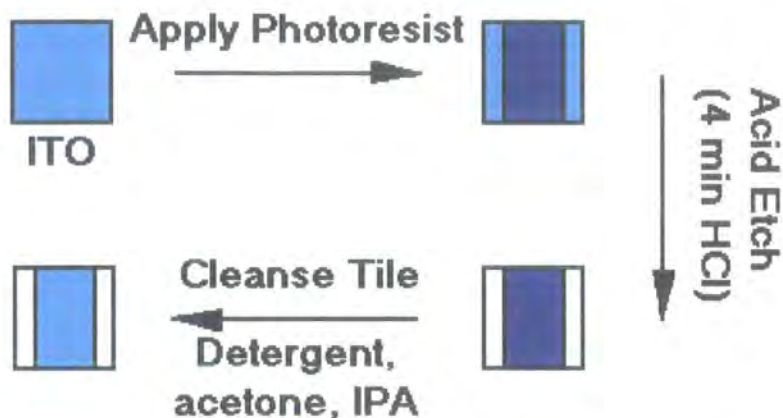
Figure 3-4 Schematic of the ITO etching process

3.123 Hole-transporting Layer Preparation

Hole-transporting layers (HTLs) PEDT:PSS, PANI:CSA, PANI:AMPSA or PANI:PSS were spin coated from solution at 2500rpm for 1 minute onto etched and cleansed tiles, with the exception of PANI:PSS which required 2 minutes and a temperature of 80^0C provided by a (heat lamp) in order to drive off the NMP solvent used. These processes were considered insufficient to drive off all residual solvent and so following this HTL coated tiles were left overnight in a vacuum oven at 50^0C and a pressure of 10^{-1} mbar, as recommended by past publications[7].

PEDT:PSS was spun from water suspension at the concentration received from Bayer-AG. The PANI:CSA, :AMPSA and :PSS were diluted down from the concentration received from Dr.N.A.Zaidi in order to produce HTL spin-cast films as close to the PEDT:PSS HTL thickness as possible. This was done in order to legitimately compare the performance of PANI and PEDT as a HTL in PLEDs.

Immediately prior to subsequent polymer layers being spun-cast on top of the HTL-coated tile it was heated at 180^0C for 3 minutes in a final attempt to drive out species detrimental to active layer performance.

3.124 Polymer Spin Coating

Each of the active layer polymers used (see Figure 3-1) were preliminarily dissolved at a range of concentrations in an appropriate solvent and spun-cast onto ITO/HTL layers. In order to minimise the amount of impurities only HPLC grade solvents were used. In addition these solvents were filtered by Dr.S.Monkman through a 5µm filter. The thickness of polymer films were then measured in order to determine the appropriate concentrations of polymer:solvent solutions for films of order 100nm. Unless otherwise stated, the standard solvent used were toluene (Tol) for PFO, PF2/6am4 and MeL-PPP, chlorobenzene (CB) for MEH-PPV and formic acid for PPY.

Typically polymers did not dissolve instantly in the solvent, and if so inhomogeneously, resulting in striations in cast films from these solutions. In order to fully mix polymer with solvent magnetic fleas were placed in the sample vial, and the solution was left to mix overnight. Of the resulting solutions PPY occasionally required filtration with glass wool and a pipette in order to remove particulate. Having fully dissolved the polymer in solution, films were then spun-cast at 2500rpm for 1 minute as above.

3.125 Cathode Evaporation

Metal electrodes were evaporated onto the polymer coated tiles, usually to a thickness of approximately 100nm, forming the cathode in forward bias. Evaporation was carried out in a nitrogen glove box background environment at a pressure of approximately 1×10^{-6} mbar. The deposition rate was held at roughly 1Å/s to minimise any detrimental effect the evaporation would have on the polymer layer. Calcium electrodes were partially protected from the effects of oxidation by subsequent evaporation of an aluminium capping layer. The arrangement of the metal electrodes is governed by the action of a shadow mask, of the authors' design, which dictates where the metal contacts are formed. The action of the mask defines an active device area of ~2 mm^2, formed where the cathode overlaps with the central ITO stripe. This means that electrical connections could be easily made with both ITO anode and metal cathode without the PLED short circuiting, as shown in

Figure 3-5. No encapsulation of the PLED was added, hence PLED characterisation immediately followed completion of the device in order to obtain optimum results.

Metal Contact

Polymer
Layer(s)

Glass Substrate

Patterned ITO
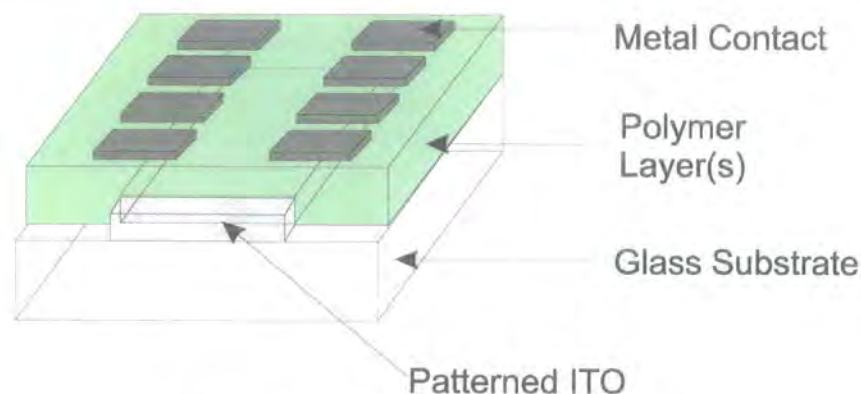
Figure 3-5 PLED device structure

3.126 Thickness Measurements

A Tencor Alpha-Step thickness profiler was used to measure the thickness of polymer and metal films. A small section of polymer/metal film was removed using a sharp scalpel and the stylus of the profiler was run over the scratch. When studying bilayer device a sample of the underlying layer was spun in addition to the full device and its thickness subtracted from that of the bilayer in order to determine the thickness of the individual layers. It was observed during the course of investigations that film thickness when spin coating was dependent on both solvent and underlying layer, hence the Alpha-Step apparatus was always used to check device dimensions. A typical trace resulting from an Alpha-Step measurement is shown below.
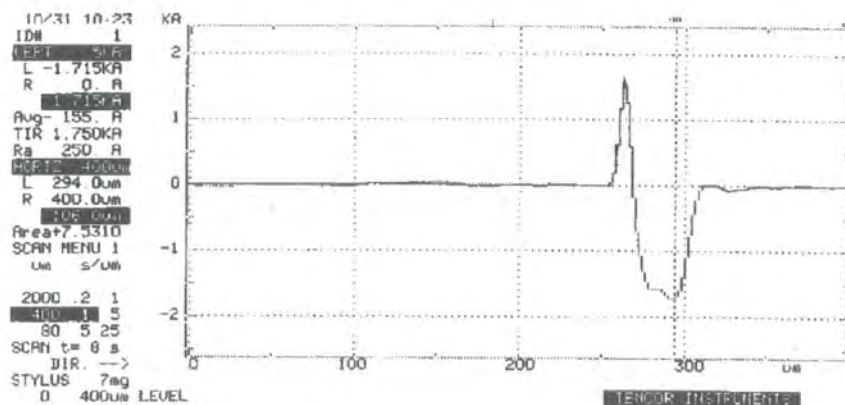
Figure 3-6 A typical measurement taken with the Alpha Step Profiler

The trace shows a flat area from around $0\mu m$ to $250\mu m$ on the x-axis. There is then a large peak of about +170nm before the trace shows a wide depression with a depth of 171.5nm (as measured). The depression is caused by the action of a scalpel scratch down the surface and the peak is a result of material from this scratch piling up on the side of the scratch.

3.2 ELECTROLUMINESCENCE CHARACTERISATION

3.21 Experimental Set-up

The PLED was mounted in a sample holder, which formed electrical connection addressing the 8 pixels. Gold sprung pins pierce the device up to the solid ITO layer. 8 of the pins encounter the cathode but no ITO due to its absence on either lengthways edge of the device. 4 central pins connect to the ITO stripe-anode.
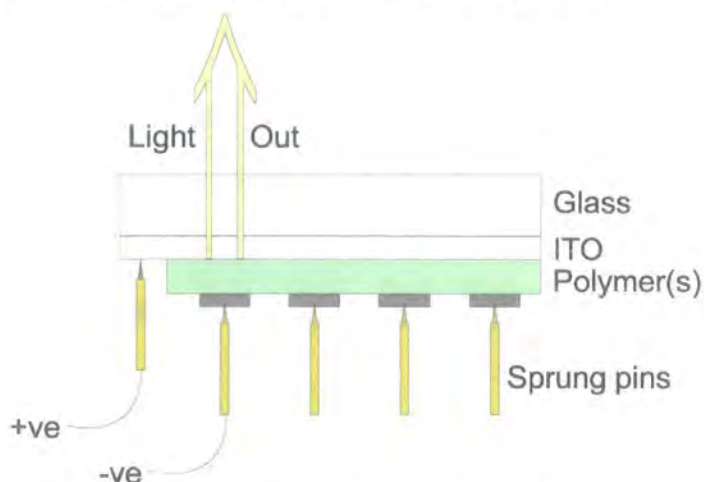
Figure 3-7 Electrical Connections to the PLED

The sample holder was then pumped down to a pressure of 10^{-2}mbar for testing. The electrical connections to the PLED were controlled by a Keithley 2400, in turn automated by NI labView PC software to allow the device to be tested under a range of current-voltage values. Simultaneously the intensity of light from the PLED was measured by a photodiode mounted in the lid of the sample holder, controlled by a Keithley 2000 again automated via PC software. Measured current, voltage and photodiode voltage is then exported as a delimited ASCII file.
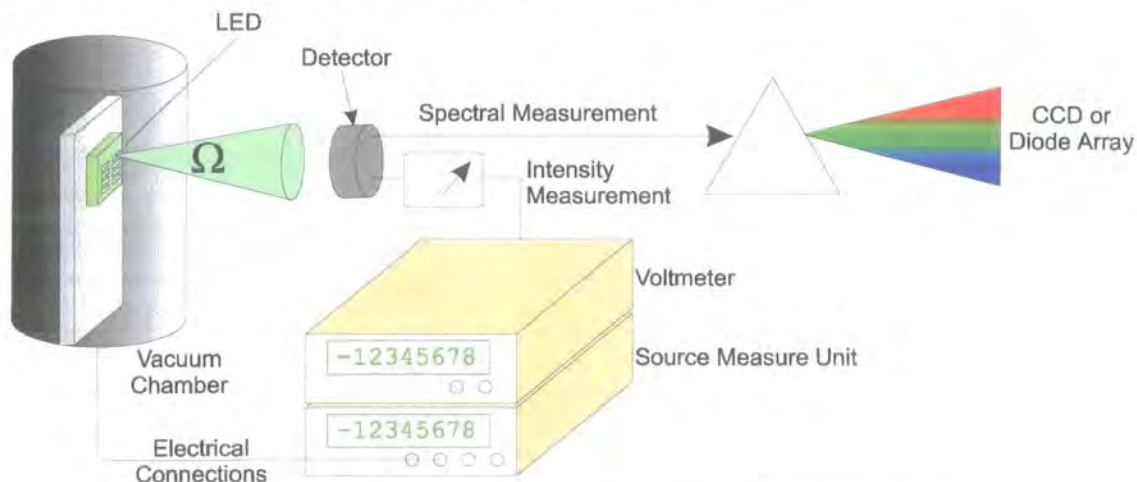
Figure 3-8 Experimental set-up for PLED characterisation

48

Electroluminescence spectra were taken with an Ocean Optics UBS2000 Spectrometer with the PLED in the sample holder but the photodiode lid removed. Spectra could easily be sampled using a fibre optic to collect the light emitted, and the GUI provided by Ocean Optics allowed one to adjust integration time, smoothing, averaging and other standard features. The electroluminescene spectrum is particularly significant in calculating device characteristics as for polymers spectra tend to be broad (relative to inorganic and small molecules). Hence when converting from our measured photovoltage to other units e.g. candelas, the spectrum must be allowed for.

3.22 Normalisation of the Electroluminescence Spectra

We use a photodiode to measure the intensity of the light from the PLED in a known collection angle, and then combine this quantitative information with the qualitative information collected by the CCD (which tells us the relative number of photons incident on the CCD for the given wavelength interval across the range of the CCD) in order to obtain a spectrum normalised by photon intensity per unit wavelength. We have already mentioned that the experimental system used results in a measured voltage from the photodiode. This photovoltage is proportional to the actual photocurrent in the device, the constant of proportionality being the gain (i.e. feedback resistance) used in amplifying the signal from the photodiode. We use a standard RS large area ($100mm^2$) photodiode that has a transimpedance amplifier built in the diode casing. The circuit layout is shown in Figure 3-9
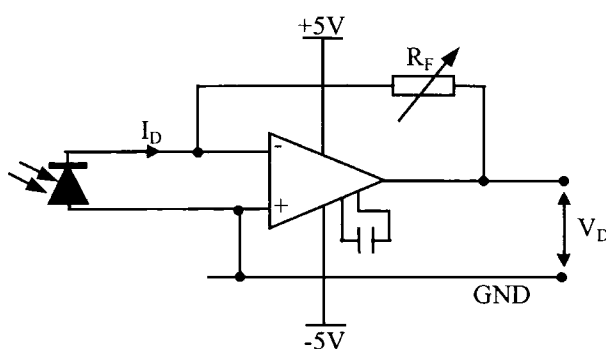
Figure 3-9 Transimpedance amplifier circuit built into the photodiode casing

In addition to this amplification an operational amplifier with a range of gains (to allow for a large variation in device performance) was built around the transimpedance amplifier. An operational amplifier merely increases the measured photovoltage rather

than convert between current and voltage like the transimpedance amplifier. Hence the total gain is given by the product of the two individual gains/feedback resistances and we can easily work back to the photocurrent using Ohm's Law, as shown in Equation 3-1.

The photodiode/feedback circuit was calibrated using an Ar^+ laser and a NIST calibrated power meter. Details of the technique employed can be found in Appendix C, and is based on techniques found in the literature[2,9,8].

$$I_D = \frac{V_D}{R_T \times R_O}$$ **Equation 3-1**

We combine this quantatative measurement of intensity with the EL spectrum (which is proportional to the total number of photons emitted at each wavelength) in order to find the absolute total number of photons at each wavelength. On integrating this value, referred to here as $S(\lambda)$, we obtain the total number of photons emitted and hence provide a route for calculating the quantum efficiency of the device. We must allow for the nature of the detector used: we correct for the responsivity variation of Silicon with photon energy.

3.221 Silicon Photodiode Responsibility

Conveniently this information is supplied to us by the manufacturer, can be found in RS Data Sheet F 232-3894 and is reproduced below:
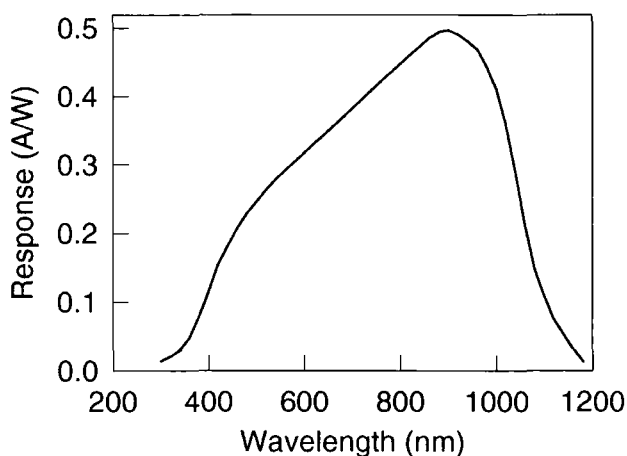
Figure 3-10 RS Photodiode Responsivity

This data can be approximated by one of two polynomials depending on which wavelength range we are interested in. A second order polynomial is accurate for the

visible range whilst the seventh order polynomial accurately fits the entire curve. In this study we always use the second order polynomial; both are shown below:

$$y_2 = -9.17965e10x^2 + 7.80834e5x - 0.119066$$

$$y_7 = 5.08611e43x^7 - 9.81884e37x^6 - 1.38876e32x^5 + 5.51266e26x^4$$
$$- 6.17115e20x^3 + 3.27231e14x^2 - 8.27777e7x + 7.99188$$

Equation 3-2 2nd and 7th Order polynomials describing the Si photdiode responsivity

3.222 Calculating the EL Spectra in terms of photons per unit wavelength

First we convert the EL spectra in terms of photovoltage, $T(\lambda)$, into a spectra in terms of amps, $A(\lambda)$, using the energy of the photon at a given wavelength $E(\lambda)$ and correcting for the response of the photodiode $Si(\lambda)$

$$A(\lambda) = T(\lambda) \times Si(\lambda) \times E(\lambda) \qquad \textbf{Equation 3-3}$$

We substitute for $E(\lambda)$ using Planck's law. Next we normalise the spectrum with respect to the measured current by introducing a numerical factor B, where B is found by equating I_D with $A(\lambda)$ and rearranging to produce Equation 3-4

$$B = \frac{I_D}{\int_0^\infty A(\lambda)d\lambda} \qquad \textbf{Equation 3-4}$$

Next we convert from intensity in amps to intensity in terms of photon number

$$S(\lambda) = \frac{B \times A(\lambda)}{Si(\lambda) \times E(\lambda)} \qquad \textbf{Equation 3-5}$$

and substituting Equations 3-3 and 3-4 into Equation 3-5 we obtain Equation 3-6

$$S(\lambda) = \frac{V_D T(\lambda)}{(R_T \times R_O)hc} \left(\int_0^\infty \frac{T(\lambda)Si(\lambda)}{\lambda} d\lambda \right)^{-1} \qquad \textbf{Equation 3-6}$$

We can then calculate the total number of photons by integrating $S(\lambda)$

$$L = \int_0^\infty S(\lambda)d\lambda \qquad \textbf{Equation 3-7}$$

3.23 Calculating the External Quantum Efficiency

The photodiode only collects light from the small cone of volume defined by joining the perimeter of the active Silicon area with the perimeter of the luminescent pixel. In order to calculate the external quantum efficiency from this we must extrapolate to the total light emitted in all directions. This involves assuming the emission to be Lambertian in distribution. Experimental evidence for this assumption is well established, and assuming a Lambertian emission profile is currently the excepted norm when calculating PLED performance values[4]. For a Lambertian source the flux as a function of angle θ is defined in Equation 3-8 and depicted in

$$F(\theta) = F_0 \cos(\theta) \qquad \textbf{Equation 3-8}$$
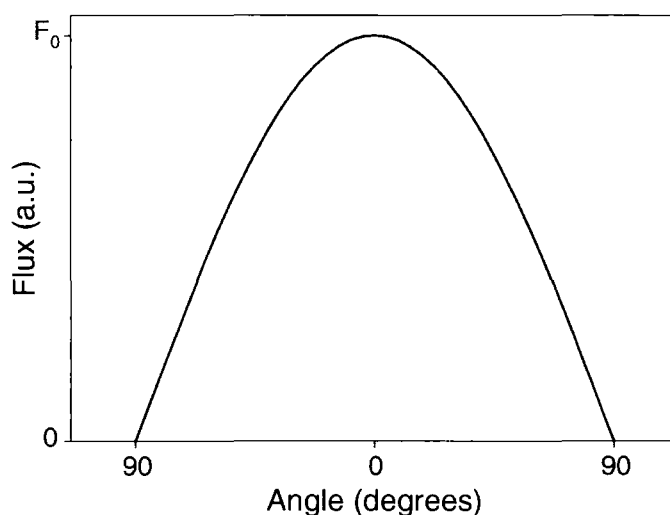
Figure 3-11 Flux as a function of angle θ for a Lambertian Source

We use the correction for the Lambertian nature of the source defined in Greenham et al.[4] The full argument can be found in either that paper or in the thesis of Dr.S.Daily[3]. Here we reproduce the end product, Equation 3-9, which allows us to calculate the total flux knowing the angle of collection which we observe with the photodiode

$$\Rightarrow F_T = \frac{\pi L r^2}{A_D} = \frac{\pi L}{\Omega} = \frac{\pi}{\Omega} \int_0^\infty S(\lambda) d\lambda \qquad \textbf{Equation 3-9}$$

here F_T is the total Flux from the PLED, L is the number of photons per second incident on the photodiode area A_D, r is the separation the detector and source and $\Omega = \frac{A_D}{r^2}$ is the solid angle of collection. It is important to note that this derivation assumes that the separation r is such that it is accurate to approximate the pixel as a point source.

The **External Quantum Efficiency** is defined as the ratio of the number of photons emitted in the forward direction to the number of injected charge pairs.

$$E_{ext} = \frac{Photons_{emiited}}{Pairs_{injected}} \qquad \textbf{Equation 3-10}$$

We find the number of injected charges from the current:

$$N_e = \frac{I_P}{e} \qquad \textbf{Equation 3-11}$$

where e is the electronic charge and I_p is the current in the PLED pixel. Substituting for F_T and N_e in Equation 3-10 we obtain Equation 3-12

$$E_{ext} = \frac{F_T}{N_e} = \frac{e\pi r^2 \int S(\lambda)d\lambda}{I_P A_D} \qquad \textbf{Equation 3-12}$$

Finally substituting for $S(\lambda)$ with Equation 3-6

$$E_{ext} = \frac{\pi e V_D}{(R_T \times R_O)I_p \Omega hc} \int_0^\infty T(\lambda)d\lambda \left(\int_0^\infty \frac{T(\lambda)Si(\lambda)}{\lambda} d\lambda \right)^{-1} \qquad \textbf{Equation 3-13}$$

The factor of V_D/I_P tells us that the External quantum Efficiency (EQE) will be proportional to the gradient of Intensity-Current Plots for PLEDs.

The calculation of external quantum efficiency is carried out using an Origin Worksheet scripted with LabTalk (script shown in Appendix A).

3.24 Calculating Power Efficiency

Power efficiency is commonly quoted in terms of either Candelas per Amp or Lumens per Watt. In this study we use the Lumens per Watt notation

$$E_{power} = \frac{Int(lumens)}{I_P V_P} \qquad \textbf{Equation 3-14}$$

This involves converting from the photocurrent in Amps to the Radiometric Lumen unit, described below.

3.25 Converting to and between Radiometric Units

3.251 Photovoltage to Watts

The Power in Watts as a function of Wavelength is the product of the EL spectrum normalised to photon number, $S(\lambda)$, and the energy of the photon at each of those wavelengths, $E(\lambda)$

$$P(\lambda) = S(\lambda) \times E(\lambda) \qquad \textbf{Equation 3-15}$$

To obtain the total power we integrate this function over all wavelengths. We can also substitute for $S(\lambda)$ using Equation 3-6 and $E(\lambda)$ using Planck's law

$$P(watts) = \frac{V_D}{(R_T \times R_O)} \int_0^\infty \frac{T(\lambda)}{\lambda} d\lambda \left(\int_0^\infty \frac{T(\lambda)Si\ (\lambda)}{\lambda} d\lambda \right)^{-1} \qquad \textbf{Equation 3-16}$$

3.252 Watts to Candela

The definition of the Candela is taken from the literature[S.Daily, 1997 #165]

$$Int = K_m \int_0^\infty C(\lambda) L(\lambda) d\lambda \qquad \textbf{Equation 3-17}$$

where K_m is the Commission Internationale de L'Eclairage (CIE) defined "maximum spectral luminous efficacy of radiation for photopic vision" and has a value of 683.002 lumens per watt. $L(\lambda)$ is the emission spectrum of the source with intensity measured in Watts per (metre cubed steradian) (W m^{-3} sr^{-1}).

$C(\lambda)$ is the *photopic relative luminous efficiency function* and it gives the ratio of the radiant flux at wavelength λ_m to that at wavelength λ, so that the two fluxes produce the same photopic luminous sensations under specified photometric conditions. Data for $C(\lambda)$ is taken from Wyszecki and Stiles' 'Color Science'[10] and can be modelled by Equation 3-18

$$C(\lambda) = a \times \exp\left[-\frac{1}{2}\left(\frac{\lambda - b}{c}\right)^2 \right] \qquad \textbf{Equation 3-18}$$

Parameters a, b and c are shown in Table 3-1 (overleaf).

54

Parameters	$\lambda \leq 555$ nm	$\lambda > 555$ nm
a	1.00	1.00
b	5.5163×10^{-7}	5.5880×10^{-7}
c	3.5761×10^{-8}	4.3678×10^{-8}

Table 3-1 Parameters for the photopic relative luminous efficiency function

To convert from Watts to Candelas per metre squared we use Equation 3-19, where A_P is the area of the PLED pixel

$$Int = \frac{K_m}{A_P \Omega} \int_0^\infty P(\lambda) C(\lambda) d\lambda \qquad \textbf{Equation 3-19}$$

Substituting for $P(\lambda)$ with Equation 3-16

$$Int = \frac{K_m V_D}{(R_T \times R_O) A_P \Omega} \int_0^\infty \frac{T(\lambda) C(\lambda)}{\lambda} \left(\int_0^\infty \frac{T(\lambda) Si(\lambda)}{\lambda} d\lambda \right)^{-1} d\lambda \qquad \textbf{Equation 3-20}$$

Again an Origin Spreadsheet embedded with LabTalk script is used for this calculation (Appendix A).

3.253 Candelas to Lumens

The conversion between Candelas per metre squared and Lumens per Watt is given in the Photonics Design and Application Handbook[8] and is reproduced in Equation 3-21

$$Int(lm) = Int(cd / m^2) \times A_P \times \pi \qquad \textbf{Equation 3-21}$$

3.26 Calculating Chromaticity Coordinates

Any interpretation of an EL spectrum using a chromatic description requires us to introduce a standard element representing the eye's filtration of light. To this end a set of colour matching functions representing a 'standard observer' are commonly used to assign a spectrum chromaticity coordinates.

3.261 X, Y, Z Coordinates

The 1931 CIE –(X,Y,Z) system is commonly used to assign spectra colour coordinates. The procedure uses three colour matching functions $\bar{x}_\lambda, \bar{y}_\lambda$ and $\bar{z}_\lambda$ which are shown in Figure 3-12
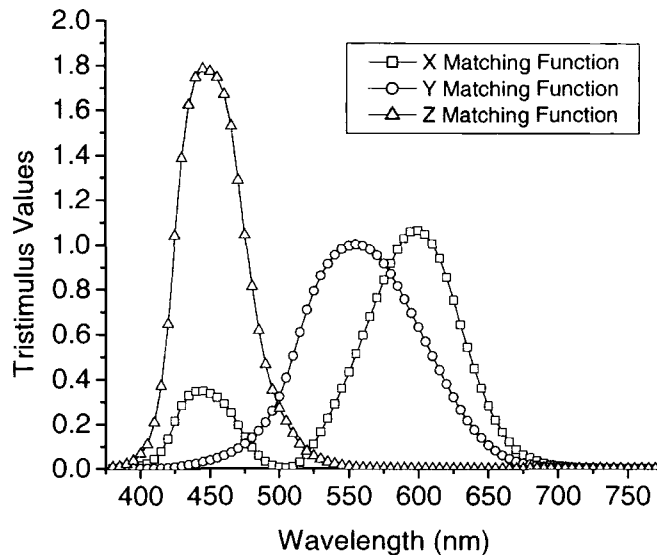
Figure 3-12 1931 CIE Colour Matching Functions

The data for these functions, along with the following method for calculating a spectrum's coordinates are taken from the literature[10].

First we calculate the values equated in Equations 3-22, known as the X,Y,Z primaries.

$$X = k\sum_\lambda T'(\lambda)\bar{x}_\lambda\Delta\lambda \approx k\int_\lambda T'(\lambda)\bar{x}_\lambda d\lambda$$

$$Y = k\sum_\lambda T'(\lambda)\bar{y}_\lambda\Delta\lambda \approx k\int_\lambda T'(\lambda)\bar{y}_\lambda d\lambda \qquad \textbf{Equation 3-22}$$

$$Z = k\sum_\lambda T'(\lambda)\bar{z}_\lambda\Delta\lambda \approx k\int_\lambda T'(\lambda)\bar{z}_\lambda d\lambda$$

T'(λ) is the measured spectrum divided by wavelength to produce intensity proportional to energy rather than number of photons. k is a constant and can be any

value, although it is commonly chosen so that the Y value will equal 100. If the measurement of T'(λ)Δλ is absolute in watts then k can be set equal to K_m, and the value of Y gives the luminous flux of the source, measured in lumens.

The x,y,z coordinates are normalised primaries such that x+y+z=1, hence z is often omitted in reports and references.

$$x = \frac{X}{(X+Y+Z)}, y = \frac{Y}{(X+Y+Z)}, z = \frac{Z}{(X+Y+Z)} \qquad \textbf{Equation 3-23}$$

Again this calculation is performed in a Labtalk scripted Origin File, code listed in Appendix B.

3.262 R,G,B Coordinates

Another commonly used coordinate set is the 1931 CIE-(R,G,B) system. This is sometimes used as the r,g,b system more intuitively expresses a spectrum in terms of the amount of red, blue and green contribution. Once again the relationship r+g+b=1 means that the final coordinates is often omitted. The coordinates can be justified as above using different colour matching functions but here we only present equations for converting between systems.

$$r = \frac{2.36461x - 0.89654y - 0.46807z}{1.85464x + 0.51546y + 0.62989z},$$

$$g = \frac{-0.51517x + 1.42641y + 0.08876z}{1.85464x + 0.51546y + 0.62989z}, \qquad \textbf{Equation 3-24}$$

$$b = \frac{0.00520x - 0.01441y + 1.00920z}{1.85464x + 0.51546y + 0.62989z}.$$

$$x = \frac{0.49000r + 0.31000g + 0.20000b}{0.66697r + 1.13240g + 1.20063b},$$

$$y = \frac{0.17697r + 0.81240g + 0.01063b}{0.66697r + 1.13240g + 1.20063b}, \qquad \textbf{Equation 3-25}$$

$$z = \frac{0.00000r + 0.01000g + 0.99000b}{0.66697r + 1.13240g + 1.20063b}$$

References

[1]   Adams, P. N.; Laughlin, P. J.; Monkman, A. P.; Kenwright, A. M. *Polymer* **1996**, *37*, 3411-3417.

[2]   Bruce, S. NIST Photodetector Measurements; NIST:, 2000.

[3]   Dailey, S. A Study of conjugated Polymers and their Applications in Light-Emitting Diodes. Doctorate, University of Durham, 1998.

[4]   Greenham, N. C.; Samuel, I. D. W.; Hayes, G. R.; Phillips, R. T.; Kessener, Y.; Moratti, S. C.; Holmes, A. B.; Friend, R. H. *Chemical Physics Letters* **1995**, *241*, 89-96.

[5]   Grell, M.; Knoll, W.; Lupo, D.; Meisel, A.; Miteva, T.; Neher, D.; Nothofer, H. G.; Scherf, U.; Yasuda, A. *Advanced Materials* **1999**, *11*, 671-+.

[6]   Gross, M.; Muller, D. C.; Nothofer, H. G.; Scherf, U.; Neher, D.; Brauchle, C.; Meerholz, K. *Nature* **2000**, *405*, 661-665.

[7]   Kiebooms, R.; Aleshin, A.; Hutchison, K.; Wudl, F.; Heeger, A. *Synthetic Metals* **1999**, *101*, 436-437.

[8]   Robert, D. A. The Photonics Design and Applications Handbook, 1993; pp p.H68-H71.

[9]   Ryer, A. Light Measurement Handbook; International Light, Inc.:, 1997; Vol. 1997.

[10]   Wyszecki, G.; Stiles, W. S. *Color Science*, 1st ed.; John Wiley & Sone Inc.:, 1967.

Chapter 4 Performance variation with architecture for various conjugated polymers

None of the work presented in this chapter has been published. It is submitted here in order to provide an introduction to PLED properties and to illustrate the wide variation in performance observable by varying charge injection layers.

4.1 SINGLE LAYER MEH-PPV LIGHT-EMITTING DIODES

poly[2-methoxy-5-(2'-ethylhexyloxy)-1, 4-phenylene vinylene] (MEH-PPV) was used as an active layer in PLEDs in to order to determine the effect on PLED performance characteristics of different types of architecture: those being cathode type, number of charge injection layers and so forth. Unless stated otherwise the polymer was dissolved in HPLC grade chlorobenzene (CB) solvent. The author found a lack of documented reports on spin casting thickness variation with solute concentration; hence the first results presented are some basic thickness measurements.

MEH-PPV concentration	Thickness on ITO after 1500rpm spin
6mg:1ml	55nm
7mg:1ml	75nm
8mg:1ml	115nm
9mg:1ml	170nm

Table 4-1 Variation of spin cast film thickness with solution concentration for MEH-PPV (CB) spun on ITO

Polymers in solution are highly non-Newtonian as the tabulated data shows. The thickness produced from spin coating is also highly dependent on the underlying layer, as will be seen when discussing bilayer systems. The thickness is expected to be dependent on the molecular weight of the polymer: for MEH-PPV 1.6×10^6.

4.11 Current-Field Characteristics for Single layer MEH-PPV PLEDs

Figure 4-1 shows the current–field characteristics for three different active layer thickness (55nm, 75nm and 155nm) sandwiched between an ITO anode and an Al cathode. The evaporation conditions are also varied using a polymer thickness of 75nm: with the venting gas either N_2 or air. As one would intuitively expect thicker films require higher field in order to drive a given current. The two thinner devices do not show the standard exponential dependence of current on voltage associated with barrier-limited injection. This is ascribed to the instability of these devices: thinner films inevitably result in inhomogenialities in field strengths due to thickness variations. This leads to pin hole formation and device breakdown.

The effect of bleeding the evaporator vacuum with N_2 appears to be a reduction in the conductivity of the film. This would suggest that the presence of O_2 is an important factor for interface formation at the metal:polymer boundary.
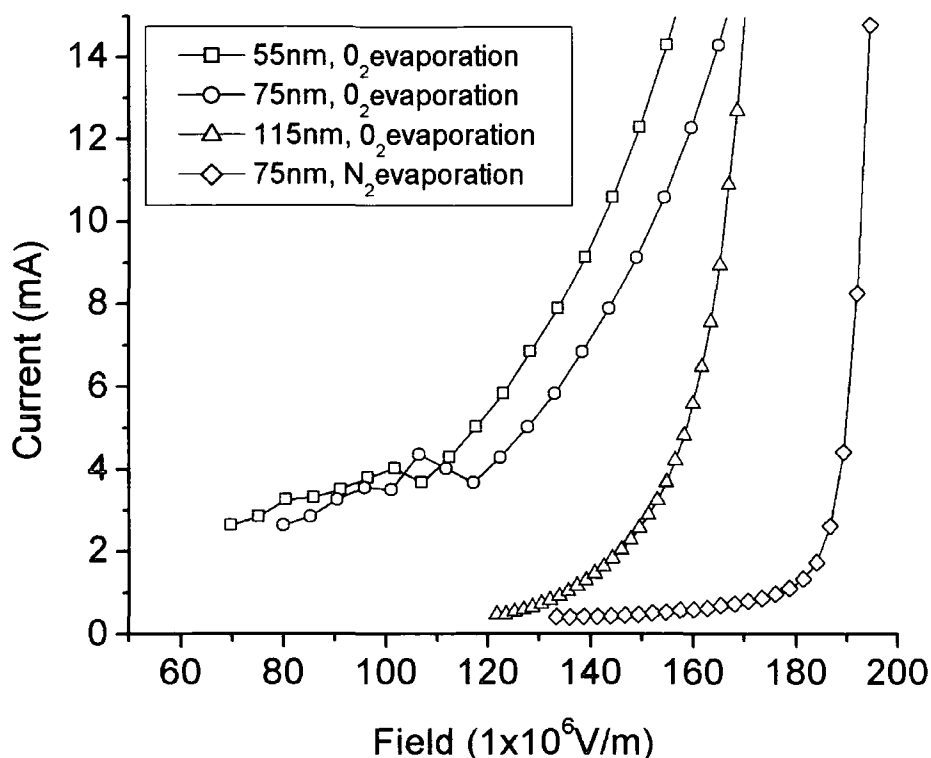
Figure 4-1 Current-Field Characteristics for a range of active layer thickness. PLED configuration was ITO/MEH-PPV/Al

4.12 Output Intensity Characteristics for Single layer
MEH-PPV PLEDs

Figure 4-2 shows the optical output intensity converted into Candelas per metre squared. The three PLEDs fabricated in an O_2 (air) evaporator follow the trend observed in the field-current plots, with output intensity inversely related to thickness of the active layer. This is expected for monolayer devices when one considers the relative mobility of electron- and hole-polarons. For thinner devices the difference has less distance over which to display itself, hence the recombination zone is closer to the middle of the device, away from any quenching interfaces. At the same time we have mentioned above that thinner devices are less stable due to thickness inhomogenialities.
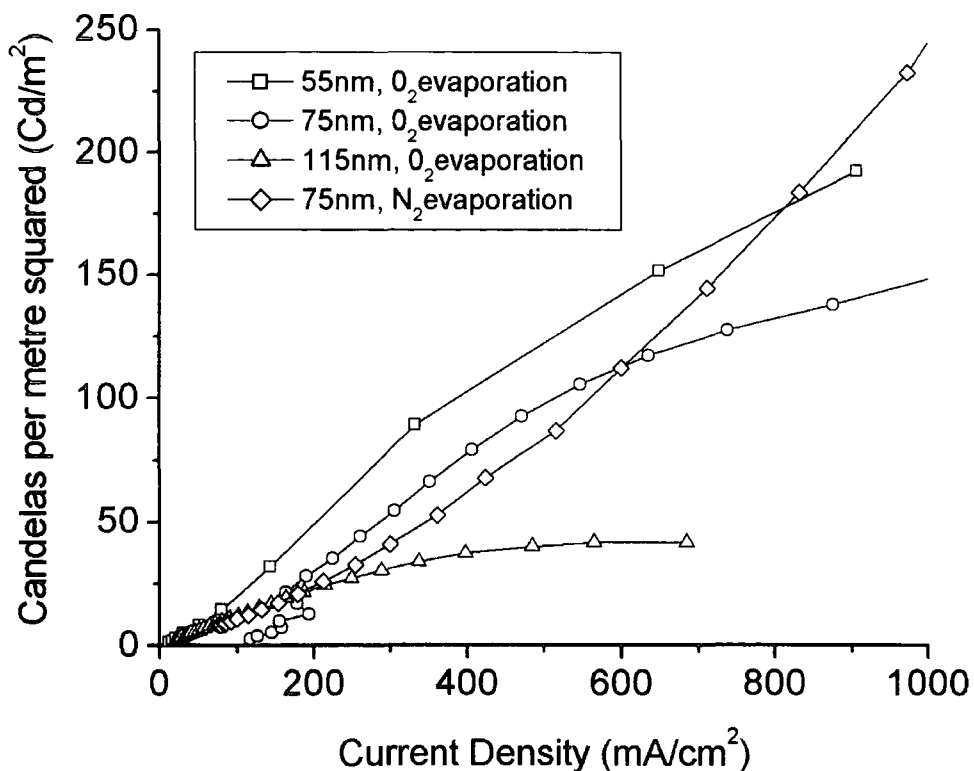
Figure 4-2 Light Output Characteristics for a range of active layer thickness. Devices tested were the same as for data shown in Figure 4-1

4.12 Electroluminescence Spectra for Single layer MEH-PPV PLEDs

Figure 4-3 shows that the electroluminescence profiles are all near identical for the monolayer systems under consideration. All show a broad, featureless peak at ~600nm (2.07eV). This is unique to monolayer devices: it shall be shown below that bilayer devices with MEH-PPV active layers typically exhibit double-peaked electroluminescence.
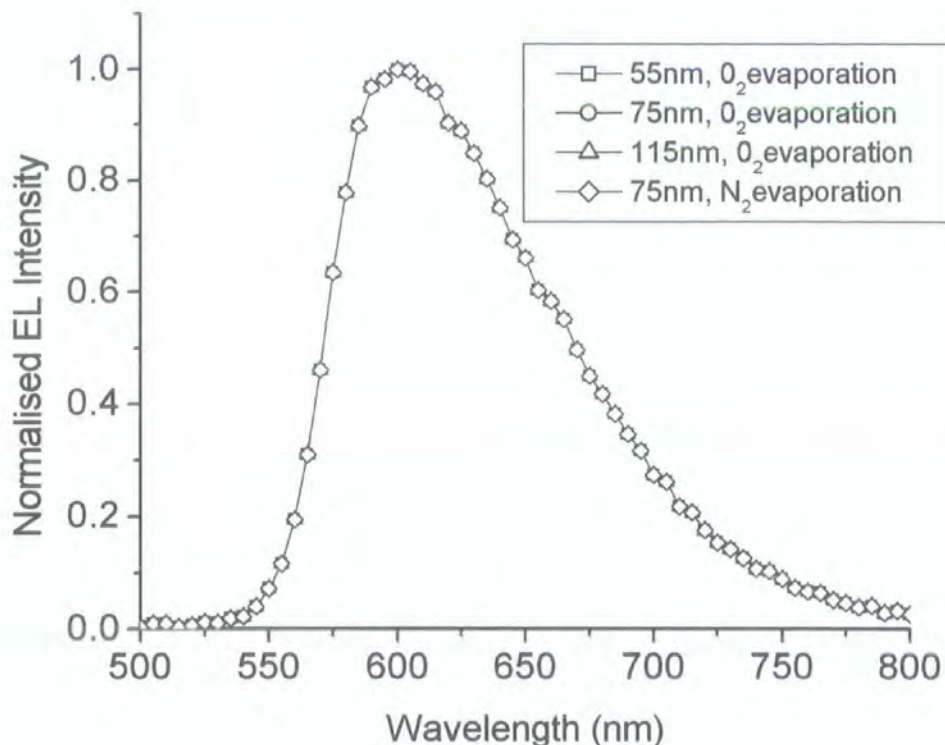
Figure 4-3 EL Spectra for all monolayer devices discussed in this section

4.12 Summary

Monolayer MEH-PPV PLEDs are generally unstable, and the high barrier for electron injection formed at the polymer:Al interface results in low device efficiencies, with measured EQEs of 0.00263%, 0.00193% and 0.00115% for 55nm, 75nm and 115nm thick active layers respectively. Evaporation with a N_2 venting gas results in a more stable device, but with a higher turn-on voltage. The EQE measured for a 75nm active layer capped in this way was 0.00497%, approximately triple the value for the 75nm thick device capped in the air-vented evaporator. This suggests that the presence of O_2 immediately after Al evaporation has an effect on the polymer:metal interface. The absence of any difference in the EL spectra suggests that the difference is not due to oxidation of the active layer.

4.2 BILAYER MEH-PPV LIGHT-EMITTING DIODES WITH ALUMINIUM

In order to compare the performance of MEH-PPV with and without hole-injecting polymer (HTL), poly(ethylenedioxythiophene) (PEDT) doped with polystyrenesulphonic acid (PSS) two PLEDs were constructed. The first was a monolayer with a thickness of 115nm (8mg/ml) sandwiched inbetween ITO and Al. The second had in addition a 30nm thick PEDT:PSS layer inbetween the ITO and MEH-PPV. Due to the difference between spin-coating MEH-PPV on PEDT:PSS compared to on ITO, a concentration of 7mg:1ml MEH-PPV:CB was used, which gave a thickness of 100nm for the active layer.
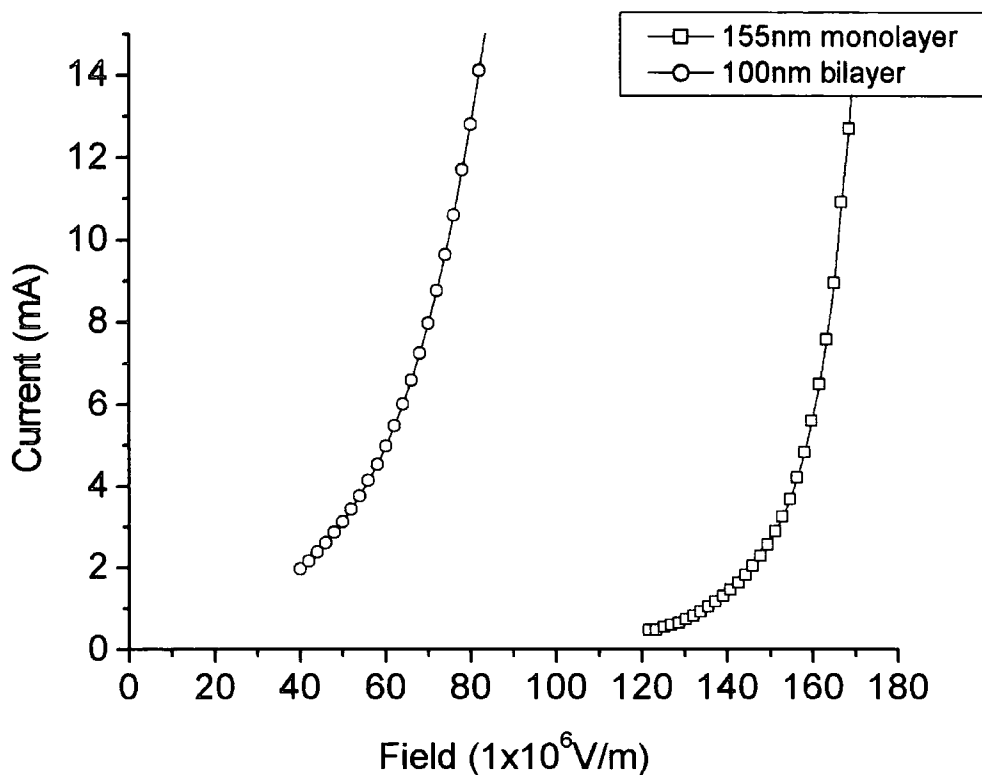
Figure 4-4 Current-Field comparison for 115nm thick monolayer and 100nm thick bilayer MEH-PPV

Figure 4-4 shows that the addition of the bilayer reduces the turn-on voltage and general drive requirements of the bilayer over the monolayer PLED, even allowing for the bilayer's thinner active layer. This shows how effective PEDT:PSS is as a heterolayer with MEH-PPV: improving electron injection by impeding holes from

entering the active layer and hence inducing electric field redistribution. This is consistent with results published elsewhere[7,1].
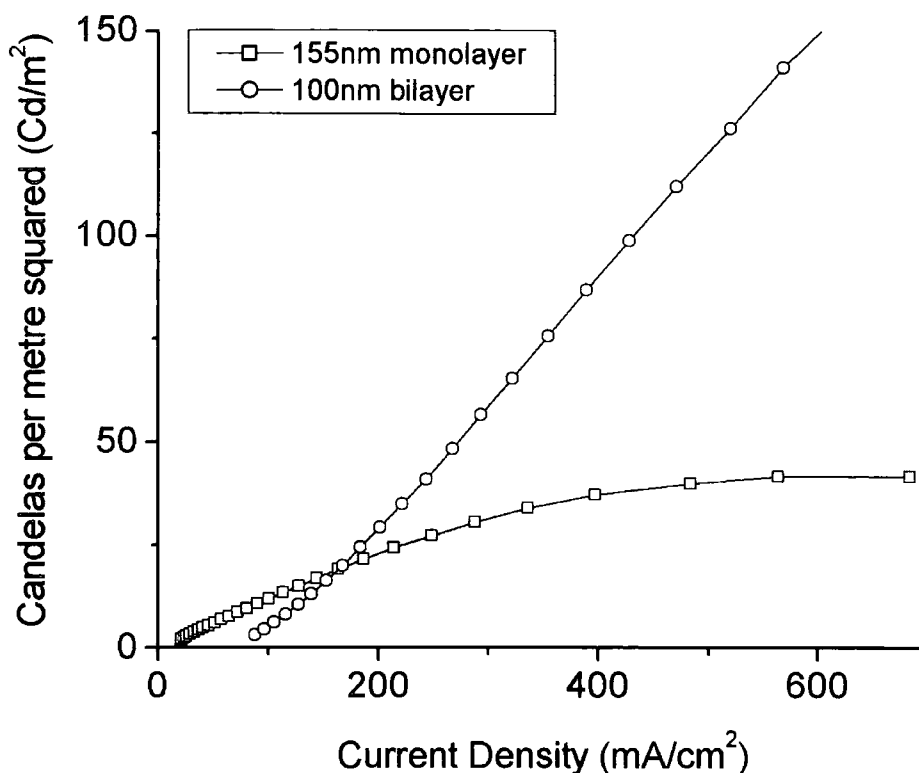
Figure 4-5 Output Intensity comparison for 115nm thick monolayer and 100nm thick bilayer MEH-PPV

Figure 4-5 shows that the output intensity has also been enhanced by the addition of a HTL, although only for current densities greater than ~150mA/cm^2. Whereas the monolayers' emission was too weak for the human eye to see, a peak emission of 300Cd/m^2 meant that the bilayer was nearly bright enough for applications.

There are important differences in the EL profiles of the two devices, shown in Figure 4-6. The bilayer has an extra peak at 630nm (1.97eV) not observed in the monolayer emission. Elsewhere this peak has been ascribed to excimer emission due to its absence in absorption spectra[10]. Whatever the excited species responsible for this peak, it is clear that PEDT:PSS is effective at injecting into its energy band(s) or level(s). In later sections of this report the manipulation of this peak through doping is investigated.
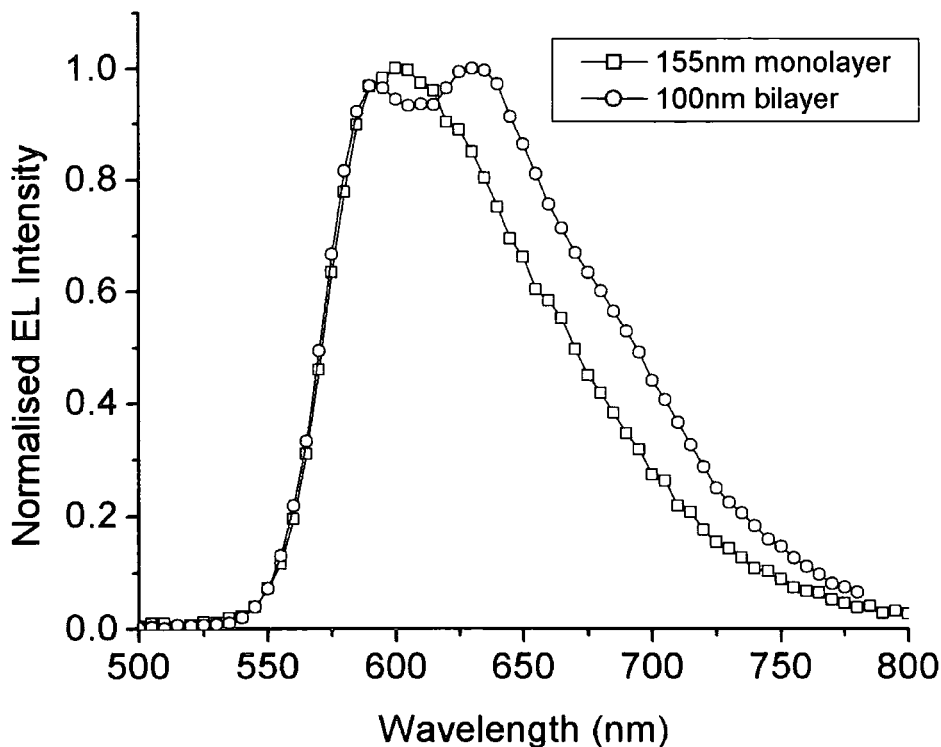
Figure 4-6 EL spectra for the monolayer and bilayer ITO/MEH-PPV/Al PLEDs

The EQE measured for the bilayer was 0.00244% (monolayer gave 0.0011%), nearly a twofold improvement over the monolayer. More significantly the reduction in voltage requirements resulted in a power efficiency peak of 0.0133 Lumens per Watt (L/W) compared to 0.00239 L/W for the monolayer. EQE and power plots are not included here as they were so erratic for the monolayer devices that a comparison would not be insightful.

In summary the addition of a HTL PEDT:PSS has been investigated. Use of the HTL reduces drive voltage requirements, complicates the emission profile through enhanced injection into excimer (or other) bands/levels, enhances EQE by a factor of 2 and PE by an order of magnitude.

4.3 BILAYER LAYER MEH-PPV LIGHT-EMITTING DIODES WITH CALCIUM

Calcium (Ca) is expected to improve electron injection and hence charge balancing by reducing the electron injection barrier. Ca has low workfunction of 3.0eV compared with 4.2eV for Al. Due to its reactivity Ca is usually capped with a protective Al layer to prolong device lifetime.

A range of MEH-PPV solution concentrations was studied in order to determine if the same trends were present as observed for monolayer MEH-PPV PLEDs: 5mg:1ml (which gave 50nm films when spun on PEDT:PSS), 6mg:1ml(90nm), 7mg:1ml(150nm), 8mg:1ml(200nm) and 9mg:1ml(240nm).

Below, Figure 4-7 depicts the current-field characteristics of the PLEDs fabricated.
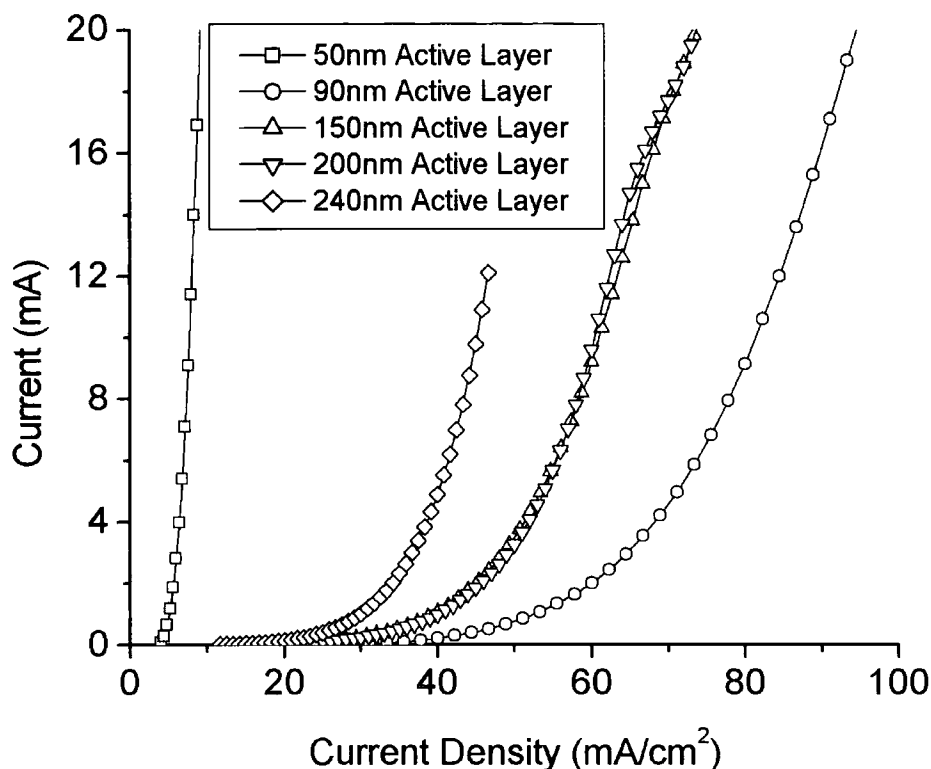
Figure 4-7 Current-Field Characteristics for the ITO/PEDT/MEH-PPV/Ca:Al bilayer PLEDs studied

Due to the large range in thickness studied there is no general trend to be observed. All devices have a current density that depends exponentially on applied field. These

PLEDs are stable to much higher current densities than either the Al monolayer or bilayer PLEDs.
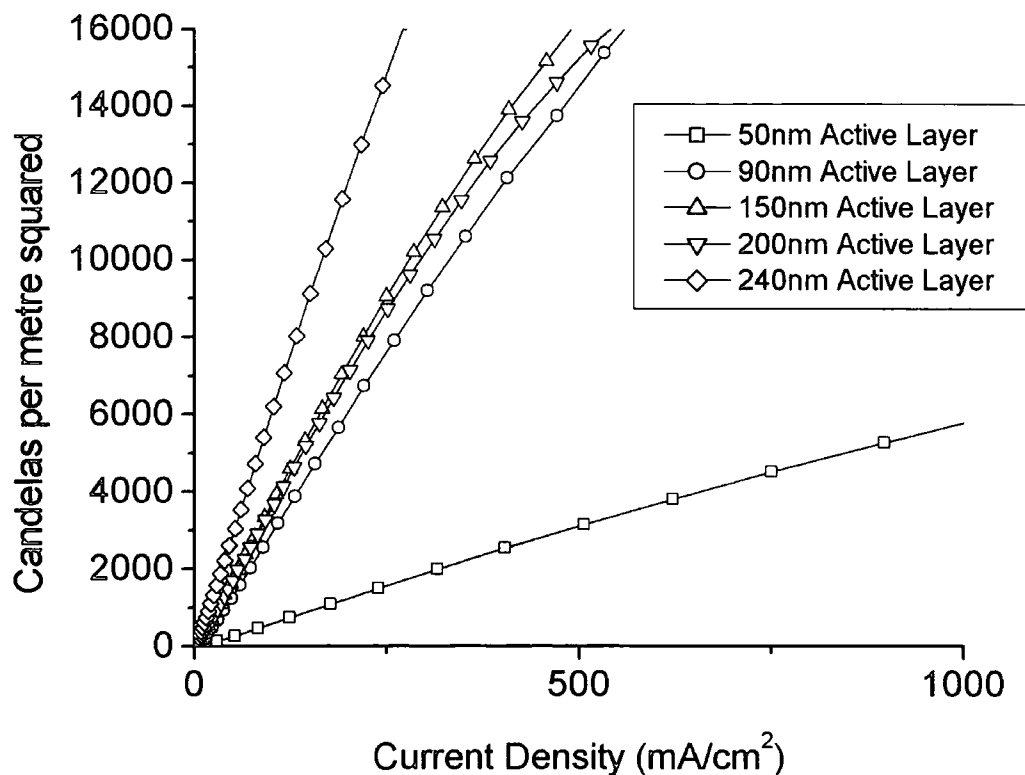
Figure 4-8 Output Intensity as a function of current density for the Ca bilayer PLEDs studied

Above, Figure 4-8 shows that the output intensity, the gradient of which is proportional to External Quantum Efficiency (EQE), increases for a given current density with active layer thickness. This is the opposite of the trend observed for monolayer PLEDs with Al cathodes, an effect of balancing hole and electron injection on the PLED.

The performance measurements of the PLEDs, EQE and PE, are shown in Figure 4-9 and Figure 4-10. They display remarkable similarity to theoretical predictions, as well as further enforcing the trend of improved performance with increased MEH-PPV thickness. They are included here to illustrate the typical performance expected of undoped active layer systems, which will become significant in later chapters when considering doped systems with markedly different performance trends.
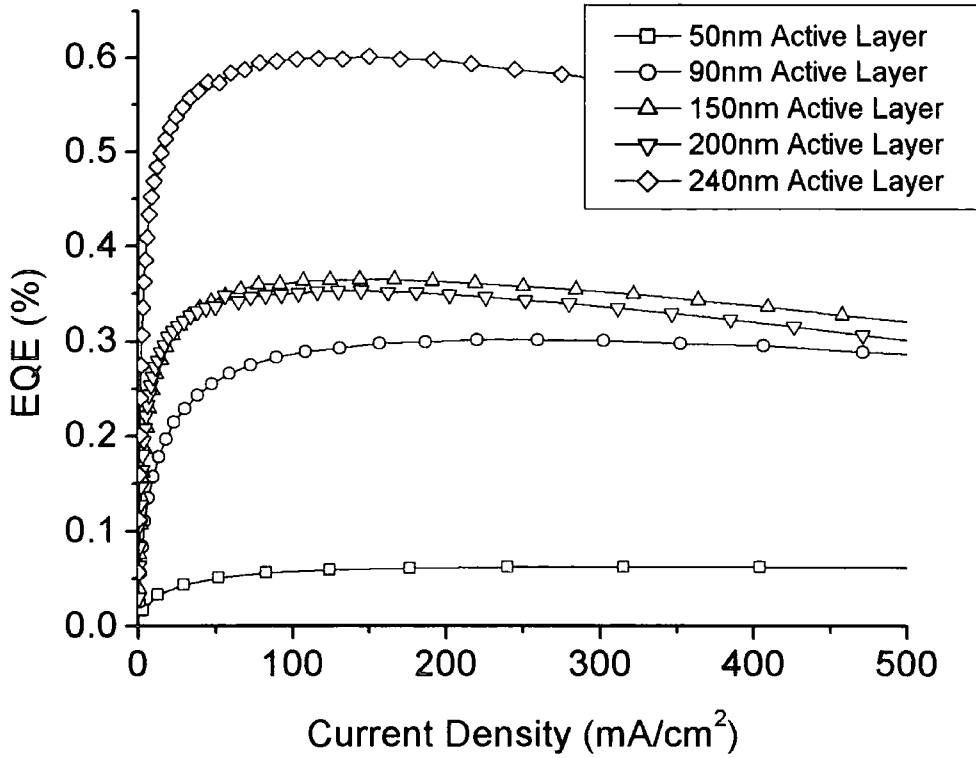
Figure 4-9 EQE as a function of current density for bilayer (ca) PLEDs
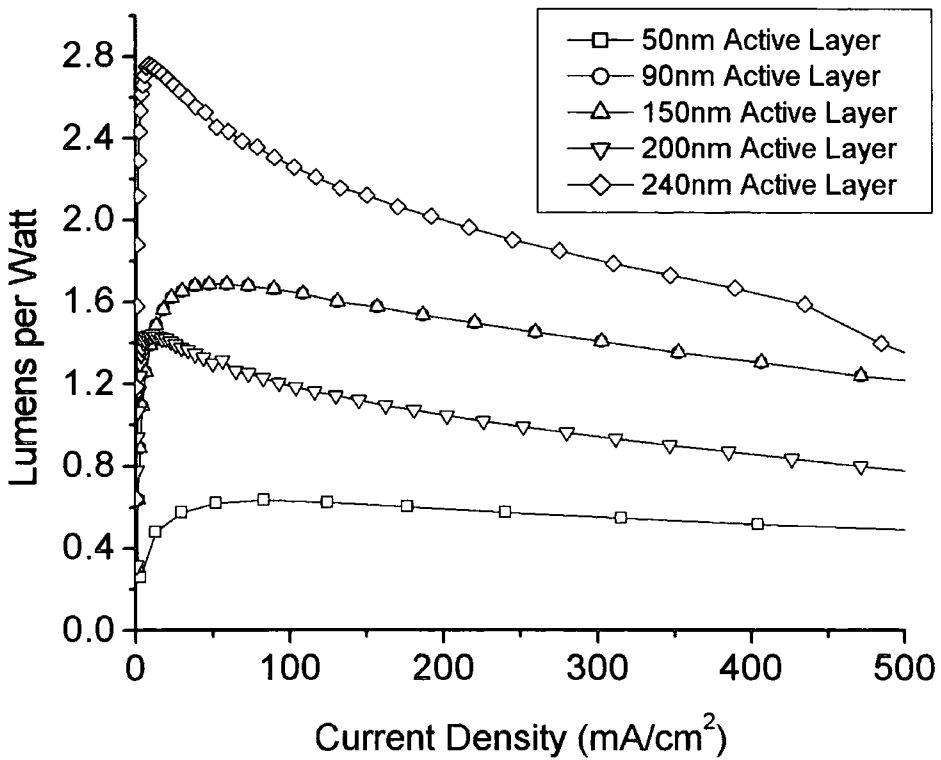
Figure 4-10 PE (in lumens per Watt) as a function of current density for the bilayer

(Ca) PLEDs

4.4 MEH-PPV PLEDS UNDER REVERSE BIAS

The problem with using a low workfunction metal like Calcium is that the metal tends to be highly reactive, as well as a good quencher of light. One idea of avoiding this is to run the PLED under effective reverse bias. Gold is known to produce an ohmic contact with MEH-PPV[13], and hence is highly suitable as a metal anode. Poly(p-pyridine) (PPY) has previously been used as an electron transporting layer (ETL) with PPV[9,3,2].

PPY was diluted in formic acid in various concentrations and spin coated on ITO to give layers 10nm(from 4mg:1ml), 20nm(5mg:1ml), 25nm(6mg:1ml), 30nm(7mg:1ml), 35nm(8mg:1ml) and 60nm(9mg:1ml) thick. A standard 6mg:1ml MEH-PPV solution was then spin cast on top of these yielding a 60nm thick active layer. The devices were completed by a 50nm thick Au anode evaporation.

All PLEDs showed a high turn-on voltage, which is ascribed to a high barrier for electron injection at the ITO:PPY interface. Below Table 4-2 summarises their performance.

PPY thickness (nm)	MEH-PPV thickness (nm)	Peak EQE (%)	Peak PE (L/W)	Turn-on Voltage	Thickness Ratio PPY:MEH-PPV
10	60	0.00724	0.01879	19	1/6
20	60	0.00720	0.01707	21	2/6
25	60	0.00391	0.01162	20	5/12
30	60	0.01097	0.02748	22	1/2
35	60	0.00800	0.02000	21	7/12
60	60	0.01587	0.04119	24	1

Table 4-2 Summary of Performance for the MEH-PPV PLEDs in upside-down configuration

There are no general trends to be observed. This device configuration was not pursued, as there was no alternative ETL available. Nevertheless these results suggest that the approach is viable if such a more suitable ETL can be found. The EQE values exceed those for monolayer and bilayer Al PLEDs under forward bias.

4.5 BILAYER PLEDS WITH OTHER ACTIVE LAYERS

4.51 Poly(9,9-bis(2-ethylhexyl)fluoren-2,7-diyl)

Poly(9,9-bis(2-ethylhexyl)fluoren-2,7-diyl) (PFO) was synthesised by Scherf and co-workers at the Max-Planck Institute[4,5]. When used in bilayer PLEDs with PEDT:PSS and Al it gives very weak emission corresponding to an EQE of ~10^{-4}%. However, the introduction of Ca gives an even more dramatic improvement than for MEH-PPV.

In similarity to MEH-PPV Ca bilayers performance is greater for thicker active layers. PFO is a blue emitter, its EL spectra has two dominant peaks (at 2.95eV and 2.76eV) as well as a broad, excimer hump (centred at 2.38eV).
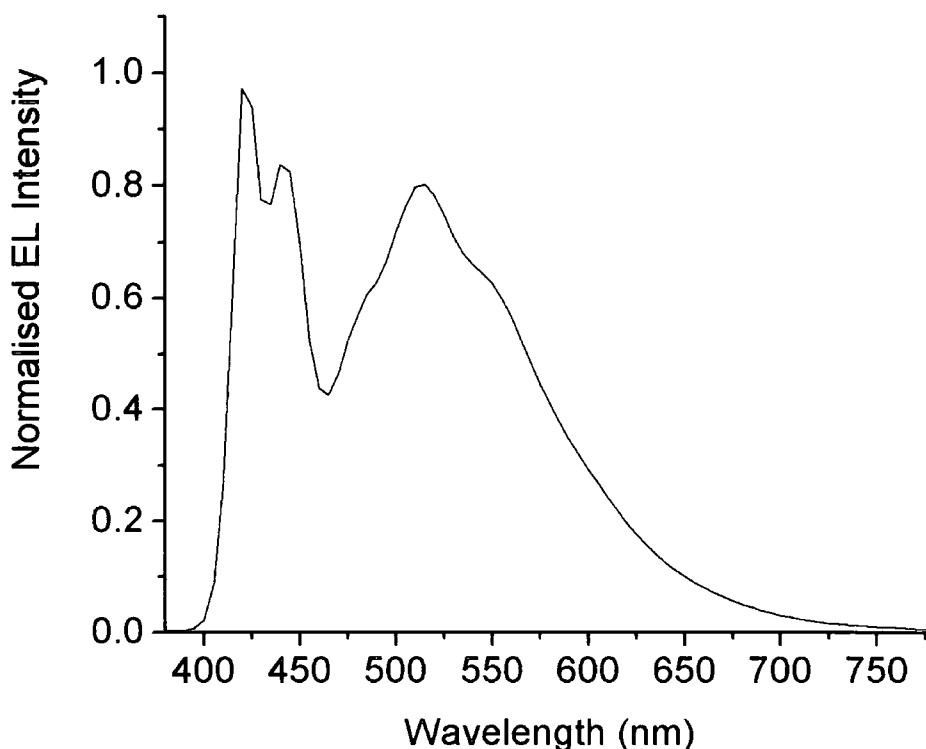
Figure 4-11 EL profile for PFO in a Ca Bilayer configuration

The spectrum was not observed to alter with active layer thickness. The EQEs were 0.398%, 0.391%, 0.318%, 0.1425 and 0.0375% for active layers 290nm(22.5mg:1ml), 190nm(20mg:1ml), 100nm(17.5mg:1ml), 60nm(15mg:1ml) and 75nm(12.5mg:1ml) respectively. EQE, PE and Output intensity dependence on current density followed trends similar to those observed for MEH-PPV in the same sandwich configuration. PFO was dissolved in CB for these measurements.

71

Unlike MEH-PPV, a significant variation in CIE color coordinates with operating voltage was observed which depended on the solvent used. For CB the spectrum was measured at 1V intervals. For simplicity Figure 4-12 only takes 5V intervals, but the trend of increasingly red-shifted emission was observed for all measurements.
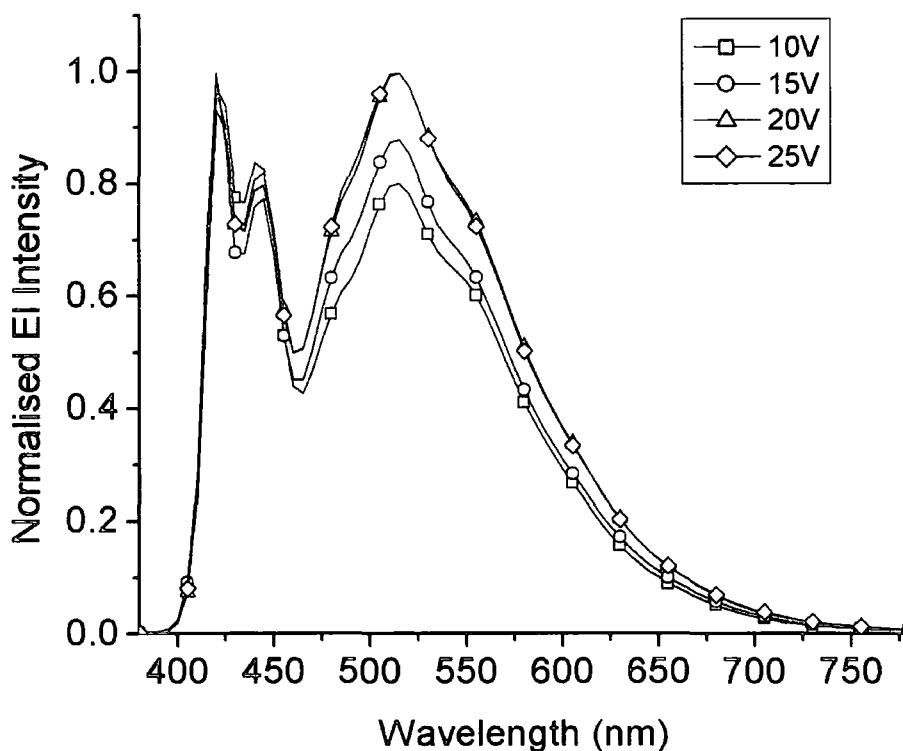
Figure 4-12 EL variation with operating voltage for PFO in ca bilayer configuration

From 10V to 25v a RGB shift of 0.077, 0.398 to 0.084, 0.432 was observed. The increased red component appears to be the excimer emission from Figure 4-12, suggesting that excimer formation is promoted under high fields.

Scherf and co-workers have also observed this behaviour. In the next section we look at their method for improving color stability.

4.511 Improving the color stability of PFO

In order to improve the color stability of PFO Scherf and co-workers have endcapped the PFO chains with amine groups. They claim that this stabilises emission by better balancing electron and hole mobility[4,5].
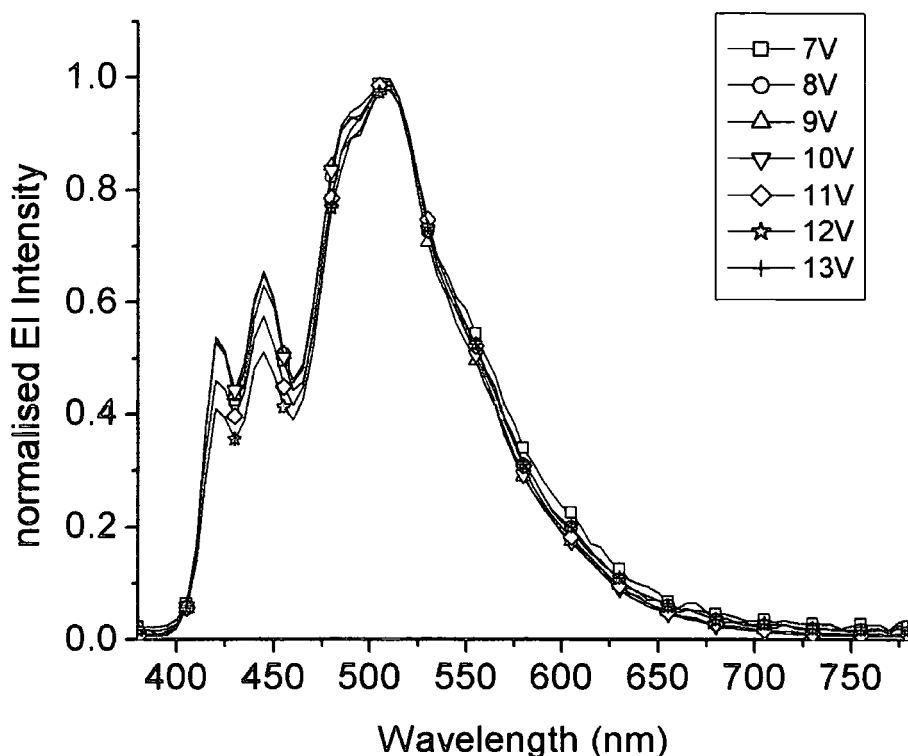
Figure 4-13 EL variation with operating voltage for PF2/6am4 in ca bilayer configuration using a CB solvent

Comparing Figure 4-13 with Figure 4-12 it is clear that endcapping has resulted in improved color stability over the PFO. α,ω-Bis[N,N-di(4-methylphenyl)aminophenyl]-poly(9,9-bis(2-ethylhexyl)fluoren-2,7-diyl) (PF2/6am4) shows a RGB variation of 0.000, 0.474 to 0.00, 0.518 from 7V to 13V. Significantly, the excimer peak at 2.38eV is now the dominant EL peak and the reason for the red0shift in emission relative to PFO. The measurements are taken at lower operating voltages than for PFO as PF2/6am4 has a lower turn-on voltage.

This shift can be reduced still further by using the less polar solvent toluene (Tol), as shown below in Figure 4-14. The excimer peak at 515nm is considerably suppressed relative to EL spectra for PLEDs fabricated via a CB solvent. This is attributed to different chain alignment in the solid state: the less polar Tol dissolves the chains completely and results in less aggregation. The emission is hence more blue

shifted than when using a CB solvent, with RGB coordinates varying between 0.100, 0.349 (7V) and 0.007, 0.297 (10V). In the region 7V-10V emission blue-shifts with increasing voltage. At higher operating voltages the emission will start to red-shift, with the re-emergence of the excimer peak. At 12V the RGB coordinates are 0.000, 0.373. However one would never need to drive the PLEDs beyond ~8V ($\cong$30,000Cd/m^2) commercially so this high voltage color instability is unimportant.

The addition of endcappers improves performance as well as color stability. For the two solvents used Tol gives the more efficient active layers, with EQEs of 1.19%, 0.98%, 0.87%, 0.22% and 0.54% for 150nm(22.5mg/ml), 100nm(20mg/ml), 80nm(17.5mg/ml), 35nm(15mg/ml) and 70nm(12.5mg/ml) thick active layers.
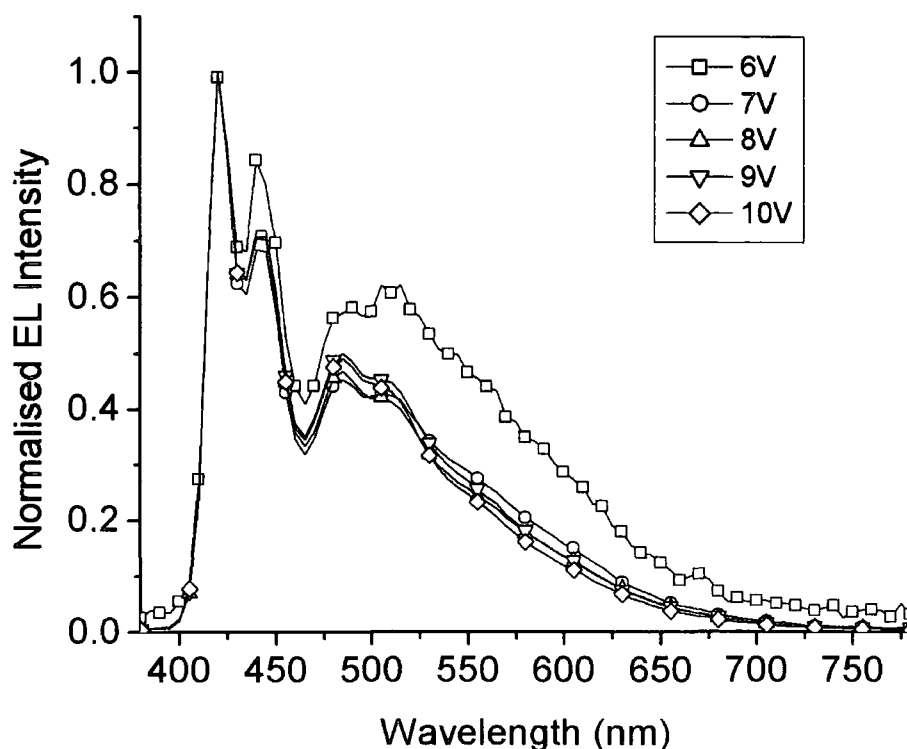
Figure 4-14 EL variation with operating voltage for PF2/6am4 in ca bilayer configuration using a Tol solvent

Power efficiencies are also higher with the 150nm thick active layers peaking at 10.63L/W. This is due to the reduction of turn-on voltages on balancing the electron and hole mobilities by endcapping.

4.52 Ladder-Type methyl-poly(p-phenylene)

Ladder-Type methyl-poly(p-phenylene) (MeL-PPP) has previously been used in triplet exciton studies due to its rigid backbone, resulting in no ring torsion[6,8,11,12,14]. It is used here for introductory purposes due to its green emission falling inbetween blue-emitting PFO and red-emitting MEH-PPV.

Mel-PPP was dissolved in Toluene. Having already seen a trend of increased performance with active layer thickness for two different polymers only a standard film thickness of 140nm(from 20mg/ml) was used. Shows the electroluminescence profile for Mel-PPP in the now standard ITO/PEDT:PSS/polymer/Ca:Al configuration.
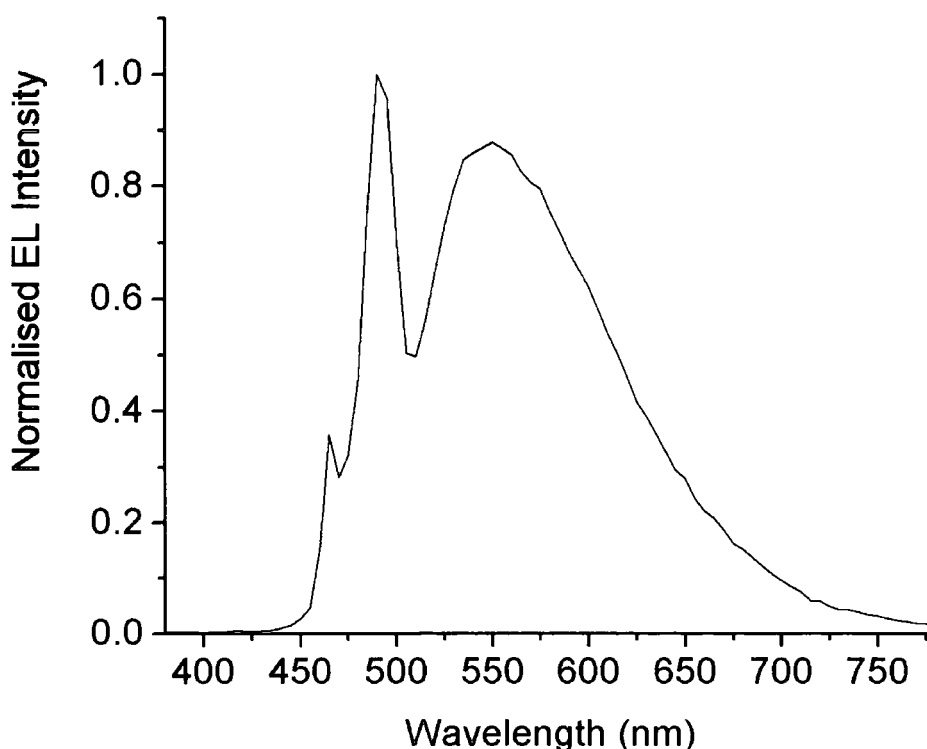
Figure 4-15 EL Spectrum of Mel-PPP in bilayer Ca configuration

The two singlet peaks at 465nm(2.67eV) and 490nm(2.53eV) are engulfed in the excimer hump peaked at 550nm(2.25eV). NMR analysis of the polymer at the Max Planck Institute for Polymer Research indicates that the synthesis route introduces carbonyl groups on the chain. These defects in the chain are significant to our understanding of excimer emission, as their presence appears to be related to the intensity of the 2.38eV EL peak.

The EQE of the device peaked at 0.149% for a current density of 23.4mA/cm^2. The PLED exhibited good color stability with CIE RGB coordinates of typically 0.33,

0.53. The EQE dependence on current density was once again similar to that seen in Figure 4-9, rising to a maximum at low current density and then gently falling away as current density is further increased.

4.53 csw-78

CSW-78 is named after its creator Dr.C.S.Wang and effectively a copolymer of phenylene- and pyridine-based monomers. Its emission spectrum is therefore expected to lie in between those of polyphenylene and polypyridine, on a wavelength scale.

It proved very unstable as an active layer and difficult to collect data for.
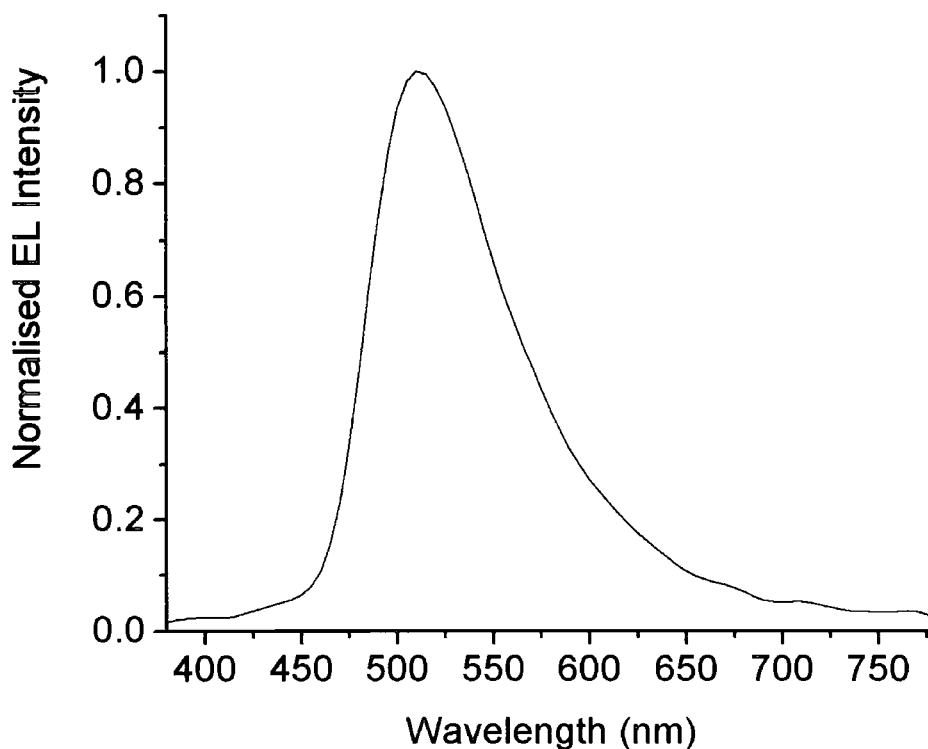
Figure 4-16 EL Spectrum for csw-78 in bilayer Ca configuration

The emission has one feature peaked at 510nm(2.43eV). This either means that excimer emission from the csw-78 is negligible, or that singlet emission and excimer emission overlap significantly leading the observer to only see one, broad feature.

The EQE value measured for a 70nm(30mg/ml in CB) thick active layer was 0.0022%, but the EQE dependence on current density was highly irregular due to instability.

Csw-78's pyridine groups can be protonated, which is expected to change its emission profile. Csw-78 was protonated with CSA in the ratio of one CSA molecule to every csw-78 chain. Protonated solution (consisting of 30mg csw-78, 30mg CSA to 1ml CB) was spun to produce active layers measuring 130nm thick. The protonated solution was notably more viscous than the pure solution. The emission of protonated csw-78 was red-shifted from that of pure csw-78 as shown in Figure 4-17.
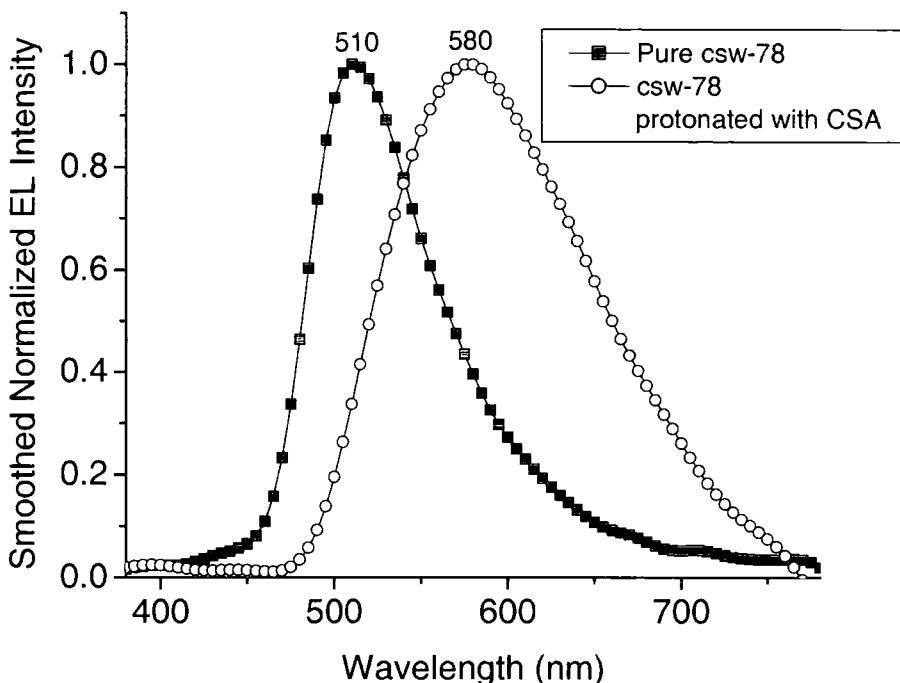
Figure 4-17 Shift in EL emission profile on protonating csw-78 with CSA

Protonation did not significantly improve the stability of the csw-78 in PLED configuration. The protonated PLED had a peak EQE of 0.0015%. However, as a method for EL tuning, protonation seems very applicable. Had we started with an efficient pure polymer we could vary the amount of protonation and hence shift in the EL spectra, leading to a range in emission. In this case one would not expect the red-shift to go significantly beyond the 70nm shift observed in Figure 4-17, as the doping ratio was calculated so as to have one CSA molecule for every available pyridine site.

4.6 SUMMARY

A range of polymers from red-emitting MEH-PPV to blue-emitting PF2/6am4 has been studied. Comparison on improving the architecture of MEH-PPV devices suggests that electron injection is the crucial factor on which device performance depends. This is further enforced by the improved performance on endcapping PFO with amide groups of high electron mobility.

The initial work with MeL-PPP brings into consideration an area of contention in conjugated polymer theory: whether the broad red-shifted (with respect to singlet emission) emission peaks in the EL spectra of all polymers studied above are due to excimers or not. The relationship of this emission to the presence of carbonyl groups on the polymer chains is contrary to understanding of excimer emission. The possibility of this emission being carbonyl linked is also supported by a relative increase in EL contribution from this peak as drive voltage is increased for PFO. The triplet exciton density is expected to increase with drive voltage/current density, and triplets have previously been shown to reduce oxygen to singlet oxygen. These free radicals could react with the polymer and form more carbonyl groups. This idea is embellished in Chapter 8.

Bilayer PLEDs are more efficient for thicker active layers due to a reduction in singlet intra-chain migration to the quenching cathode. It may also be that a recombination zone well insulated from atmospheric degradation by a thick active layer either side is less susceptible to oxygen diffusion. For practical reasons active layer thickness of ~100nm will be used in later chapters. There is generally no need for high undoped results as the rest of this report is interested in relative improvements due to doping and injection.

References

[1]   Campbell, A. J.; Bradley, D. D. C.; Antoniadis, H. *Journal of Applied Physics* **2001**, *89*, 3343-3351.

[2]   Dailey, S.; Halim, M.; Rebourt, E.; Horsburgh, L. E.; Samuel, I. D. W.; Monkman, A. P. *Journal of Physics-Condensed Matter* **1998**, *10*, 5171-5178.

[3]   Dailey, S.; Monkman, A. P.; Samuel, I. D. W. *Synthetic Metals* **1999**, *102*, 945-946.

[4]   Grell, M.; Knoll, W.; Lupo, D.; Meisel, A.; Miteva, T.; Neher, D.; Nothofer, H. G.; Scherf, U.; Yasuda, A. *Advanced Materials* **1999**, *11*, 671-+.

[5]   Gross, M.; Muller, D. C.; Nothofer, H. G.; Scherf, U.; Neher, D.; Brauchle, C.; Meerholz, K. *Nature* **2000**, *405*, 661-665.

[6]   Hertel, D.; Romanovskii, Y. V.; Schweitzer, B.; Scherf, U.; Bassler, H. *Synthetic Metals* **2001**, *116*, 139-143.

[7]   Kim, J. S.; Granstrom, M.; Friend, R. H.; Johansson, N.; Salaneck, W. R.; Daik, R.; Feast, W. J.; Cacialli, F. *Journal of Applied Physics* **1998**, *84*, 6859-6870.

[8]   Monkman, A. P.; Burrows, H. D.; Hamblett, I.; Navaratnam, S.; Scherf, U.; Schmitt, C. *Chemical Physics Letters* **2000**, *327*, 111-116.

[9]   Monkman, A. P.; Halim, M.; Dailey, S.; Samuel, I. D. W.; Horsburgh, L. E. *Synthetic Metals* **1999**, *101*, 208-209.

[10]   Nguyen, T. Q.; Martini, I. B.; Liu, J.; Schwartz, B. J. *Journal of Physical Chemistry B* **2000**, *104*, 237-255.

[11]   Schweitzer, B.; Arkhipov, V. I.; Scherf, U.; Bassler, H. *Chemical Physics Letters* **1999**, *313*, 57-62.

[12]   Schweitzer, B.; Bassler, H. *Synthetic Metals* **2000**, *109*, 1-6.

[13]   Scott, J. C.; Malliaras, G. G.; Chen, W. D.; Breach, J. C.; Salem, J. R.; Brock, P. J.; Sachs, S. B.; Chidsey, C. E. D. *Applied Physics Letters* **1999**, *74*, 1510-1512.

[14]   van der Horst, J. W.; Bobbert, P. A.; Michels, M. A. J.; Bassler, H. *Journal of Chemical Physics* **2001**, *114*, 6950-6957.

Chapter 5 Polyaniline as an alternative to poly(3,4-ethylenedioxythiophene) as a hole-transporting layer in polymer light-emitting diode

This work later submitted to Advance Materials under the title' A study of emeraldine base polyaniline (PANI) with various counter ions as an alternative to poly(3,4-ethylenedioxythiophene) (PEDT) as a hole-transporting layer in polymer light-emitting diodes'. Currently under consideration.

5.1 INTRODUCTION

PEDT:PSS is commonly used as a hole-transporting layer (HTL) in PLEDs. It has a reasonable conductivity and can be spun very thin, (30nm) which minimizes the increased requirements on the applied bias that an extra layer introduces. It also increases the workfunction to ~5.2eV[4] when used to treat ITO. When used in devices improved efficiency and reduced turn-on voltage relative to a monolayer device is observed.

In this work alternative HTLs to commercial PEDT:PSS are investigated: namely PANI:CSA, PANI:AMPSA and PANI:PSS in bilayer devices with poly(2-methoxy, 5-(2'ethyl-hexyloxy)-*p*-phenylene vinylene) MEH-PPV and later ladder-type methyl-poly(p-phenylene) Me-LPPP as active layers for all devices. By doing this we hope to gain more insight into what makes PEDT-PSS such a good HTL, by varying the mobility of the PANI counter ion used, the conductivity and the effective workfunction of the HTL (by varying the doping ratio) and the thickness of the HTL (by varying the percentage wt. of the PANI-counter ion in solvent). Previously other groups fabricated HTLs with PANI:CSA[10,9], and compared them with ITO hole injection suitability. Since then PEDT:PSS has been developed commercially whilst PANI in general has been commonly used for its conducting properties. We have already established PANI's excellent stability and applicability to conducting fibres[11,7,8,1]; if this long-term stability can be transferred to PLEDs then it is of obvious benefit to their development into commercial products.

A standard thickness of 150nm for MEH-PPV or 140nm for Me-LPPP was used for all PLEDs. The cathodes were of standard thickness as described in the experimental technique section.

5.11 Transparency of untreated and treated ITO

Figure 5-1 shows the transmission spectra of untreated ITO, ITO coated in PEDT:PSS (measuring 70nm thick) and ITO coated in PANI-CSA (measuring 70nm thick). All show high transmission over the visible range of the spectrum. There is a small drop in transmission for PANI-CSA over the high-energy end of the spectrum, making PANI more suitable as a HTL when used with green or red emitters, although PANI is still suitable for blue-green emitters given the typical film thickness of ~30nm used for HTLs. PANI:AMPSA and PANI:PSS transmission spectra were similar to PANI:CSA and hence only one is shown in Figure 5-1.
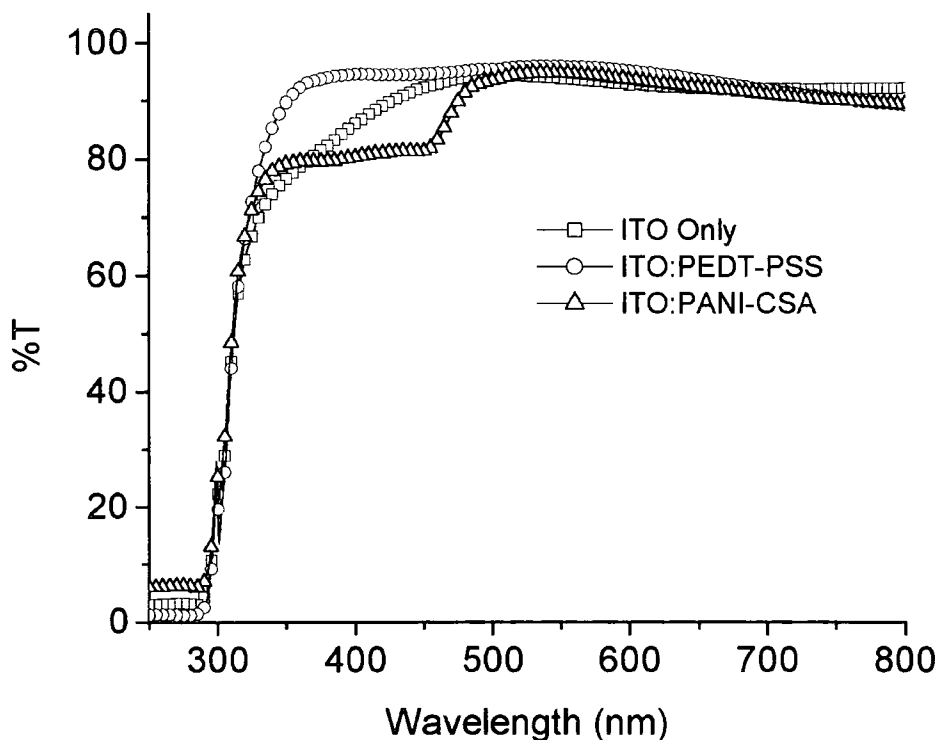
Figure 5-1 Transmission Spectra of untreated ITO, ITO:PEDT and ITO:PANI

5.12 Performance of Bilayer PLEDs with PANI:CSA(45%) compared to PEDT:PSS as a HTL

The performance of HTLs in MEH-PPV bilayer PLEDs for PANI doped 45% wt. with CSA were measured. Figure 5-2 and Figure 5-3 show the Field-Current and Current-EQE curves for 0.2%, 0.3%, 0.5% and 1% wt. PANI:CSA(45%) dissolved in m-cresol/1,1,1,3,3,3,-hexafluoro-2-ol (F_6IPA) HTLs. The performance is also summarised in Table 5-1, and compared with the standard PEDT:PSS HTL device. Repeat IV runs for a sample device are also taken, in this case the 1% wt. device, as a measure of the stability of the devices. This repeat measurement is shown in Figure 5-4 (and the PEDT:PSS standard in Figure 5-5).
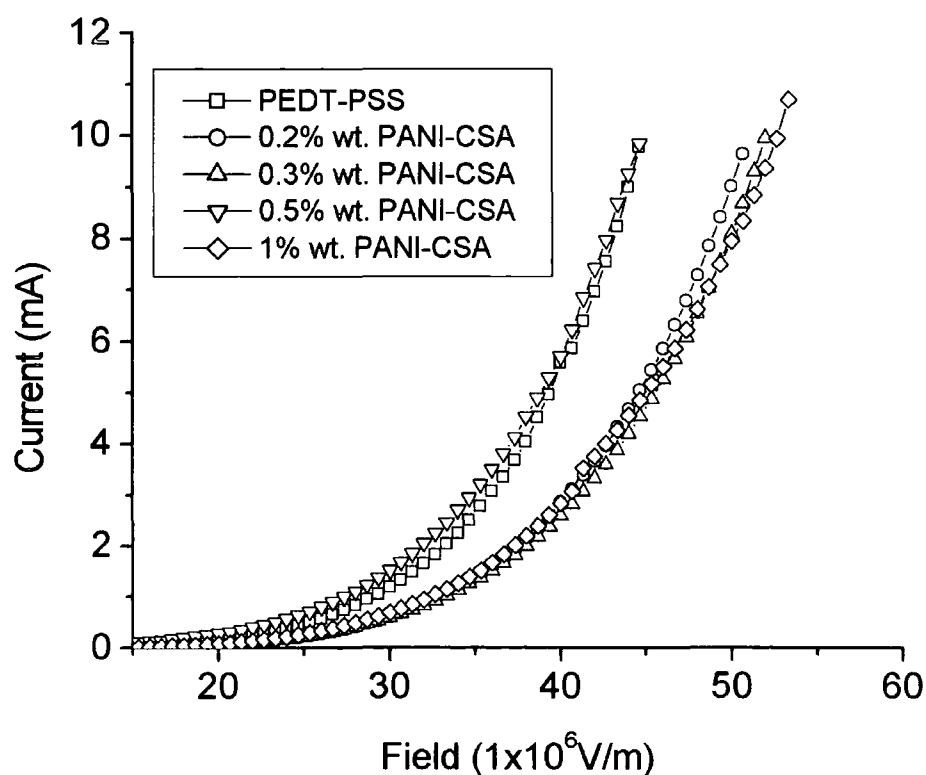
Figure 5-2 Field-Current Characteristics for the PANI-CSA (45% doped) HTL PLEDs tested

An increase in drive voltage with increasing percentage by weight PANI:CSA in solution was observed. This is attributed to the increase in HTL thickness, measured on a Tencor Alpha Step Stylus (Table 5-1). The Peak EQE values of all PANI-CSA(45%) devices are well below that of the PEDT:PSS device, although they do exhibit good 'initial run' stability. On repeating the I-V measurements a fall of the

gradient of the each curve was observed for repeat measurements, representing a drop in performance.
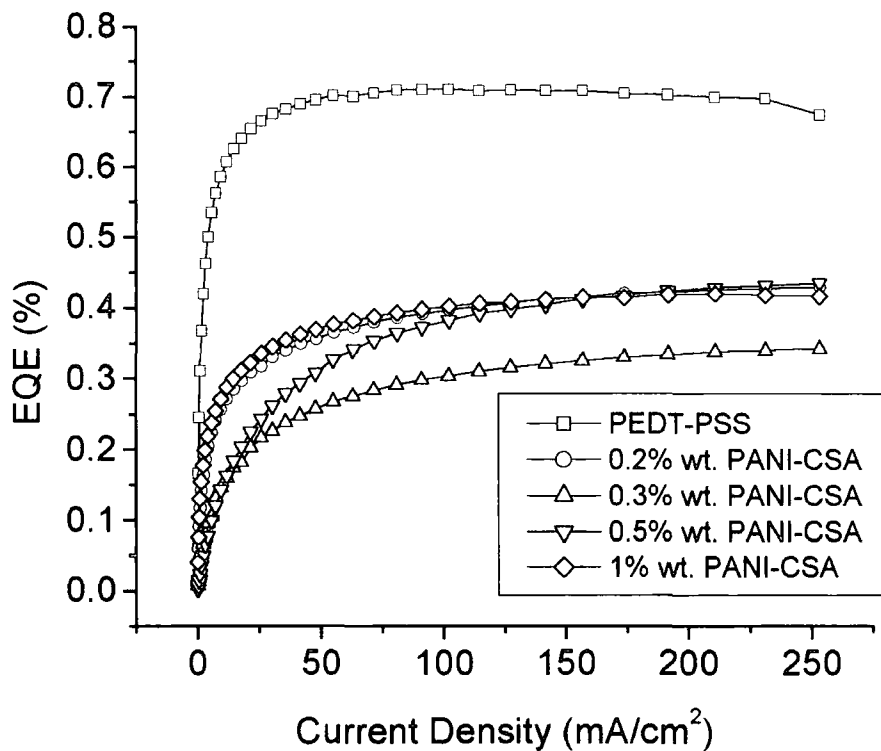
Figure 5-3 Current-EQE Curves for the PANI-CSA (45% doped) HTL PLEDs tested
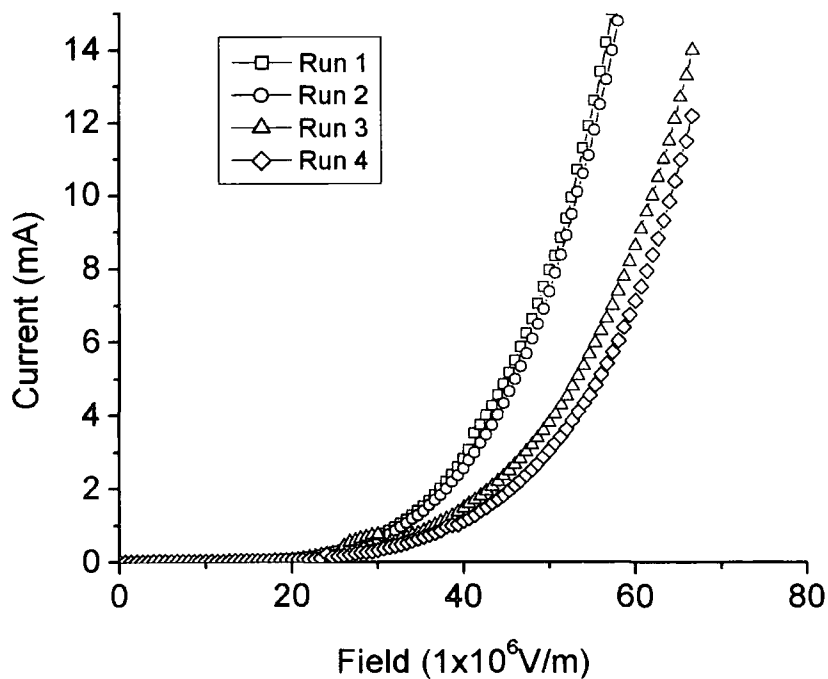
Figure 5-4 Variation of Field-Current characteristics with repeat runs for the 1%wt. PANI-CSA (45% doped) HTL PLED

84

Sharp turn-on 'spikes' in the Field-Current curves were observed, especially for the thicker HTLs. Below it is suggested that the fact that these peaks are more significant in the PANI:CSA(60%) HTL devices suggest that the CSA molecules are mobile enough to migrate in the active layer and once there damage its emission performance.
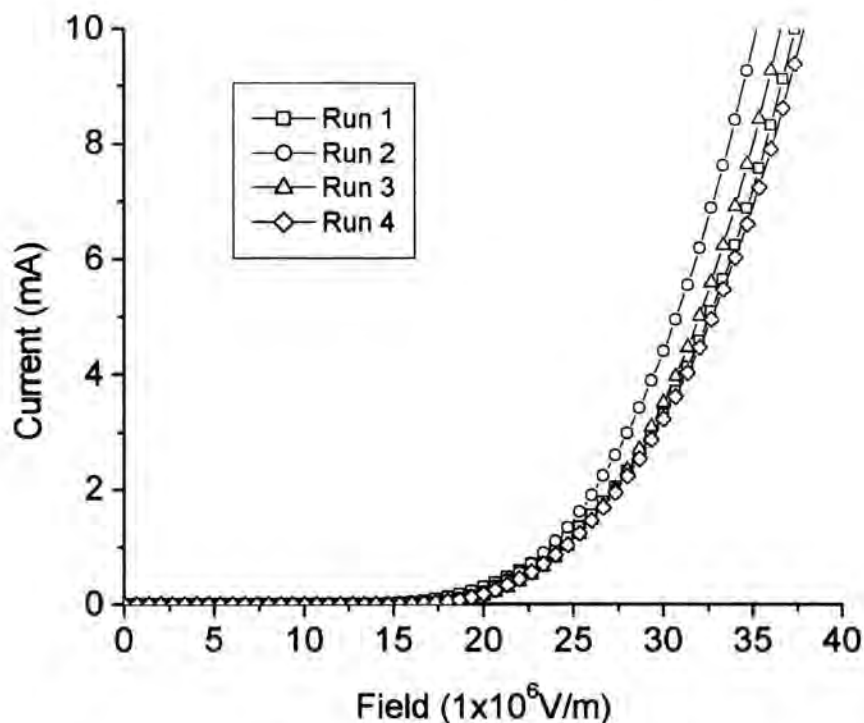
Figure 5-5 Variation of Field-Current characteristics with repeat runs for the 1%wt. PEDT-PSS HTL PLED

5.13 Performance of Bilayer PLEDs with PANI:CSA(60%) compared to PEDT:PSS as a HTL

Figure 5-6 and Figure 5-7 show the Field-Current and Current-EQE curves for 0.2%, 0.3%, 0.5% and 1% wt. PANI:CSA(60%) dissolved in m-cresol/F_6IPA HTLs. The performance is also summarised in Table 5-1, and compared with the standard PEDT-PSS HTL device. Again repeat IV runs for a sample device were taken, in this case the 1% wt. device, as a measure of the stability of the devices. This repeat measurement is shown in Figure 5-8 (compare with Figure 5-5).

Again an increase in drive voltage with increasing percentage by weight PANI:CSA in solution was observed. Peak EQE decreases with increasing HTL

thickness, again suggesting expected due to the increase in field requirements for a thicker PLED.
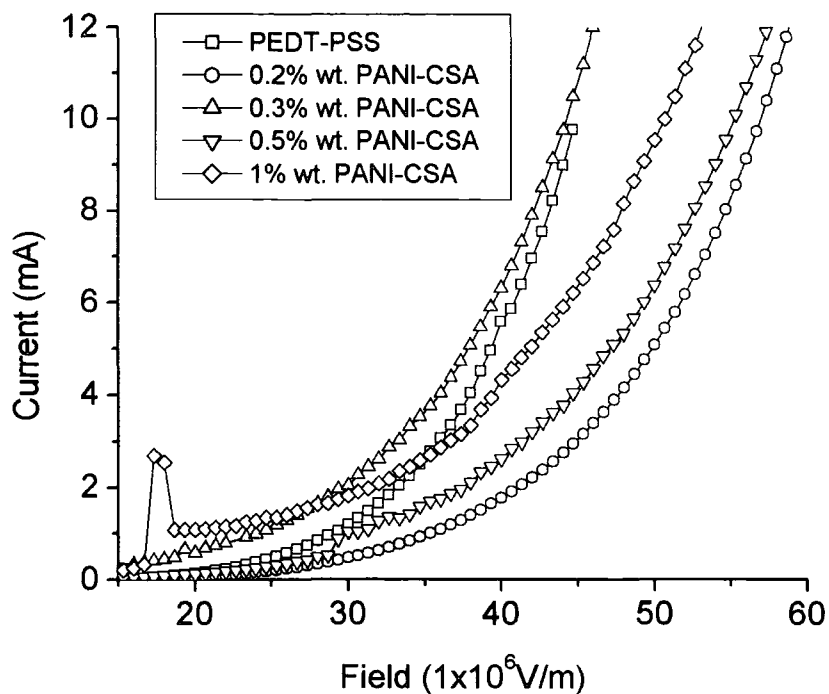
Figure 5-6 Field-Current Characteristics for the PANI-CSA (60% doped) HTL PLEDs tested
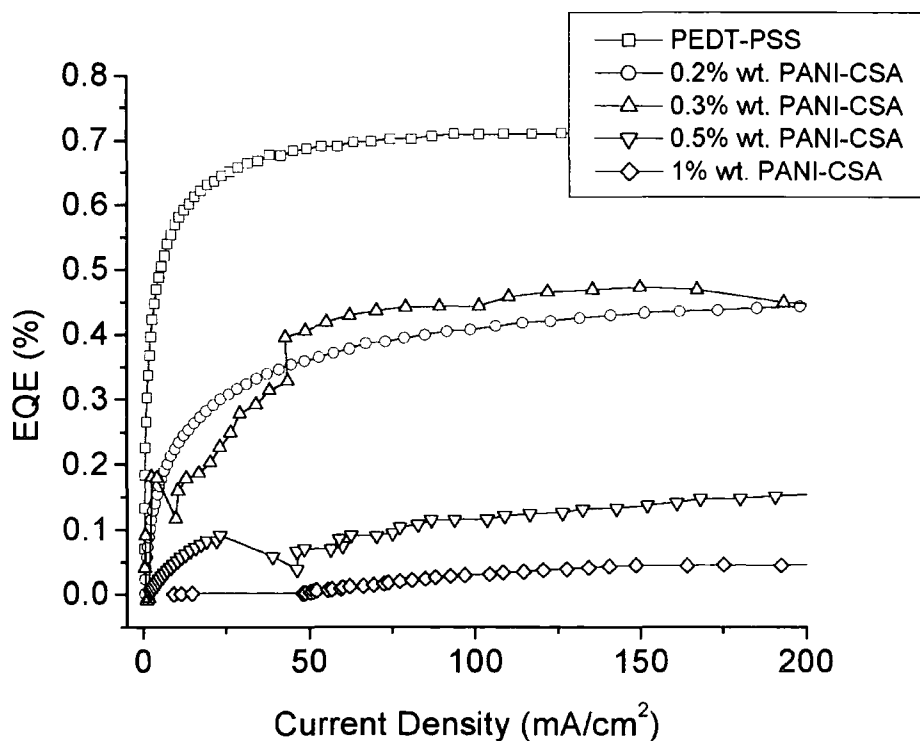
Figure 5-7 Current-EQE Characteristics for the PANI-CSA (60% doped) HTL PLEDs tested
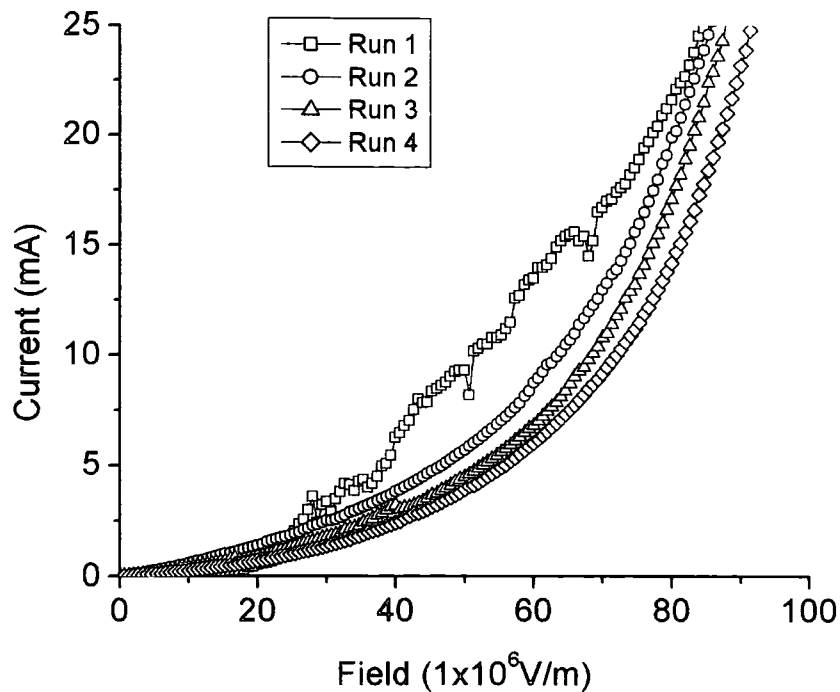
Figure 5-8 Variation of Field-Current characteristics with repeat runs for the 1%wt. PANI-CSA (60% doped) HTL PLED

Peak EQEs are generally better than the equivalent thickness PANI:CSA(45%) HTL device, although, but the stability is less good. For these devices the Field-Current curves are highly irregular, and on repeating the I-V measurements the gradient of curve falls for repeat measurements (Figure 5-8 contrasted with Figure 5-4). This increase in poor repeat performance and curve irregularities relative to the PANI:CSA(45%) HTL devices, coincident with the increase in HTL CSA content, is noted.

5.14 Performance of Bilayer PLEDs with PANI:AMPSA(60%) compared to PEDT:PSS as a HTL

Figure 5-9 and Figure 5-10 show the Field-Current and Current-EQE curves for 0.2%, 0.3%, 0.5% and 1% wt. PANI:AMPSA(60%) dissolved in dichloroacetic acid (DCA) HTLs. Cross referencing with Table 5-1 one observes a repetition of the general characteristics of PANI:CSA HTL devices: an increase in operating voltages with film thickness, and higher peak EQE values for devices with thinner HTL layers, suggesting that thinner layer offer better current balancing.

The repeat I-V runs for these devices are not displayed as there are hardly any changes in gradient, indicating the better stability of the larger counter-ion AMPSA relative to CSA. This is more evidence for the theory that in PANI:CSA devices the mobility of the relatively small CSA molecules is a problem for device stability. Unfortunately the peak EQE values of the PANI:AMPSA(60%) devices are lower than for either of the two PANI:CSA ratios used.
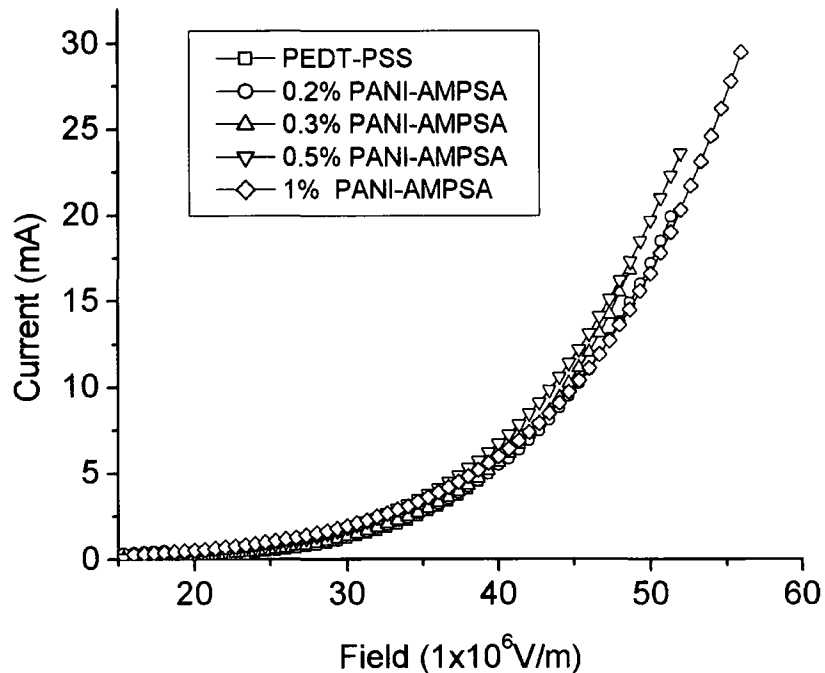
Figure 5-9 Field-Current characteristics for the PANI-AMPSA (60% doped) HTL PLEDs tested
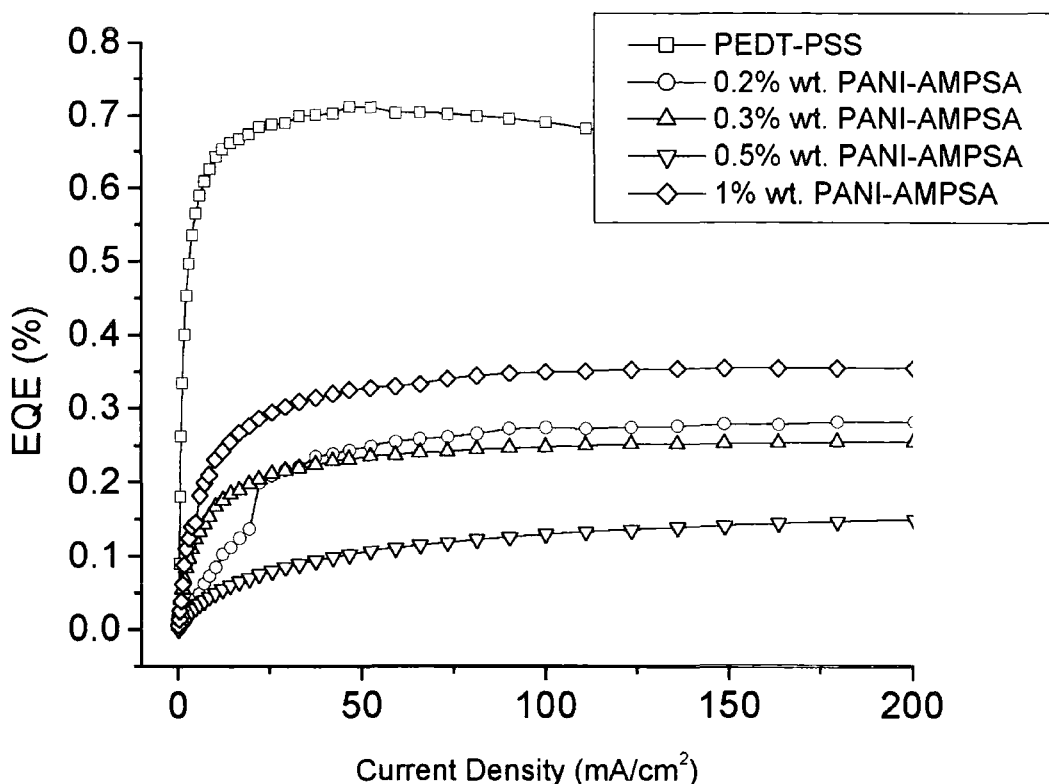
Figure 5-10 Current-EQE characteristics for the PANI-AMPSA (60% doped) HTL
PLEDs tested

5.15 Performance of Bilayer PLEDs with PANI:PSS(1:1, 1:2, 1:5 and 1:10 by weight) compared to PEDT-PSS as a HTL

From the experiments using PANI:CSA and PANI:AMPSA it is clear that one should employ a thin HTL film in order to minimise its detrimental effect on a PLED electric field requirements. For this reason we vary only the ratio of PANI to counter-ion PSS when investigating the HTL properties of such films. Figure 5-11 and Figure 5-12 show the Field-Current and Current-EQE curves for 1:1, 1:2, 1:5 and 1:10 by weight PSS doped PANI, all dissolved in N-methyl-2-pyrolidinone (NMP) to concentrations of 5%wt in order to produce 25nm films when spin cast. Conductivity is expected to fall with increasing counter-ion concentration, given similar effects already measured elsewhere for PANI:CSA and PANI:AMPSA films[1].

A general trend of increasing drive voltage with increasing counter-ion concentration is observed, with the 1:5 and 1:10 doped HTL effectively acting as

highly offset barriers (Figure 5-11). The performance variation with current is summarised in Table 5-1 and Figure 5-12.
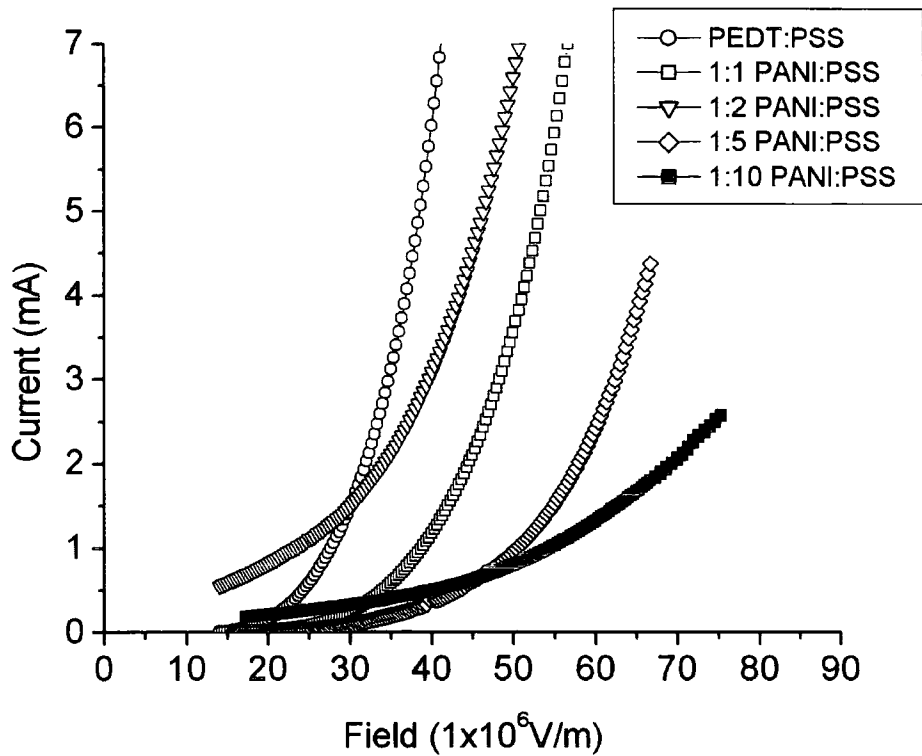
Figure 5-11 Field-Current characteristics for the PANI-PSS (1:1, 1:2, 1:5 and 1:10 doped) HTL PLEDs tested (with MEH-PPV active layer)
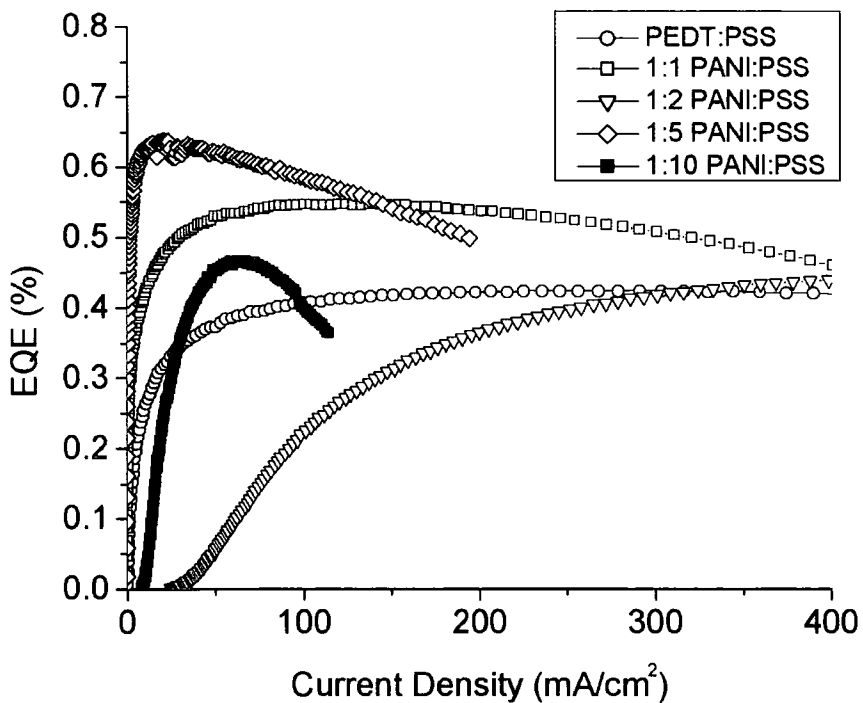
Figure 5-12 Current-EQE characteristics for the PANI-PSS (1:1, 1:2, 1:5 and 1:10 doped) HTL PLEDs tested (with MEH-PPV active layer)

Markedly different behaviour for the PANI:PSS relative to the other PANI:counter-ion combinations is observed. All PANI devices outperform the PEDT:PSS device in various current density regions. The 1:1 doped HTL appears most suitable for current densities below ~400mA/cm^2 (≡22,000Candelas per metre output intensity) and the 1:2 doped HTL for higher current densities. Again the 1:5 and 1:10 doped HTLs appear to act as high offset barriers and are unstable for realistic operating requirements.

Having found a combination of PANI:counter-ion that outperforms PEDT:PSS with MEH-PPV active layers, it is appropriate to investigate its performance with another polymer with a different conjugated backbone. Here Me-LPPP is used, and the results displayed in Table 5-1. Unfortunately all PANI:PSS HTL types performed poorly with Me-LPPP, resulting in unstable devices.

HTL		HTL Thickness (nm)	Abs EQE(%)	Relative to PEDT:PSS Standard
PEDT:PSS with MEH-PPV		30	0.4231	-
with MEL-PPP			0.1492	-
PANI:CSA (45%)	0.2% wt.	35	0.2573	0.6081
	0.3% wt.	35	0.2377	0.5618
	0.5% wt.	70	0.2623	0.6200
	1% wt.	140	0.2500	0.5909
PANI:CSA (60%)	0.2% wt.	35	0.2717	0.6422
	0.3% wt.	35	0.2813	0.6649
	0.5% wt.	70	0.1190	0.2812
	1% wt.	140	0.0800	0.1890
PANI:AMPSA (60%)	0.2% wt.	30	0.1709	0.4039
	0.3% wt.	30	0.2118	0.5005
	0.5% wt.	60	0.1522	0.3598
	1% wt.	180	0.1051	0.2483
PANI:PSS (1:1)	5.0% wt.	25	0.5468	1.2925
with Me-LPPP Active Layer			0.0190	0.1271
PANI:PSS (1:2)	5.0% wt.	25	0.4457	1.0534
with Me-LPPP Active Layer			0.0124	0.0833
PANI:PSS (1:5)	5.0% wt.	25	0.6362	1.5037
with Me-LPPP Active Layer			0.0168	0.1129
PANI:PSS (1:10)	5.0% wt.	25	0.4657	1.1007
with Me-LPPP Active Layer			0.0516	0.3459

Table 5-1 Performance Summary of all PLEDs studied in this work. Unless stated otherwise MEH-PPV was used as the active layer.

5.16 Discussion

PANI:PSS appears to be the best combination of PANI and counter-ion for use as a HTL with MEH-PPV active layers. Other more mobile counter-ions result in poorer stability and lower performance. Repeated use of devices indicates that in order of stability PANI:PSS and PANI:AMPSA are approximately the same, with PANI:CSA markedly worse. Although HTLs are in general required to provide an offset to hole injection, the results appear to suggest that there are limits to how low one can make the HTL conductivity before the performance starts to suffer.

The performance of the PANI:PSS films with MEH-PPV and MeL-PPP suggests that the workfunction of the PANI is higher than that of PEDT:PSS, and is above the level of the MeL-PPP HOMO: MeL-PPP having a larger bandgap than MEH-PPV (MEH-PPV peak electroluminescence (EL) at 590nm, MeL-PPP at 495nm). Me-LPPP shares its phenylene backbone with the family of polyfluorenes (PFOs) that have proved highly suitable to PLEDs recently[2,3,5,6], and so one expects the PANI:PSS HTLs to be unsuitable for PFOs.

PEDT:PSS has been developed from being inferior to highly superior over PANI:CSA as a HTL material in the past 7 years[9]. It has been shown that a PANI:CSA HTL results in poor stability, and this is attributed to the relatively high mobility counter-ion CSA. Even ignoring the poor stability the peak performance of PANI:CSA PLEDs is significantly below that of the PEDT:PSS PLED. These films will have reasonable conductivity and it is conceivable that the PANI:CSA films fail to balance electron and hole injection into the active layer.

PANI:AMPSA HTLs show improved stability but again the performance is below that of the PEDT:PSS. PANI:PSS HTLs however outperform PEDT:PSS HTLs. The large polymeric counter-ion may provide improved PANI chain alignment and device stability. Performance of PANI:PSS HTLs varies markedly with counter-ion concentration, with the more conductive films producing performance more suitable to PLED applications.

The PANI:PSS films are not suitable for use with higher bandgap active layers, as illustrated by the poor performance of Me-LPPP active layer PLEDs fabricated here. This is expected to be due to a higher workfunction for PANI:PSS relative to PEDT:PSS which for high bandgap active layers with lower HOMOs is detrimental to PLED performance.

In addition to use with low bandgap active layer polymers in PLEDs PANI:PSS be suitable to other applications. The expected thermal stability of PANI films due to the polymeric counter-ion may make it suitable for use in electric circuits that require heat treatment during their preparation. In order to determine this futher studies will measure the conductivity of PANI:PSS films before and after heat treatment.

References

[1]   Adams, P. N.; Pomfret, S. J.; Monkman, A. P. *Synthetic Metals* **1999**, *101*, 685-685.

[2]   Bernius, M. T.; Inbasekaran, M.; O'Brien, J.; Wu, W. S. *Advanced Materials* **2000**, *12*, 1737-1750.

[3]   Cadby, A. J.; Lane, P. A.; Mellor, H.; Martin, S. J.; Grell, M.; Giebeler, C.; Bradley, D. D. C.; Wohlgenannt, M.; An, C.; Vardeny, Z. V. *Physical Review B* **2000**, *62*, 15604-15609.

[4]   Campbell, A. J.; Bradley, D. D. C.; Antoniadis, H. *Journal of Applied Physics* **2001**, *89*, 3343-3351.

[5]   Gross, M.; Muller, D. C.; Nothofer, H. G.; Scherf, U.; Neher, D.; Brauchle, C.; Meerholz, K. *Nature* **2000**, *405*, 661-665.

[6]   Millard, I. S. *Synthetic Metals* **2000**, *111*, 119-123.

[7]   Pomfret, S. J.; Adams, P. N.; Comfort, N. P.; Monkman, A. P. *Polymer* **2000**, *41*, 2265-2269.

[8]   Vaschetto, M. E.; Monkman, A. P.; Springborg, M. *Theochem-Journal of Molecular Structure* **1999**, *468*, 181-191.

[9]   Yang, Y.; Heeger, A. J. *Applied Physics Letters* **1994**, *64*, 1245-1247.

[10]   Yang, Y.; Heeger, A. J. *Molecular Crystals and Liquid Crystals Science and Technology Section a-Molecular Crystals and Liquid Crystals* **1994**, *256*, 537-542.

[11]   Zhou, J.; Tzamalis, G.; Zaidi, N. A.; Comfort, N. P.; Monkman, A. P. *Journal of Applied Polymer Science* **2001**, *79*, 2503-2508.

Chapter 6 Effects of singlet and triplet energy transfer to molecular dopants in polymer light-emitting diodes and their usefulness in chromaticity tuning

This work later submitted to Applied Physics Letters. Now accepted for publication July 23rd 2001

6.1 *EFFECTS OF SINGLET AND TRIPLET ENERGY TRANSFER TO MOLECULAR DOPANTS IN POLYMER LIGHT-EMITTING DIODES AND THEIR USEFULNESS IN CHROMATICITY TUNING*

Rubrene has previously been used in molecular blending experiments with poly [2-methoxy-5-(2-ethylhexyloxy)-1,4-phenylene-vinylene] (MEH-PPV)[2] and in a polystyrene based dispersion with 8-hydroxyquinoline aluminium (Alq3)[3]; its fluorescence efficiency being 100%, although the phosphorescence yield is poor . Rubrene's singlet and triplet energies have been measured at 2.23eV and 1.14eV respectively[7], below that of the PF2/6am4 singlet energy at 2.79eV. The non-endcapped PFO triplet energy has been measured at 2.3eV[5]).
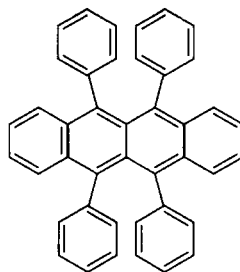
Figure 6-1 Molecular Structure of Rubrene (Rb)

Here rubrene was added to standard PF2/6am4 solutions (20mg/ml Tol) to produce doped active layers when spin-cast. The standard bilayer configuration was used. A range of dopant concentrations was used: 1%wt, 2%wt, 3%wt and 4%wt. Each PLED was then characterised.

6.1 Results

Figure 6-2 and Figure 6-3 respectively show the Field-Current and brightness output curves of the devices tested. In similarity with other polyfluorene/dopant systems[9,10] an increase in turn-on voltage with dopant concentration was observed, with the voltage required for a current of 1×10^{-5}A in the device at 4, 5, 7.1, 10.1 and 10.2V for the undoped, 1%, 2%, 3% and 4% doped devices respectively. Note that the IV characteristics of the 3% and 4% doped devices are similar, yet the output from the 4% device was poor, indeed too unstable to measure.
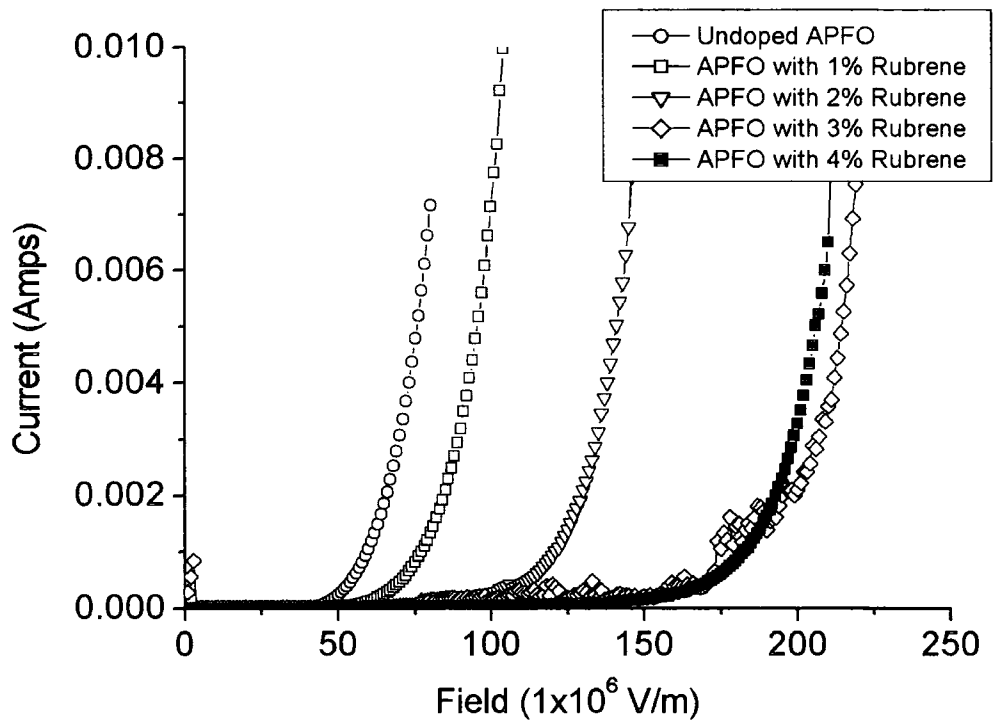
Figure 6-2 Field-Current Cruves for the PF2/6am4:Rb devices tested
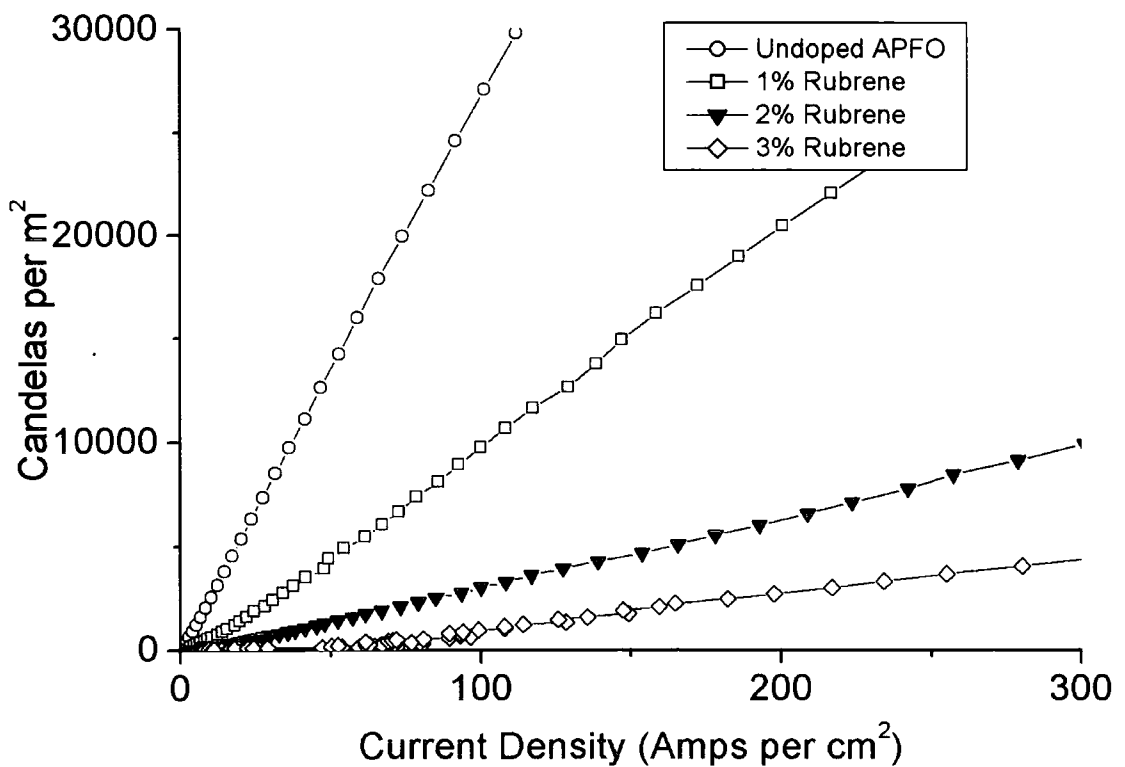
Figure 6-3 Power Output Curves for the PF2/6am4:Rb devices tested

The EL spectra are increasingly red-shifted with increasing dopant concentration, as shown in Figure 6-4.
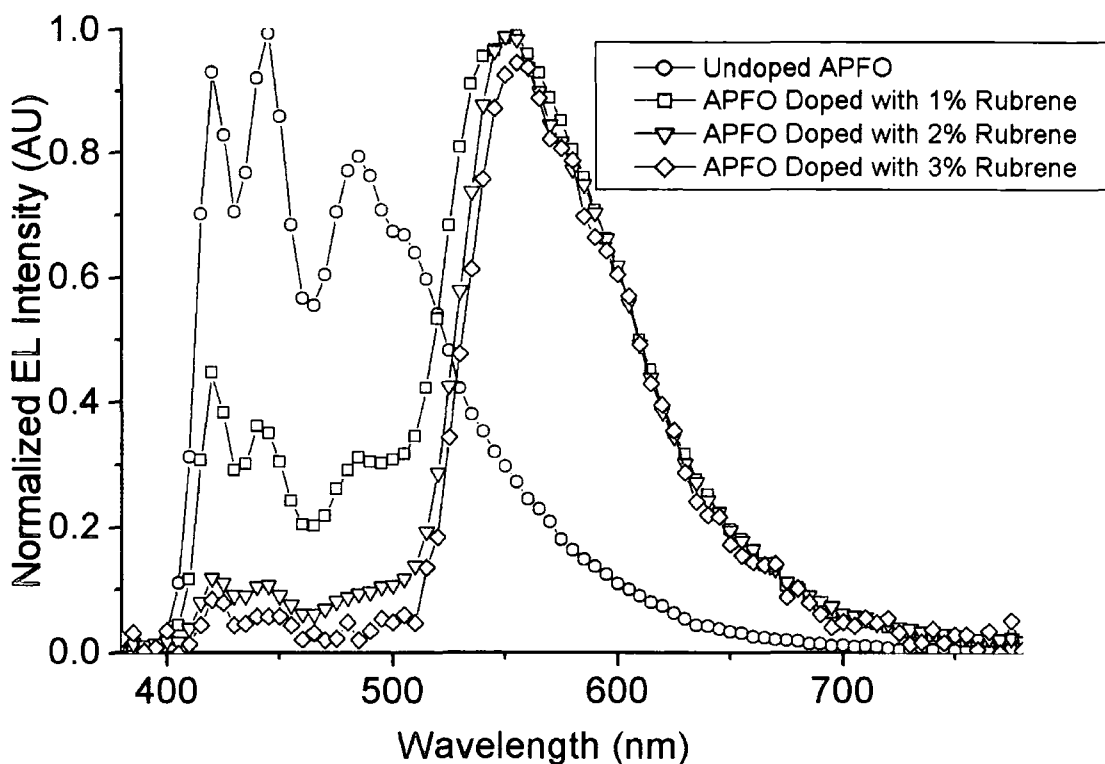
Figure 6-4 Representative EL Spectra for each device (Undoped at 6V, 1% doped at 8V, 2% at 12V, 3% at 19V)

From this plot is appears that the peaks associated with the PF2/6am4 in its undoped state become increasingly suppressed as dopant concentration is increased until at 3% there are only trace peaks. Table 1 presents a summary of the CIE coordinates for each device under a range of operating voltages. A small variation in CIE coordinates with operating voltage for the undoped PF2/6am4 was observed, in agreement with previous studies[1]. This has been ascribed to voltage dependant aggregate states, which the endcapper units suppress considerably relative to the original polymer. These small variations can be seen in the doped samples although they are increasingly negligible at higher dopant concentrations.

The efficiencies of the doped devices are lower than the undoped device, as shown in table 1. However with X, Y coordinates of 0.33, 0.42 the 1% wt. rubrene doped device offers good white emission at a high efficiency of 1.04742% at 9.0V. This efficiency compares well to other white-emitting polymeric devices and is a result

Device	Peak EQE (Voltage at peak)	Spectral Output (in CIE Coordinates)					
		Voltage	R	G	B	X	Y
Undoped PF2/6am4	1.30141% (6.0V)	6	0.1	0.349	0.552	0.238	0.273
		7	0.049	0.31	0.642	0.215	0.232
		8	0.027	0.296	0.677	0.206	0.217
		9	0.019	0.305	0.676	0.204	0.221
		10	0.007	0.297	0.696	0.199	0.213
1% Rubrene Doped PF2/6am4	1.04742% (9.0V)	7	0.34006	0.46627	0.19367	0.35439	0.44669
		8	0.32143	0.45657	0.222	0.34414	0.43105
		9	0.30807	0.44938	0.24255	0.3369	0.41984
		10	0.30496	0.44236	0.25268	0.33452	0.41285
2% Rubrene Doped PF2/6am4	0.5059% (15.0V)	10	0.4598	0.48145	0.05874	0.4188	0.51293
		11	0.44548	0.48573	0.06879	0.41153	0.51
		12	0.43658	0.47986	0.08356	0.40581	0.50057
		13	0.43569	0.4816	0.08271	0.40558	0.50172
		14	0.4347	0.47962	0.08568	0.40475	0.49949
		15	0.43073	0.47195	0.09732	0.40149	0.49083
3% Rubrene Doped PF2/6am4	0.29572% (22.4V)	17	0.4708	0.45388	0.07531	0.42079	0.49308
		18	0.4815	0.47228	0.04622	0.42963	0.51498
		19	0.4815	0.47228	0.04622	0.42963	0.51498
		20	0.48291	0.47176	0.04533	0.43035	0.51519
		21	0.48351	0.47364	0.04285	0.43099	0.51721

Table 6-1 External Quantum Efficiency & Variation in Color Coordinates with Operating Voltage for each device

of emission from both host and dopant sites, and by fine tuning the concentration of dopant the color coordinates could be refined further. EQE values do not take into account the operating voltage and so these results would appear to suggest

either that the transfer process is intrinsically inefficient or singlet annihilation increases upon transfer to the dopant. Were there Dexter transfer of PF2/6am4 triplet excitons one would expect the EQE of the doped devices to be significantly enhanced relative to the undoped device, but this is not observed. Instead the process is radiative or Förster transfer of singlet excitons, which conserves the spin of the excited species. Rubrene molecules do not act as charge traps in the beneficial way observed by other groups where there was a reduction the amount of triplet-singlet-annihilation[8]. It is however possible that triplet energy transfer occurs from the polymer to the rubrene which has a long triplet lifetime $\geq 120\mu s$[7]. Forster and/or radiative transfer is efficient as seen by the complete quenching of the PF2/6am4 elextroluminescnce at >3% wt. doping levels. However as can be seen by the measured EQE values rubrene singlet quenching must occur. Previous studies have shown that triplet energy transfer from small molecules to polymers readily occurs in solution[6] and polymer triplets are quenched by triplet energy transfer to molecular oxygen[6], thus it must be assumed that a proportion of polymer triplets are transferred to the rubrene which has a lower triplet energy than the PF2/6am4. The rubrene triplets are long lived $\tau_T \geq 120\mu s$ thus singlet-triplet-annihilation can occur on the dopant, i.e. $S_1 + T_1 \rightarrow T_n + S_0$. This will reduce considerably the overall EQE of the doped devices. If effective charge trapping occurs at the rubrene sites leading to excited singlet state formation on the rubrene[3] then one might well expect an increased device EQE as observed in Rubrene doped Alq_3 devices[3]. Since this does not obviously occur in PF2/6am4 doped devices (using very similar concentrations to those used in the Alq_3 devices) it must be concluded that such a mechanism in the polymer case is not effective. Thus the decrease in overall EQE of the APO doped PLEDs is ascribed to singlet-triplet annihilation at the rubrene sites mediated by the long lived trapped triplets on the dopant arising from triplet energy transfer from the PF2/6am4. As the singlet-triplet-annihilation processes regenerate the triplet state, one trapped triplet may quench many singlet states. Further singlet-triplet annihilation is effectively a Förster transfer from the singlet to the triplet it will be efficient in the confines of the singlets and triplets localized on the dopant rubrene molecules. This difference between polymeric systems and small molecule systems may well be caused by higher interchain triplet mobility[4]. Thus triplets in the polymer device can more readily migrate to the dopant sites.

6.2 Discussion

Rubrene does not produce an increase in External Quantum Efficiency when used as a dopant in PF2/6am4 PLEDs. The long-lived rubrene Triplet, $\tau_T \geq 120\mu s$, results in singlet-triplet annihilation on the dopant rubrene sites that exceeds the singlet-triplet-annihilation present in devices of undoped PF2/6am4. However, due to the highly efficient nature of the undoped PF2/6am4 (with a device EQE of 1.30141% at 6V), an efficient white emitting device with CIE coordinates 0.33, 0.42 was fabricated whose peak EQE measured 1.04742% at 9V. This performance level is most competitive when compared to other white emitters based on conjugated polymers, and is a result of EL emission from both the host and acceptor. Upon increasing the dopant concentration further, saturation is observed at circa 4% wt. rubrene. The 'failure' of rubrene to enhance the efficiency of PF2/6am4 PLEDs is significant given rubrene's high fluorescence efficiency. The result illustrates that the choice of molecular dopant for use in PLEDs may be complicated by properties other than dopant energy levels and fluorescence efficiency. Performance enhancement is dependant on not only the efficient transfer of energy to the dopant centers, but just as importantly on fast decay of the dopant excitons, avoiding singlet-triplet annihilation quenching resultant from the high triplet density around dopant sites.

References

[1]   Gross, M.; Muller, D. C.; Nothofer, H. G.; Scherf, U.; Neher, D.; Brauchle, C.; Meerholz, K. *Nature* **2000**, *405*, 661-665.

[2]   Jang, M. S.; Song, S. Y.; Shim, H. K.; Zyung, T. Y.; Jung, S. D.; Do, L. M. *Synthetic Metals* **1997**, *91*, 317-319.

[3]   Jin, Y. D.; Yang, J. P.; Heremans, P. L.; Van der Auweraer, M.; Rousseau, E.; Geise, H. J.; Borghs, G. *Chemical Physics Letters* **2000**, *320*, 387-392.

[4]   Monkman, A. P.; Burrows, H. D.; Hamblett, I.; Navaratnam, S. *Chemical Physics Letters* **Submitted**.

[5]   Monkman, A. P.; Burrows, H. D.; Hartwell, L. J.; Horsburgh, L. E.; Hamblett, I.; Navaratnam, S. *Physical Review Letters* **2001**, *86*, 1358-1361.

[6]   Monkman, A. P.; Burrows, H. D.; Miguel, M. d. G.; Hamblett, I.; Navaratnam, S. *Synthetic Metals* **2001**, *116*, 75-79.

[7]   Murov, L.; Carmichael, I.; Hug, G. L. *Handbook of Photochemistry*, 2nd ed.; New York: New York, 1993.

[8]   O'Brien, D. F.; Giebeler, C.; Fletcher, R. B.; Cadby, A. J.; Palilis, L. C.; Lidzey, D. G.; Lane, P. A.; Bradley, D. D. C.; Blau, W. *Synthetic Metals* **2001**, *116*, 379-383.

[9]   Virgili, T.; Lidzey, D. G.; Bradley, D. D. C. *Advanced Materials* **2000**, *12*, 58-+.

[10]   Virgili, T.; Lidzey, D. G.; Bradley, D. D. C. *Synthetic Metals* **2000**, *111*, 203-206.

Chapter 7 Electrophosphorescence and Chromaticity tuning in polymer light-emitting diodes

This work later submitted to Journal of Applied Physics under the title 'A study of the energy transfer to porphyrin derivatives when used as dopants in polymer light-emitting diodes'. Currently under consideration.

7.1 INVESTIGATING TRANSFER MECHANICS BY VARYING DOPANT PROPERTIES WITHIN THE PORPHYIN FAMILY

The study of rubrene in a highly efficient host polymer suggests that efficient dopant emission is not enough to ensure device enhancement. Unless the singlet excitons are offered a fast route to decay they are vulnerable to singlet-triplet annihilation at the dopant site. In order to further investigate this effect three porphyin derivatives were used as dopants in PF2/6am4: 2,3,7,8,12,13,17,18-octaethyl-21H,23H- porphyrin zinc(II) (ZnOEP), 2,3,7,8,12,13,17,18-octaethyl-21H,23H- porphyrin palladium(II) (PdOEP) and 2,3,7,8,12,13,17,18-octaethyl-21H,23H- porphyrin platinum(II) (PtOEP). Their chemical structure is shown in
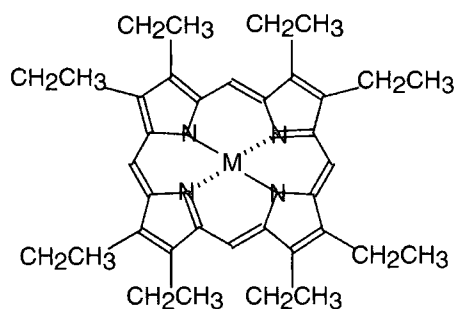
Figure 7-1 The common structure of ZnOEP, PdOEP and PtOEP, where M is either Zn, Pd or Pt respectively

Varying the central metal atom of the porphyrin can change the amount of spin-orbit coupling exerted on the host by the dopant, as well as the fluorescence efficiency and excited state lifetimes of the dopant molecule itself (as summarized in table 1, values taken from the literature[14,11,17]). Thus by comparing the performance of electroluminescent devices incorporating each of these molecules we may be able to determine which if any of the dopant properties are crucial for an efficient device.

Dopant Molecule	Triplet Lifetime	Luminescence Quantum Yield
PtOEP	91μs	0.5
PdOEP	990μs	0.2
ZnOEP	57ms	0.065

Table 7-1 Summary of the Fluorescence efficiency and Luminescence Quantum Yield of the porphryin derivatives PtOEP, PdOEP and ZnOEP

7.11 ZnOEP doped PF2/6am4 PLEDs

Figure 7-3 and Figure 7-4 show the Field-Current and brightness output curves of the devices tested. In similarity with other polyfluorene/dopant systems[16] (and in poly(N-vinylcarbazole) doped with 2,4,7-trinitrofluorenone[10]) an increase in turn on voltage with dopant concentration was observed, with the voltage required for a current of 1×10^{-5}A in the device at 4.05, 5.20, 5.35, 5.45, 7.75 & 7.80V for the undoped, 0.5% 1%, 2%, 3% and 4% wt. doped devices respectively. Previously other authors have ascribed this increase in drive voltage to charge trapping at the dopant centers[16]. This is possible when either the electron affinity of the dopant is lower than that of the polymer host, or the ionization potential is higher. It is likely that a similar process occurs in these ZnOEP doped devices, with the trapped charge resulting in a redistribution of the electric field across the active layer. This is supported by the data in Figure 7-2, which suggests that all three of the porphyrin dopants will act as hole traps in PF2/6am4.
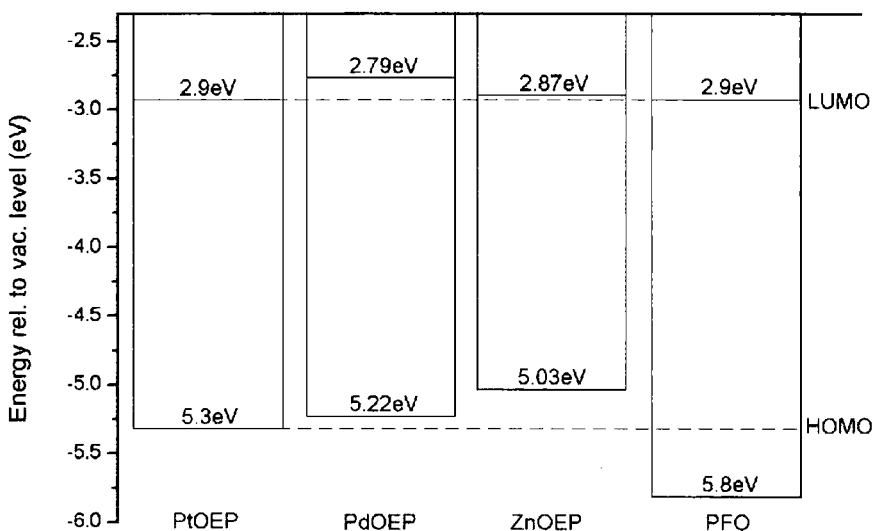
Figure 7-2 HOMO and LUMO levels for the polymer and porphyrin dopants used. Data was taken for PtOEP and PFO from reference[2], and for ZnOEP and PdOEP from reference[6]

105

The peak External Quantum Efficiencies (EQEs) of all the ZnOEP doped PLEDs are substantially lower than the undoped PLED and decline with increasing dopant concentration, as summarized in Table 7-2, and illustrated in the trend seen in Figure 7-4: the gradient of the power curve being proportional to the efficiency of the device. Figure 7-5 shows that for dopant concentrations greater than 2% wt. the ZnOEP Electroluminescence (EL) emission (peaked at 628.5nm) dominates over the PF2/6am4 EL emission. The ZnOEP emission in PF2/6am4 is peaked at the same wavelength as that observed when the dopant was spin coated in a film of poly(methyl methacrylate) PMMA, hence we conclude that the ZnOEP molecules are behaving as secondary emitters in their own right, and not as complexes formed with the host chains. This is important as it allows the use of the values contained in Table 7-1 when assessing the relative performance of ZnOEP, PdOEP and PtOEP doped devices.

It is interesting to note the current densities at which all ZnOEP doped devices achieved peak EQE are similar to that for the undoped device. This important observation becomes increasingly relevant when we later contrast this result with the other porphyrin dopants.
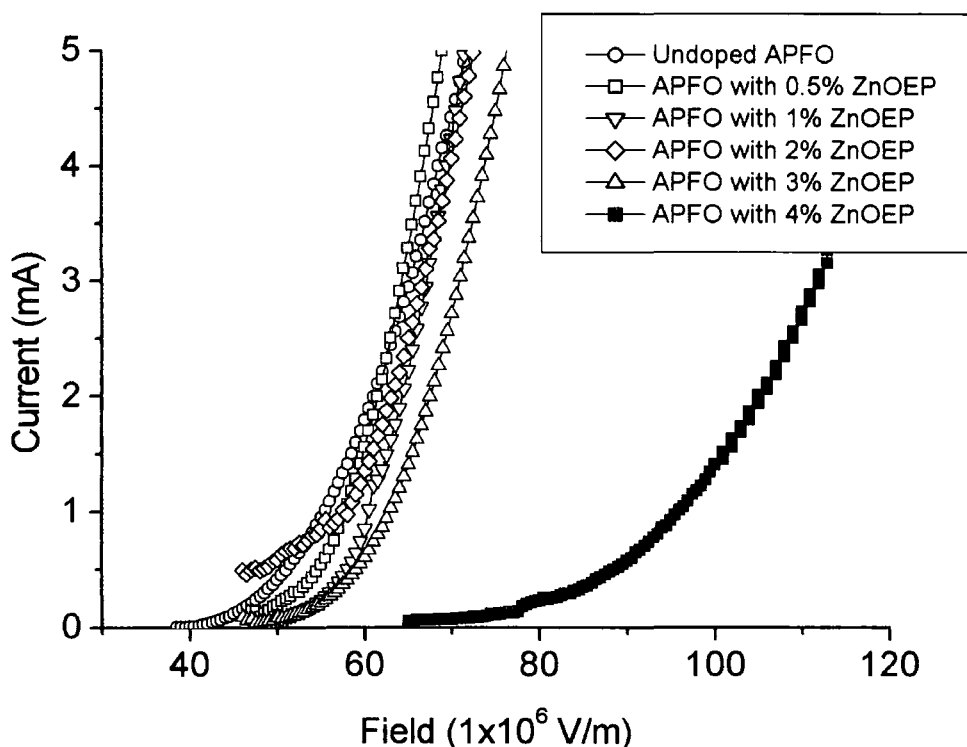
Figure 7-3 Current-field Profiles for ZnOEP Devices tested
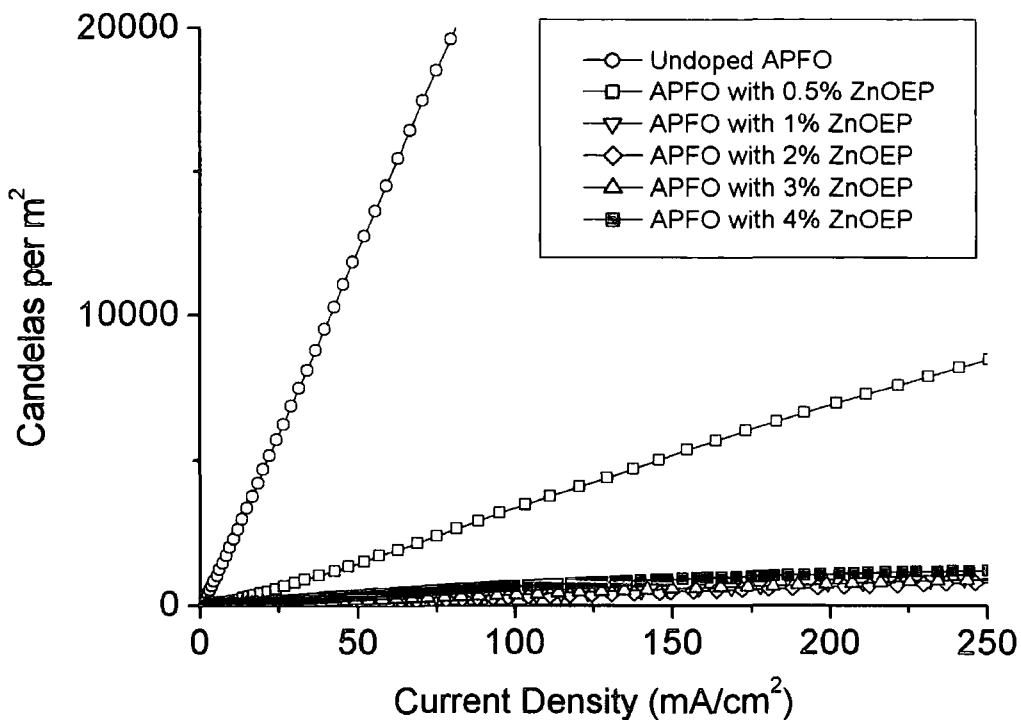
Figure 7-4 Power Output curves for the ZnOEP PLEDs tested
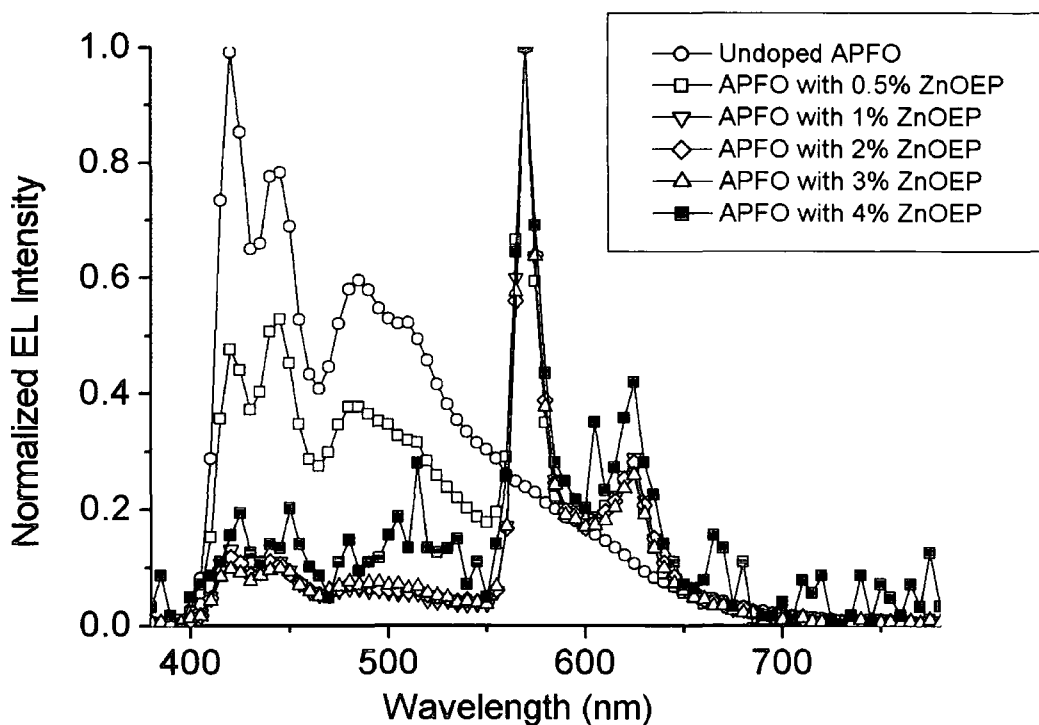
Figure 7-5 Electroluminescence Spectra for ZnOEP Devices tested

Device	Dopant %wt.	Peak EQE [at mA/cm^2]	Operating Voltage (V)	CIE Coordinates X	Y
Undoped		1.19	5	0.23683	0.2678
		[70.67]	6	0.20727	0.22705
			7	0.198	0.21056
PF2/6am4	0.5	0.22	6	0.2900	0.3090
Doped with ZnOEP		[173.33]	7	0.2760	0.2870
			8	0.2750	0.2870
	1	0.04	6	0.4100	0.3760
		[242.67]	7	0.4840	0.4250
			8	0.4160	0.3810
	2	0.04	7	0.49355	0.43604
		[236.89]	8	0.41817	0.38690
			9	0.4183	0.38878
	3	0.04	7	0.41869	0.39292
		[141.78]	8	0.41644	0.39362
			9	0.40955	0.38890
	4	0.04	10	0.40101	0.39268
		[54.22]	11	0.39034	0.3820
			12	0.41319	0.40126
PF2/6am4	0.5	1.06	8	0.22466	0.24599
Doped with PdOEP		[0.21]	10	0.21267	0.25376
			12	0.2149	0.29029
	1	1.08	8	0.36141	0.28039
		[0.56]	10	0.26229	0.24139
			12	0.23185	0.23936
	2	0.82	8	0.45453	0.28224
		[0.69]	10	0.44344	0.30407
			12	0.35026	0.2647
	3	0.62	9	0.42616	0.28743
		[1.36]	11	0.35732	0.24786
			13	0.29316	0.24267
	4	0.91	10	0.43086	0.29257
		[0.88]	12	0.40141	0.25607
			14	0.34995	0.26402
PF2/6am4	0.5	2.36	5	0.47415	0.2621
Doped with PtOEP		[15.6]	6	0.37664	0.23279
			7	0.29889	0.21543
	1	2.75	7	0.62007	0.29379
		[9.16]	9	0.62324	0.27526
			11	0.56166	0.25607
	2	1.99	9	0.60512	0.29352
		[1.92]	11	0.64774	0.27721
			13	0.63147	0.27137
	3	1.29	12	0.64189	0.28112
		[2.13]	14	0.64467	0.27134
			16	0.61804	0.26976
	4	1.28	10	0.64189	0.28112
		[7.78]	12	0.64468	0.27134
			14	0.61805	0.26976

Table 7-2 External Quantum Efficiency & Variation in Color Coordinates with Operating Voltage for each device.

7.12 PdOEP doped PF2/6am4 PLEDs

Figure 7-6 and Figure 7-7 show the Field-Current and brightness output curves of the devices tested. A general trend of increase in turn on voltage with dopant concentration was observed, with the voltage required for a current of 1×10^{-5}A in the device at 4.05, 5.90, 5.80, 6.20, 6.25 & 7.1V for the undoped, 0.5% 1%, 2%, 3% and 4% wt. doped devices respectively. The increase is by no means as severe as for the ZnOEP devices, and suggests less charge trapping at the PdOEP centers.

Again a decrease in peak EQE of doped devices with increasing dopant concentration was observed (Table 7-2 & Figure 7-7). The magnitude of EQE reduction is less than that for ZnOEP, even for higher dopant concentrations. The dopant EL emission dominates for higher dopant concentrations, and again this EL peak corresponds to the fluorescence of the dopant at 662.5nm, see Figure 7-9.

PdOEP doped devices this current densities at which peak EQEs were observed were several orders of magnitude lower than for the undoped device (Table 7-2). Of equal significance, whereas the high performance of the undoped device is maintained up to high current densities (circa 400Cd/m^2), the EQE of all PdOEP devices falls off sharply with increasing current density beyond the bracketed values contained in Table 7-2.

109

Figure 7-6 Current-field Profiles for PdOEP PLEDs tested

Figure 7-7 Power Output curves for the PdOEP PLEDs tested

Figure 7-8 Electroluminescence Spectra for PdOEP Devices tested

Figure 7-9 Fluorescence Spectra of the dopant studied in an inert PMMA host. Films of PMMA:Dopant blends were drop cast into quartz disks and then analysed in a FluoroMax 4 Fluorometer

111

7.13 PtOEP doped PF2/6am4 PLEDs

Figure 7-10 and

Figure 7-11 show the Field-Current and brightness output curves of the devices tested. A general trend of increase in turn on voltage with dopant concentration was observed again, with the voltage required for a current of 1×10^{-5}A in the device at 4.05, 3.40, 4.65, 6.25, 7.6 & 5.85V for the undoped, 0.5% 1%, 2%, 3% and 4% wt. doped devices respectively. Again this increase in drive voltage is predicted by the offset in HOMO levels between host and dopant.

Unlike the other dopants, an increased peak EQE for all of the doped devices relative to the undoped device was observed, with the 2% wt. PtOEP doped device showing a factor of improvement in peak EQE of 2.29 (for all devices' EQE see Table 7-2). The dopant EL emission dominates for higher dopant concentrations, and corresponds to the dopant fluorescence spectrum (Peak at 643.5nm, see Figure 7-9).

These values should be treated with great care as the improvement is only for low current densities (and correspondly low EL emission intensity). For all PtOEP doped devices the peak in EQE was observed at current densities several orders of magnitude lower than for the undoped device (Table 7-2), and at high current densities the EQE of the doped devices fall off to low values of the order of 0.3%, well below that of the undoped device at equivalent current densities. There is an observed increase from the PF2/6am4 in the blends at high current density, suggesting that past the peak performance conditions there is a small increase in the probability of recombination and subsequent emission from the host (Figure 7-15).
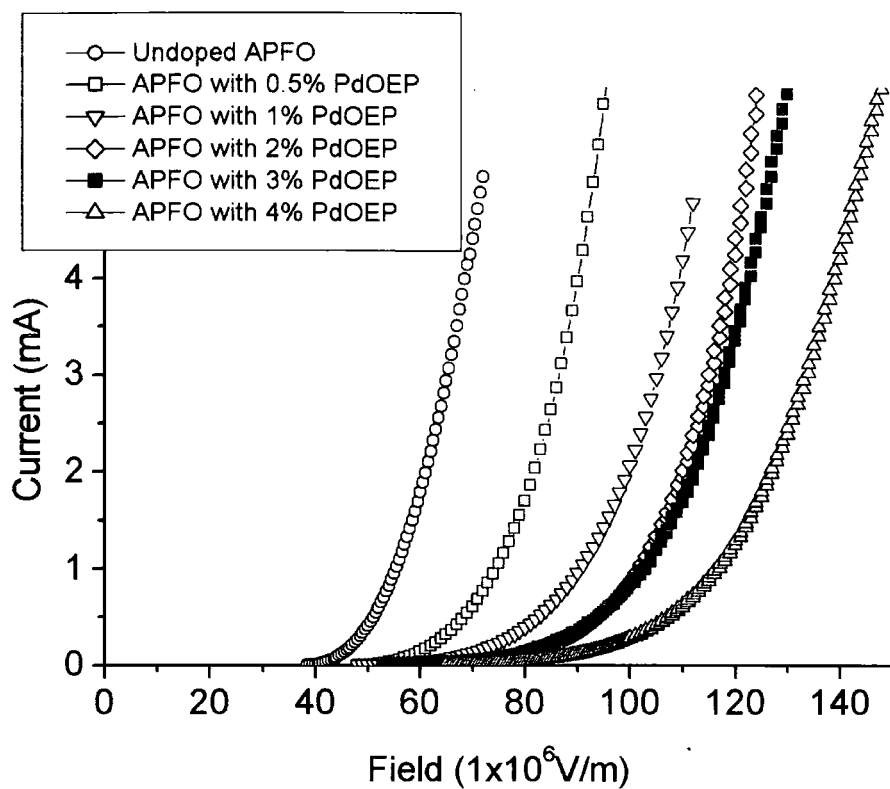
112
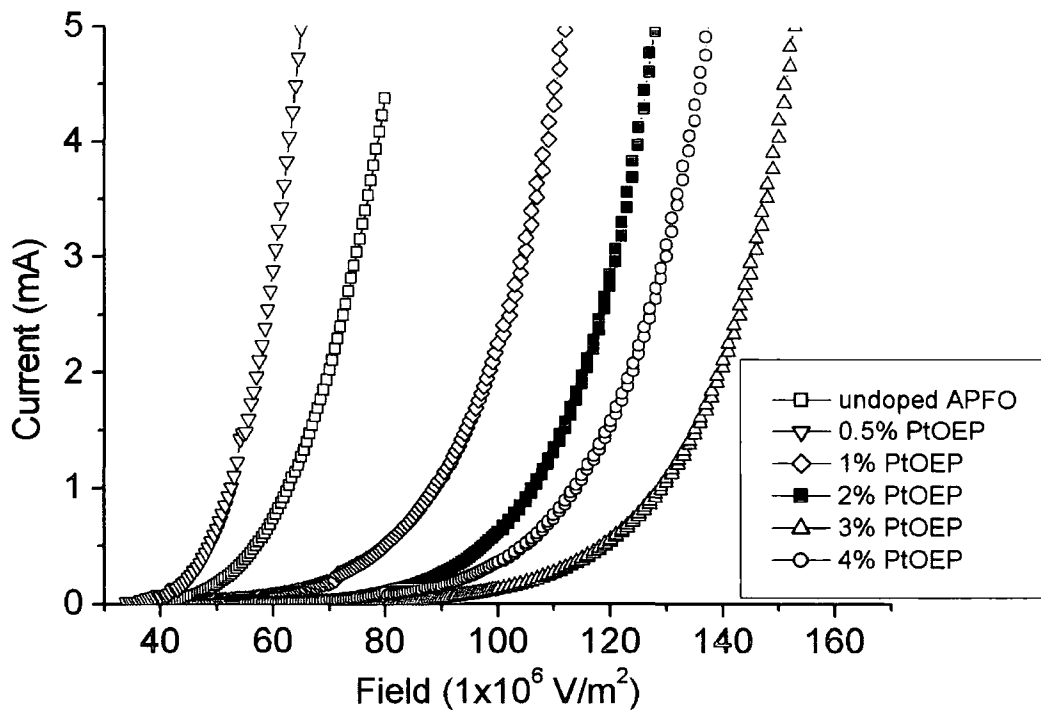
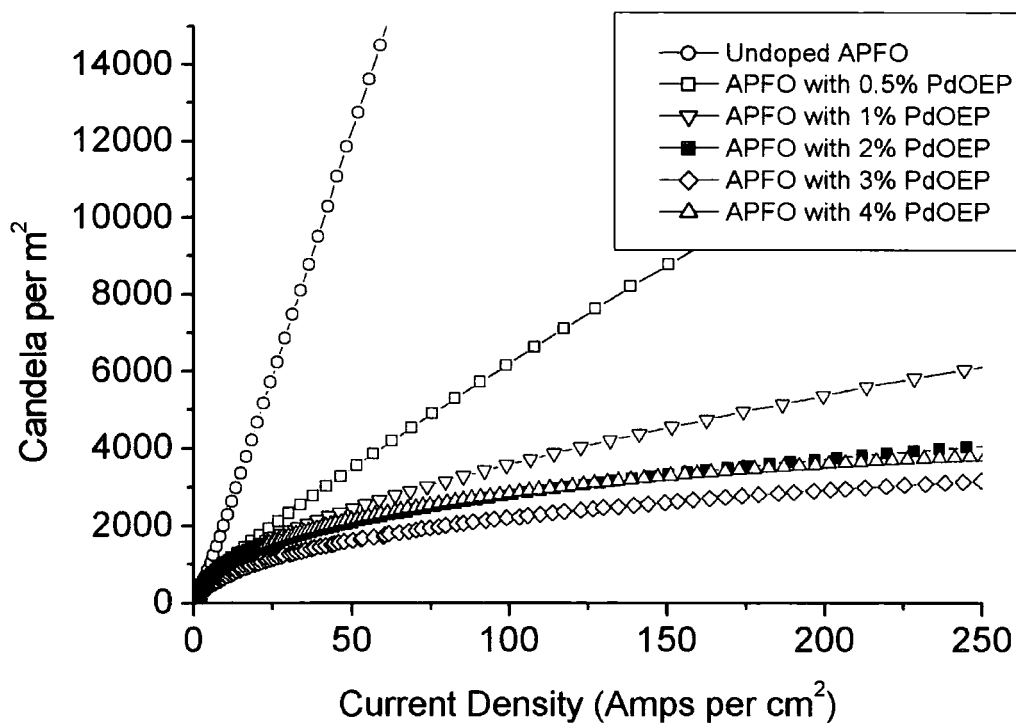**Figure 7-10** Current-field Profiles for PtOEP PLEDs tested
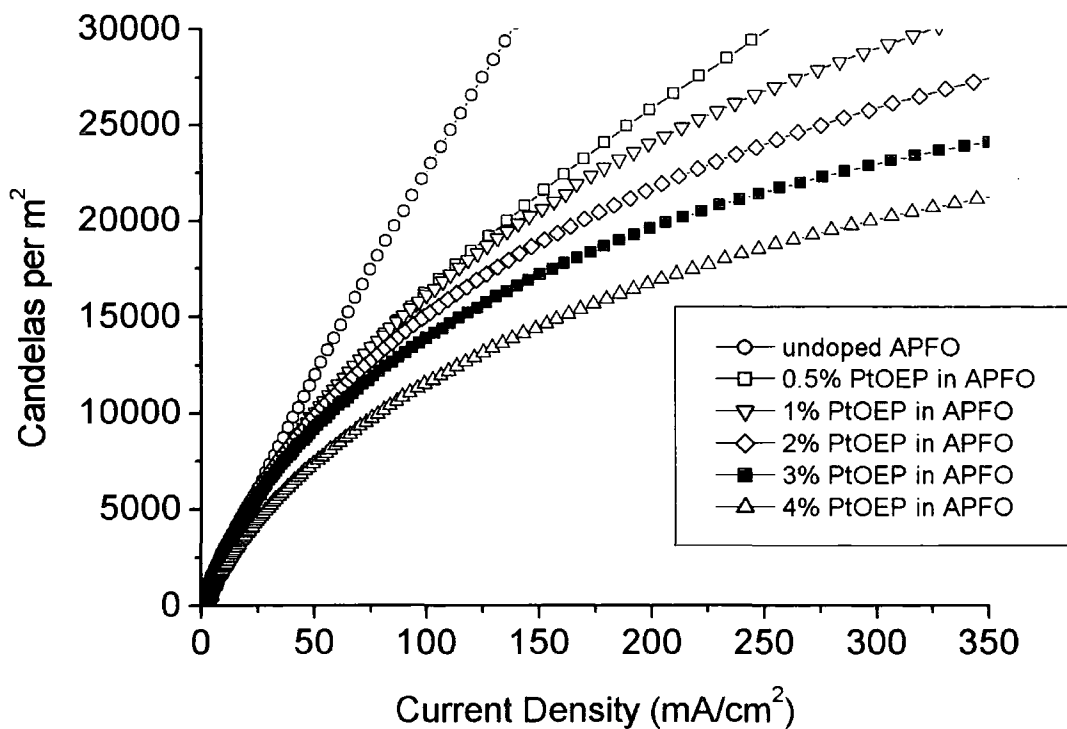
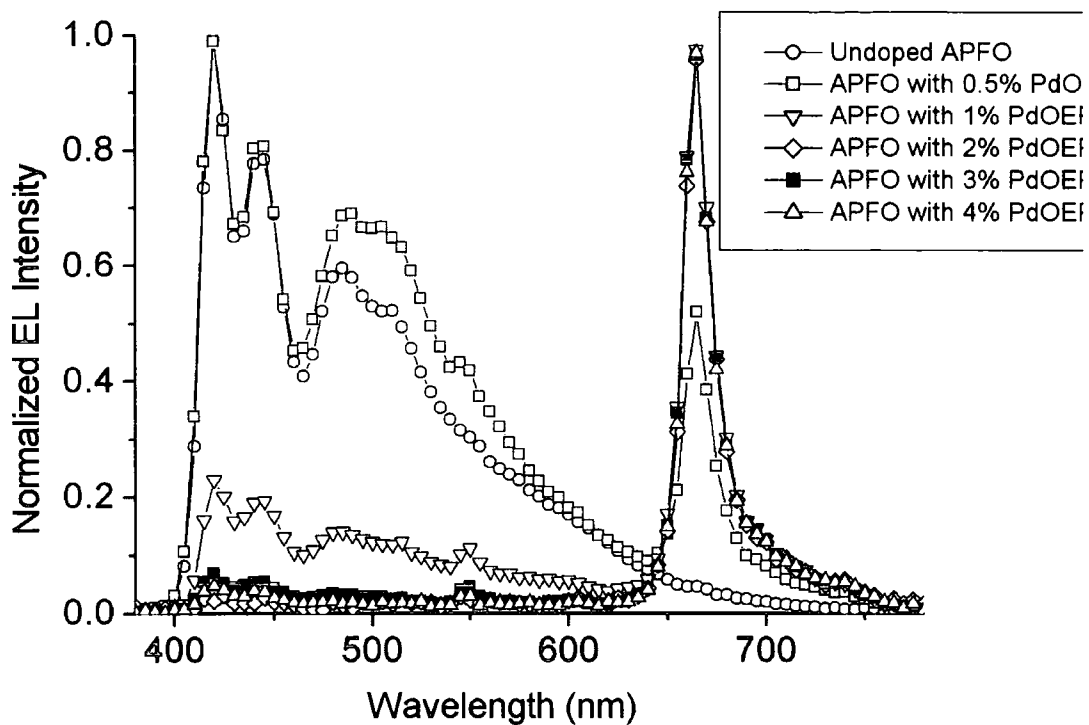**Figure 7-11** Power Output curves for the PtOEP PLEDs tested

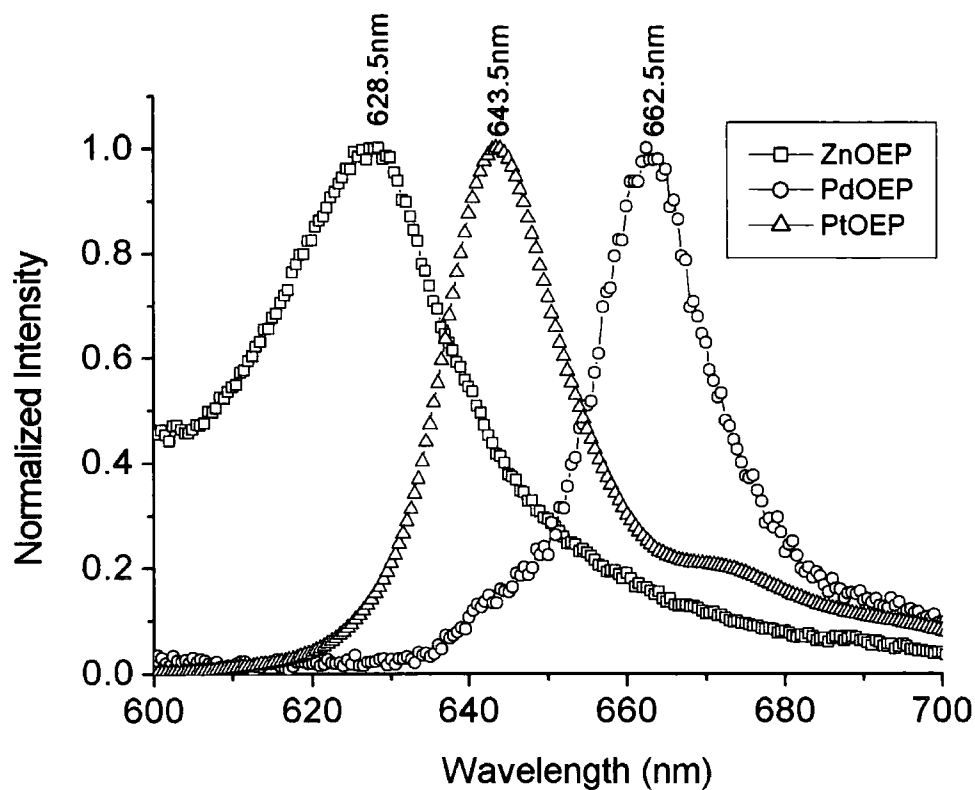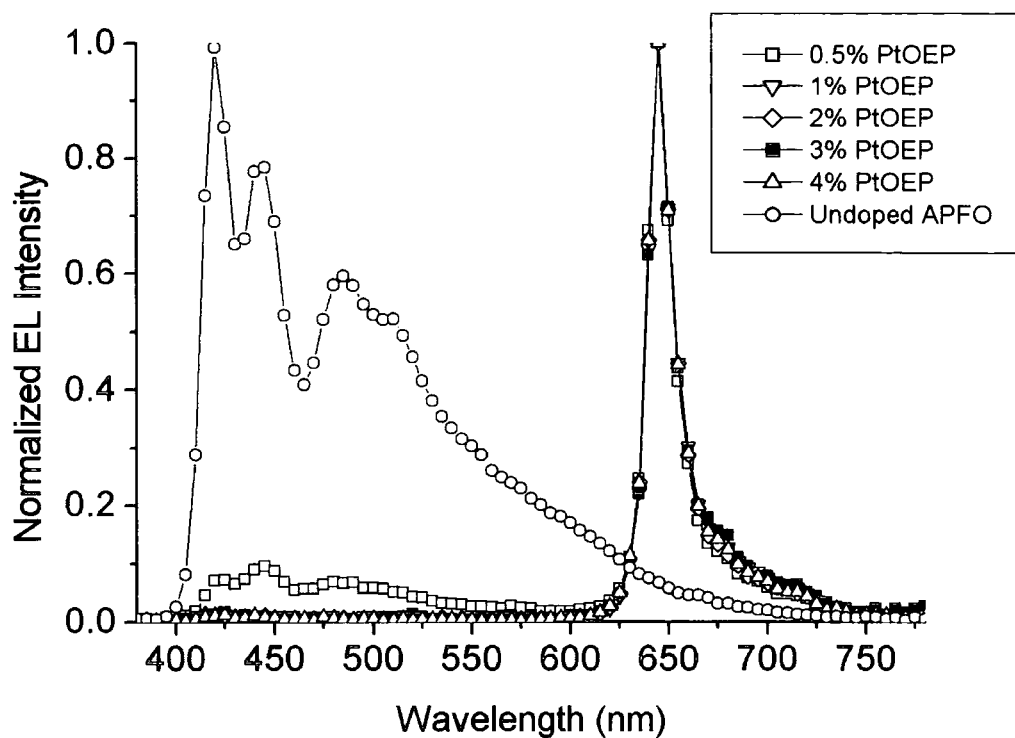**Figure 7-12** Electroluminescence Spectra for PtOEP Devices tested
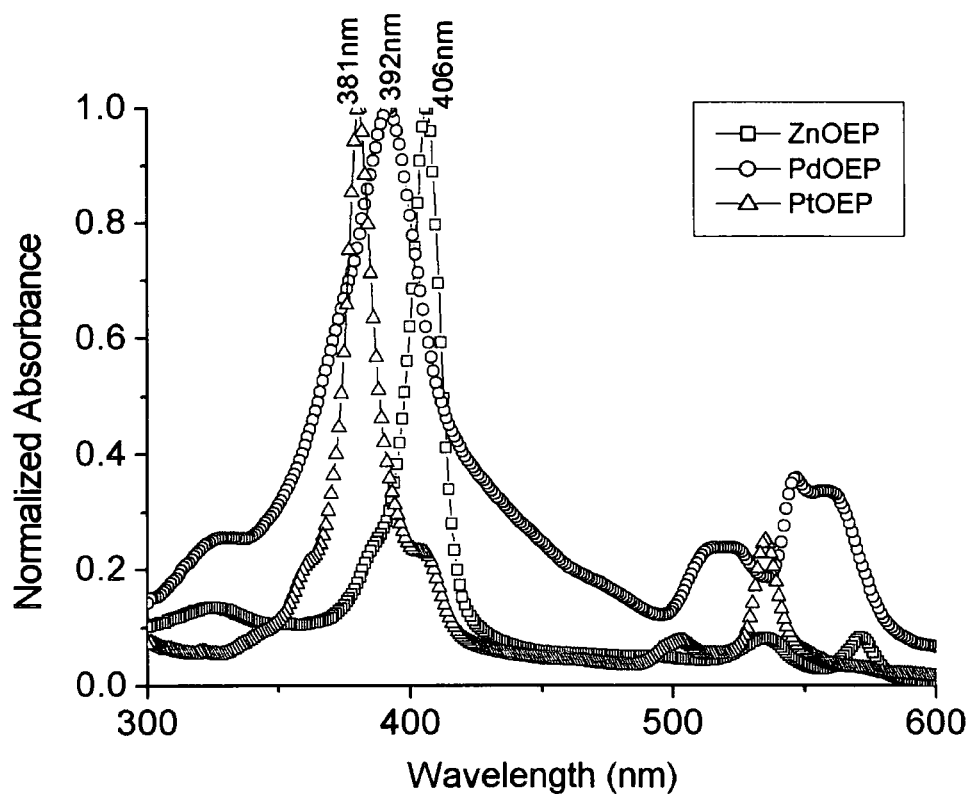
Figure 7-13 Absorption Spectra of the dopant studied in an inert PMMA host. Films of PMMA:Dopant blends were drop cast into quartz disks and then analysed in a UV Spectrometer

7.14 Discussion

Of the three dopants used in this study, PtOEP has previously received the most attention[16,15]. High values of EQE combined with the ability to finely tune the color of emission between the blue of PF2/6am4 to the red of PtOEP by varying the blend ratio. What has been neglected is that this EQE enhancement is only for low current densities and output intensities. The majority of practical applications would require significantly more intensity (i.e. circa $100Cd/m^2$ average in actively addressed matrix displays[8], which for pulsed operation would mean 64 times this average for 1/64 of the time), at which correspondingly high current densities our PtOEP devices have fallen significantly in efficiency. Figure 7-14 compares the shape of EQE vs. Current Density curves for undoped PF2/6am4 and 2% wt. PtOEP, ZnOEP and PdOEP doped PF2/6am4. The EQE have been normalized in order to clearly see differences in behaviour over operational current densities (for absolute values refer to Table 7-2). The shape of the PtOEP curve is markedly different to that of the undoped device. The undoped device EQE rises to a maximum value and then remains there until the device is pushes into breakdown at very high current densities. In the PtOEP device, conversely, EQE peaks at lower current density and then EQE falls away, until at $100mA/cm^2$ the EQE is approximately half the peak value. The EQE curve levels out at higher current densities to a value of ~0.3%.

Including the PdOEP and ZnOEP curves of Figure 7-14 in the analysis helps to explain this behaviour. Referring to Table 7-1 is can be seen that as dopant phosphorescence efficiency increases so do the peak EQE values, with PtOEP the most suitable dopant, then PdOEP and finally ZnOEP. This is intuitive and is the reason PtOEP is a popular dopant: it is selected for its high efficiency of emission.

What are more interesting are the current densities at which the doped devices peak in EQE. From Table 7-2 it can be seen that the longer the phosphorescence lifetime of the dopant, the lower the current density for peak EQE is. This is also shown in the normalised EQE curves in Figure 7-14. This would appear to suggest that the reason for the poor performance of the doped devices at high current densities relative the undoped device is the capacity of the dopant centres to radiately dissipate excitons efficiently. As current density increases the amount of trapped charge centred on dopant sites will increase, as well as any Forster and/or radiative transfer to the dopant. The overlap between porphyin absorption and PF2/6am4 fluorescence is small, which correspondingly means any Forster transfer would be small. This information,

115

combined with the observed domination of EL spectra by porphyrin emission for ZnOEP, PdOEP and PtOEP, indicates that we have observed recombination directly on the dopant sites initiated by trapped hole polarons. If the dopant molecules cannot emit fast enough they will become saturated in excitons, exposing those excited species 'queuing' at the dopant sites to the possibility of non-radiative quenching by singlet[18] or triplet[12] annihilation or triplet-ion[4] quenching of the form $T_1+^2D{\rightarrow}S_0+^2D^*$, where T_1 is the first triplet excited state, S_0 is the ground state and ^2D and $^2D^*$ are the ground and excited charge states respectively. Hence the efficiency of the device falls off as current density increases. The current density at which EQE is a maximum is directly related to the dopants' phosphorescence lifetime.
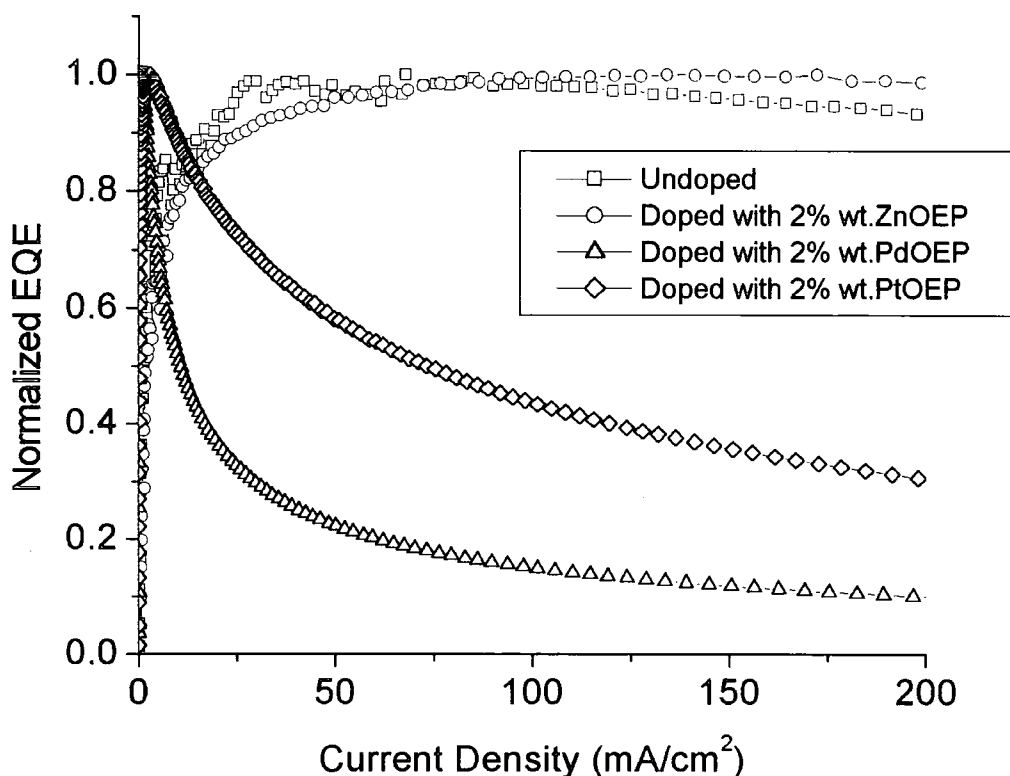
Figure 7-14 Normalized EQE-Current Plots for representative Devices: Undoped PF2/6am4 with 2% wt. ZnOEP, PdOEP and PtOEP doped PF2/6am4 doped PF2/6am4. For absolute EQE values refer to Table 7-2. The purpose of normalizing the curves is to compare the curve shapes and the positions of the peaks for different dopant species

Further evidence for this saturation effect can be seen looking closely at the doped PLED electroluminescence spectra in the wavelength range of PF2/6am4 fluorescence. For larger drive voltages we observe an increase in the amount of

116

PF2/6am4 emission contributing to the electroluminescence. This can be seen in Table 7-2, with the CIE-b coordinate increasing, and is also depicted in Figure 7-15 for the 1% wt. PtOEP doped PF2/6am4 PLED. This suggests that at higher drive voltages saturation of the dopant enables positive charge to reside on the polymer long enough for recombination to occur without transferring to the dopant, giving rise to emission from the polymer.
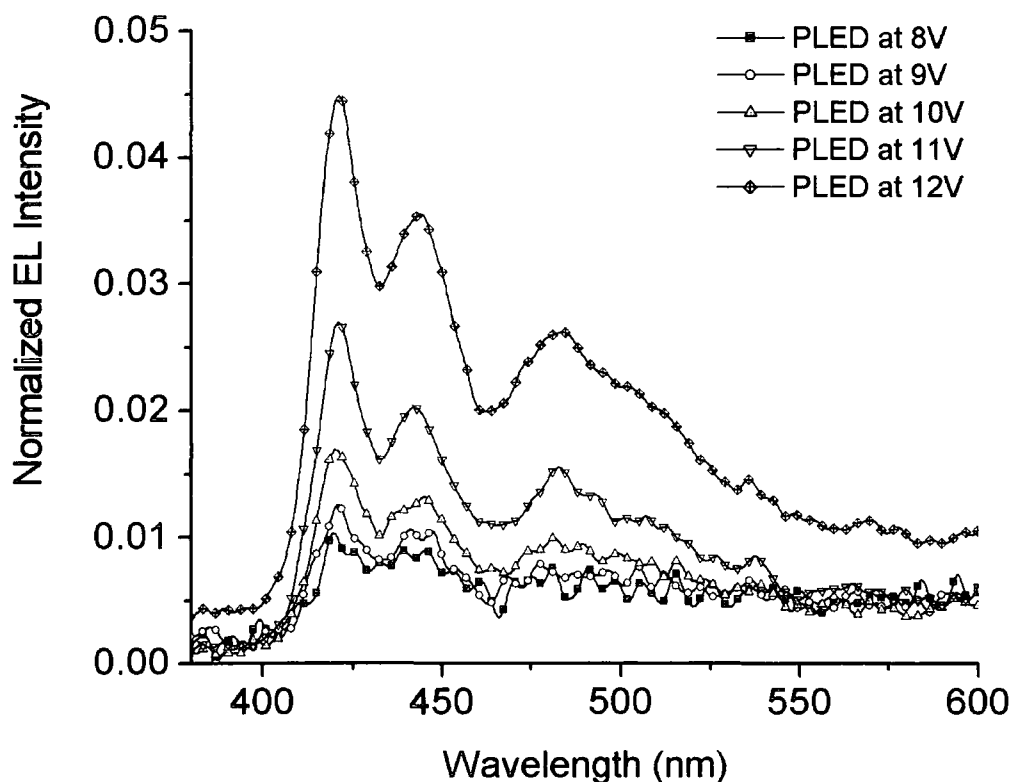
Figure 7-15 Variation in Electroluminescence (EL) contribution from the host polymer as drive voltage is increased for the 1%wt. PtOEP doped PLED

Thus, ideally one would employ a dopant molecule with a short phosphorescence lifetime and a high phosphorescence efficiency in order to achieve a high peak EQE and maintained performance over operational current densities. Recent results from Baldo et al. using bis(2-(2'-benzo[4,5-a]thienyl)pyridinato-N,C-3') iridium(acetylacetonate) (Btp(2)Ir(acac)) confirm these findings[1].

A final remark should also be made concerning the outcome of triplet-triplet annihilation, which should be a rather favoured process on the localised dopant sites. The intermediate triplet pair formed during the annihilation process will have some charge separated character[19]. Given the very high electric field across the device,

decay of the triplet pair to a cationic species would be enhanced at higher current densities by this process. Therefore at high current densities, the long lived excited state lifetimes of the dopants directly leads to massive quenching of the excitons by excited state annihilation and further quenching by the products of annihilation.

7.2 SUMMARY

The results obtained allow us to highlight key design considerations when choosing dopants for use in PLEDs. In addition to high phosphorescence efficiency the dopant needs to have a short emission lifetime in order to avoid dopant saturation over the operational current densities and required output intensity of the PLED. The dopant should also be chosen so as to minimise any loses in power efficiency, i.e. charge trapping at the dopant sites results in increases in turn-on voltage. Ideally we would have no charge trapping at all, with the electron affinity and ionisation potential respectively below and above those of the host polymer. In this regime we would rely solely on efficient excitation energy transfer from the polymer to the dopant. In the case of poly(N-vinylcarbazole) (PVK) doped with tris(2-phenylpyridine) iridium $(Ir(ppy)_3)$[9] where this is very nearly the case, EQE still falls of at high current densities as once again the relatively long lifetime of the dopant excited state degrades efficiency through effective quenching mechanisms. In that case the EQE drop was not as severe as observed in this study, suggesting that enhanced triplet-ion quenching may have been avoided, but that singlet or triplet annihilation concentrated on the sites does occur.

Indeed the results presented here bring into question the whole issue of doping PLEDs with small molecules in order to enhance device performance. Specifically: there are few known dopants with high efficiencies that also have short excited state lifetimes. Those dopants with lifetimes usually incorporate heavy metals that introduce significant spin-orbit coupling: an additional complication to dopant selection. More fundamentally the idea of energy transfer to more efficient chomaphores than present in the pure host requires that the dopant energy levels lie below those of the host. Thus red light-emitting devices are possible by blending a blue host with a red emitter: but this methodology cannot work for devices that emit in the blue end of the spectrum. Triplet transfer would be worse as E_T of such blue-emitting polymers is of order 1eV below E_s[13]. We would need to start with a polymer that efficiently emitted in the UV in order to obtain the correct energy level positioning. In addition the difference in energy between the host exciton and the dopant exciton must be translated to a phonon(s), and this will heat the PLED and change its properties.

With recent experimental and theoretical results[7,3,5,20] questioning the validity of the spin-independent recombination, and hence the maximum theoretical Internal

Quantum Efficiency of 25% predicted by simplistic quantum statistics, these results would suggest that efforts would be better served investigating how we can enhance the singlet yield of conjugated polymers, without changing their emission profiles. The long lived excited state lifetimes of the dopants studied here directly leads to massive quenching of the excitons by excited state annihilation and further quenching by the products of annihilation. We need a full range of colours emitted at high efficiency for PLEDs to fulfil their commercial potential, and energy transfer to dopant molecules seems to not only limit our colour range but also the range of operation at high efficiency. From our results in the cases with or without charge trapping, the most important criterion for an effective dopant will be a short excited state lifetime, which decays radiatively with high yield.

References

[1]   Adachi, C.; Baldo, M. A.; Forrest, S. R.; Lamansky, S.; Thompson, M. E.; Kwong, R. C. *Applied Physics Letters* **2001**, *78*, 1622-1624.

[2]   Cleave, V.; Yahioglu, G.; Le Barny, P.; Hwang, D. H.; Holmes, A. B.; Friend, R. H.; Tessler, N. *Advanced Materials* **2001**, *13*, 44-+.

[3]   Dyakonov, V.; Frankevich, E. *Chemical Physics* **1998**, *227*, 203-217.

[4]   Ern, V.; Bouchriha, H.; Fourny, J.; Delacote, G. *Solid State Communications* **1971**, *9*, 1201.

[5]   Frankevich, E.; Ishii, H.; Hamanaka, Y.; Yokoyama, T.; Fuji, A.; Li, S.; Yoskino, K.; Nakamura, A.; Seki, K. *Physical Review B* **2000**, *62*, 2505-2515.

[6]   Fuhrhop, J.; Fuuhrhop, I.; Kadish, K. M.; Davis, D. G. *Journal of the American Chemical Society* **1973**, *95*, 5140.

[7]   Hong, T. M.; Meng, H. F. *Physical Review B* **2001**, *6307*, 5206-+.

[8]   Kido, J. *Polymers for Advanced Technologies* **1997**, *8*, 379-379.

[9]   Lee, C. L.; Lee, K. B.; Kim, J. J. *Applied Physics Letters* **2000**, *77*, 2280-2282.

[10]   Marc, N.; Moisan, J. Y.; Andre, B.; Lever, R. *Philosophical Magazine B- Physics of Condensed Matter Statistical Mechanics Electronic Optical and Magnetic Properties* **1996**, *73*, 779-791.

[11]   Mills, A.; Lepre, A. *Analytical Chemistry* **1997**, *69*, 4653-4659.

[12]   Monkman, A. P.; Burrows, H. D.; Hamblett, I.; Navaratnam, S. *Chemical Physics Letters* **Submitted**.

[13]   Monkman, A. P.; Burrows, H. D.; Hartwell, L. J.; Horsburgh, L. E.; Hamblett, I.; Navaratnam, S. *Physical Review Letters* **2001**, *86*, 1358-1361.

[14]   Murov, L.; Carmichael, I.; Hug, G. L. *Handbook of Photochemistry*, 2nd ed.; New York: New York, 1993.

[15]   O'Brien, D. F.; Baldo, M. A.; Thompson, M. E.; Forrest, S. R. *Applied Physics Letters* **1999**, *74*, 442-444.

[16]   O'Brien, D. F.; Giebeler, C.; Fletcher, R. B.; Cadby, A. J.; Palilis, L. C.; Lidzey, D. G.; Lane, P. A.; Bradley, D. D. C.; Blau, W. *Synthetic Metals* **2001**, *116*, 379-383.

[17]   Papkovsky, D. B. *Sensors and Actuators B-Chemical* **1995**, *29*, 213-218.

[18]   Rahman, T. S.; Kuox, C. R. S. *Physica Status Solidi B* **1973**, *58*, 715.

[19]   Scherr, H.; Orlowski, T. E. *Physics Review Letters* **1983**, *50*, 775.

[20]   Wohlgenannt, M.; Tandon, K.; Mazumdar, S.; Ramasesha, S.; Vardeny, Z. V. *Nature* **2001**, *409*, 494-497.

Chapter 8 Heavy Atom and Paramagnetic Triplet Quenching effects in polymer light-emitting diodes

This work later submitted to Physical Review B under the same title. Currently under consideration

8.1 MANIPULATING THE SINGLET YIELD IN POLYMER LIGHT-EMITTING DIODES WITH HEAVY METAL DOPANTS

Heavy atoms have been known for their perturbing effect on the neighbouring atomic/molecular orbitals for many years[7]. Here samples of both MEH-PPV and PF2/6am4 are doped with a variety of rare-earth lanthanide metal-organic complexes. This is due with the intention of perturbing the inter-system crossing (ISC). This ideology is discussed in more detail above.

Active layers with emissive host polymer MEH-PPV were doped to a variety of concentrations between 0.5 and 4% wt. with tris(2,2,6,6-tetramwthyl-3,5-hepanedionato)gadolinium(III)] (Gd-thd₃), tris(2,2,6,6-tetramwthyl-3,5-hepanedionato)lanthanum(III)] (La-thd₃), tris(2,2,6,6-tetramwthyl-3,5-hepanedionato)dysprosium(III)] (Dy-thd₃) and cerium(III) 2-ethylhexanoate (Ce-eh₃). The emissive host PF2/6am4 was doped with Gd-thd₃ in order to determine the effect of doping a blue emitting polymer with a heavy metal-ligand complex.
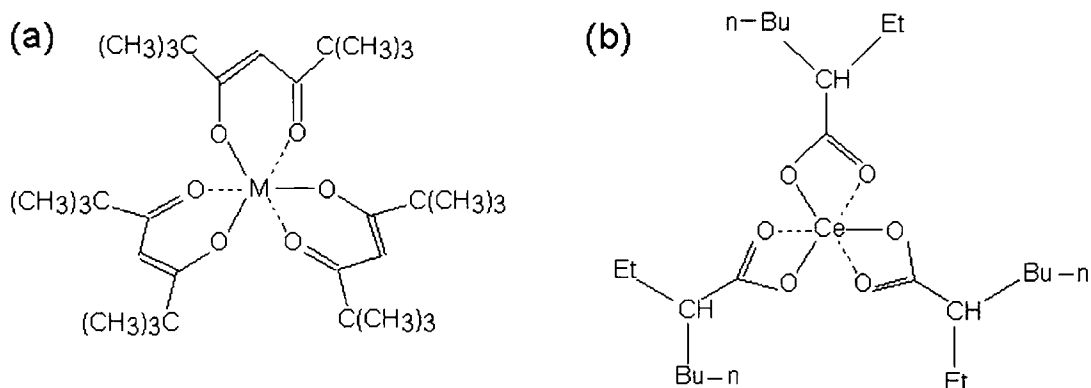
Figure 8-1 Chemical stuctures of (a)M-thd₃, where M=Gd, La or Dy (b)Ce-EH₃

8.11 MEH-PPV doped with Gd-thd₃, La-thd₃, Dy-thd₃ and Ce-eh₃

Figure 8-2, Figure 8-3, Figure 8-4 and Figure 8-5 show the field-current, candela output, EL spectra and current density-EQE characteristics respectively for all Gd-thd$_3$ doped MEH-PPV PLEDs studied. There was no significant change in turn-on voltage with dopant concentration observed relative to other dopant systems[6], with 2.35, 2.30, 2.40, 2.50, 2.80 and 3.60V required for a current of 1×10^{-5}A in the undoped, 0.5%, 1%, 2%, 3% and 4% wt. Gd-thd$_3$ doped MEH-PPV PLEDs. This would suggest that there is no charge trapping at the dopant sites.

There are no significant shifts in CIE coordinates for any of the doped devices relative to the undoped device for all operating voltages (Table 8-2/Figure 8-4), but the relative heights of peaks in the EL spectra vary. An increase in the height of the peak at 590nm (2.10eV) relative to the 635nm (1.95eV) peak was observed, which is usually highest for undoped MEH-PPV PLEDs. At higher dopant concentrations the height of the higher energy peak usually associated with pure singlet fluorescence in MEH-PPV exceeds that of the lower energy peak. The EQE values of all doped PLEDs (see Table 8-2) are significantly greater than that of the undoped device. The order of magnitude of current densities at which peak EQEs for the doped PLEDs were measured were comparible with that of the undoped PLED. The enhancement in EQE is maintained for all operating current-voltage values, and EQE curves are similar to those typically observed in undoped systems (Figure 8-5).

An exhaustive a display of results for the La-thd₃, Dy-thd₃ and Ce-eh₃ PLEDs is not presented here as the other doped samples behave similarly to the Gd-thd₃ experiment; displaying a reduction in the 1.95eV EL peak which appears proportional to the enhancement observed in the EQE of the PLED (referring to Figure 8-6 and Table 8-1). This peak has been previously been ascribed to excimer emission[4] Again we observe the enhancement in EQE to be prolonged over all operating voltages with relatively small drive voltage increases with dopant concentration.
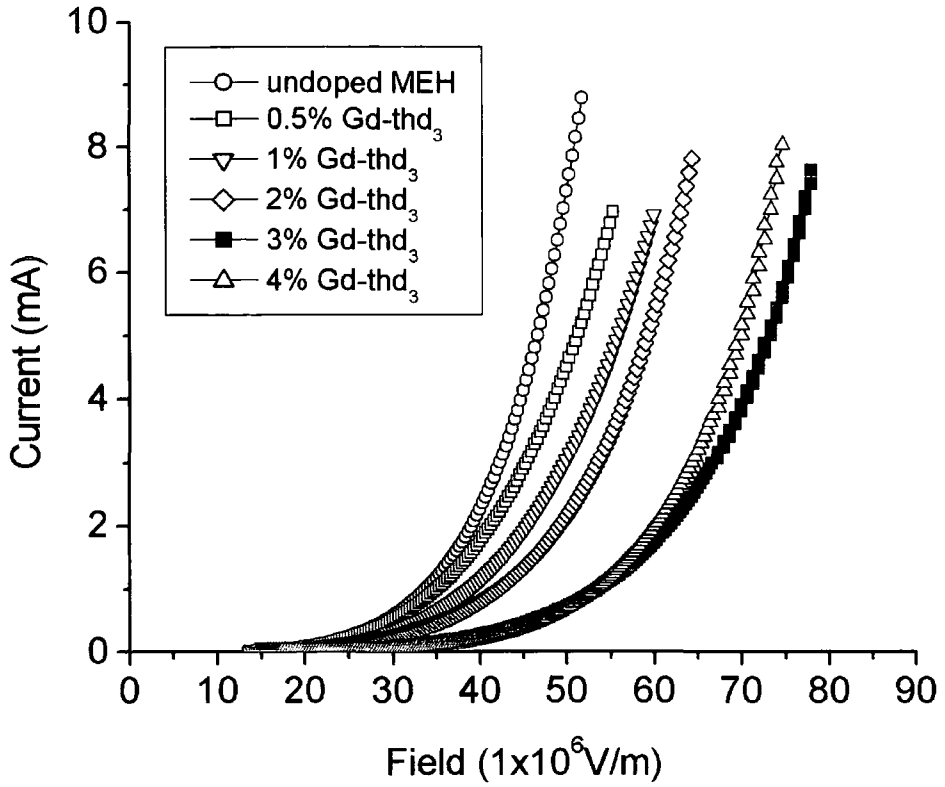
Figure 8-2 Field-Current Curves for the Gd-thd$_3$ doped MEH-PPV devices tested

Figure 8-3 Current Density-Candela Output Curves for the Gd-thd$_3$ doped MEH-PPV

devices tested

125
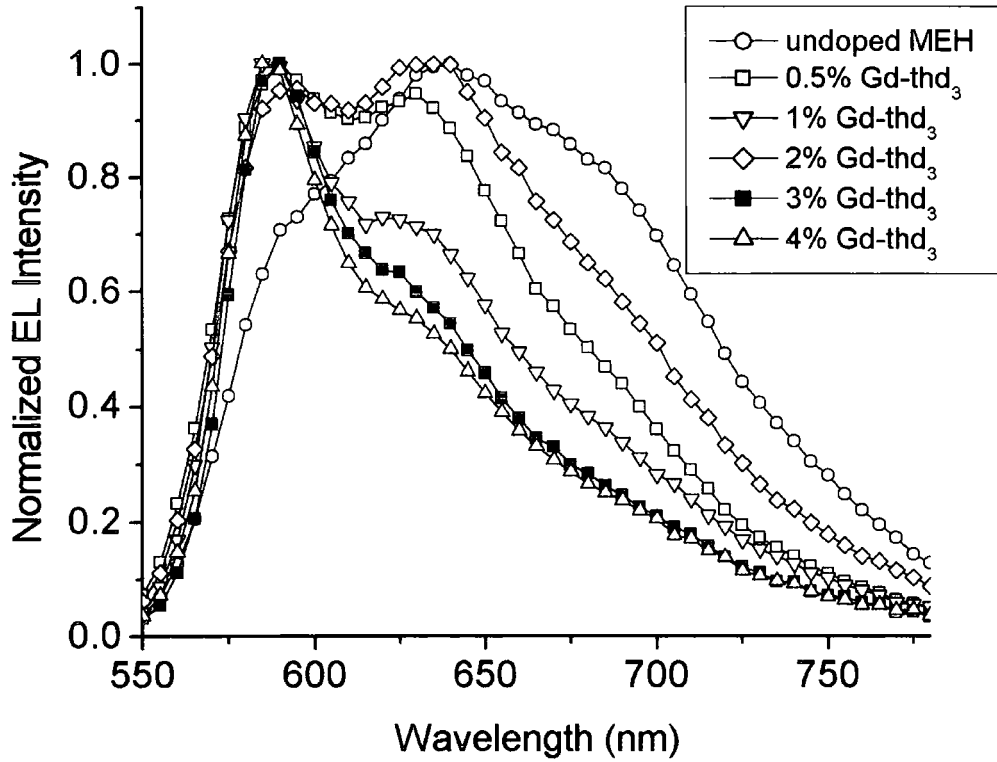
Figure 8-4 EL Spectra for the Gd-thd$_3$ doped MEH-PPV devices tested
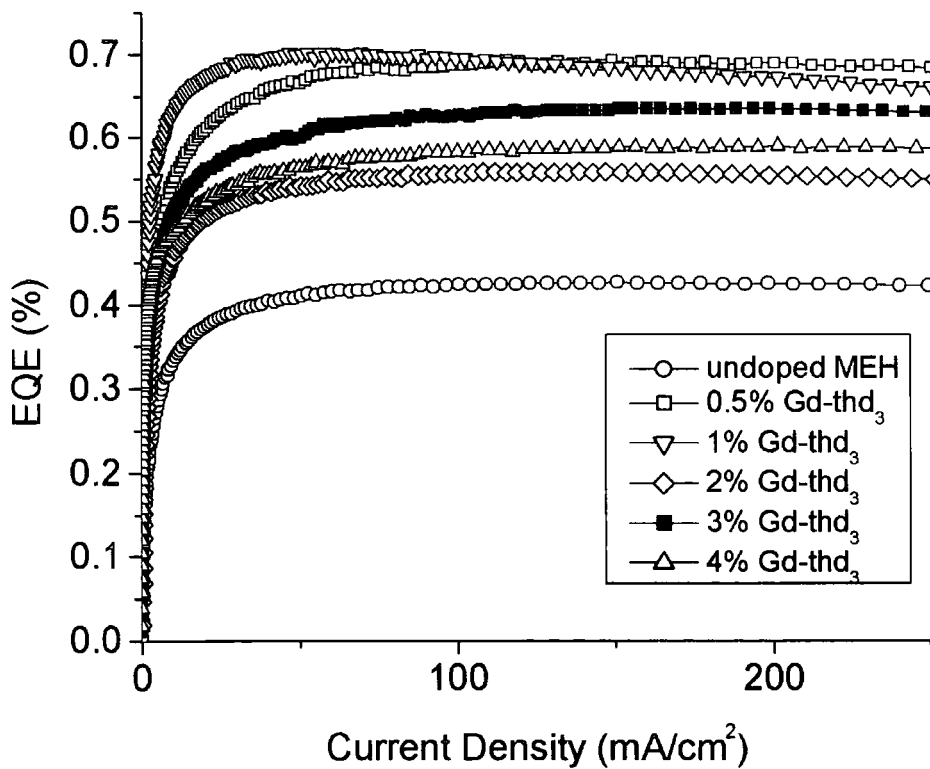
Figure 8-5 EQE Curves for the Gd-thd$_3$ doped MEH-PPV devices tested
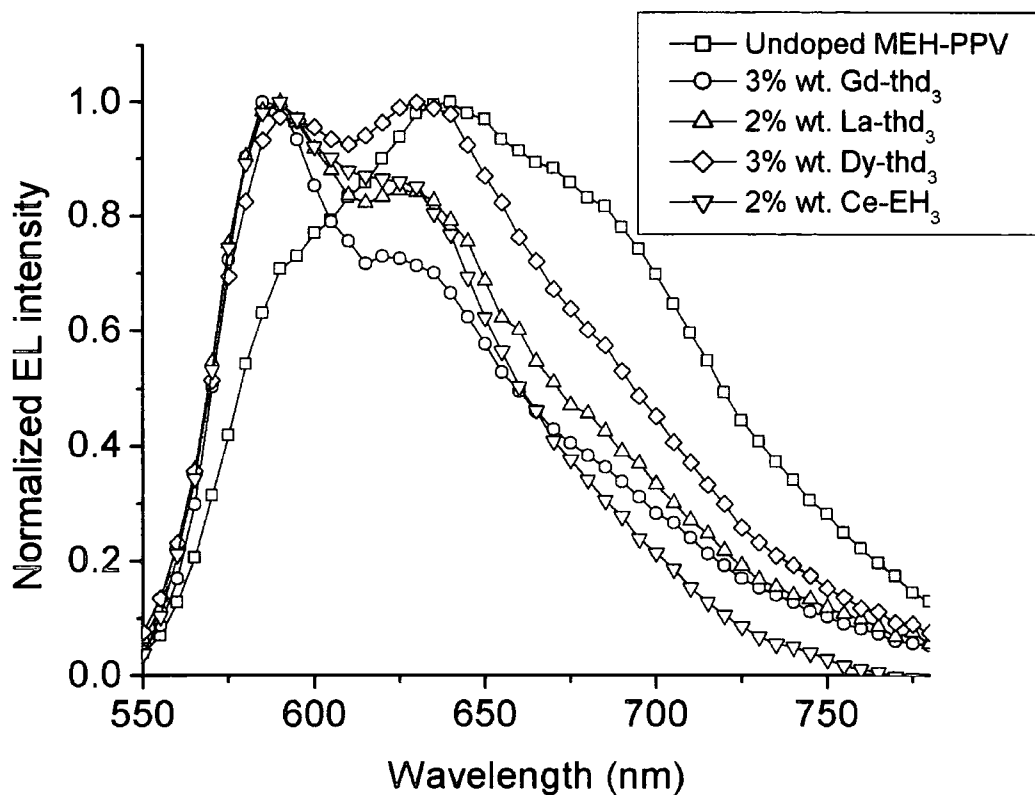
Figure 8-6 EL Spectra for each 'best of batch' MEH-PPV-dopant combination

Dopant [%wt.]	Peak EQE (%)	Factor Improvement	M^{3+} Electronic Configuration	Measured Magnetic Moment at 300K (Bohr magnetons)
undoped	0.4263	-		
Gd-thd₃	0.7013	1.645	*[Xe]4f₇*	8
La-thd₃	0.5657	1.327	*[Xe]*	0
Dy-thd₃	0.4702	1.103	*[Xe]4f₉*	10.5
Ce-eh₃	0.4992	1.171	*[xe]4f₁*	2.6

Table 8-1 Summary of the highest performance dopant:MEH-PPV combinations of each dopant (spin configurations and magnetic moments taken from the literature[1])

127

Device	Dopant %wt.	Peak EQE [at mA/cm^2]	Operating Voltage (V)	CIE Coordinates X	Y
Undoped PF2/6am4		1.19 [70.67]	5	0.237	0.268
			6	0.207	0.227
			7	0.198	0.211
PF2/6am4 Doped with Gd-thd3	0.5	0.15 [56.44]	5	0.182	0.203
			6	0.179	0.196
			7	0.182	0.204
	1	0.14 [109.33]	5	0.185	0.206
			6	0.176	0.196
			7	0.178	0.219
	2	0.18 [96.89]	5	0.192	0.213
			6	0.175	0.192
			7	0.180	0.215
	3	0.11 [202.22]	5	0.195	0.270
			6	0.177	0.248
			7	0.176	0.245
	4	0.18 [42.18]	6	0.213	0.258
			7	0.198	0.244
			8	0.194	0.244
Undoped MEH-PPV		0.43 [150.67]	5	0.601	0.383
			7	0.619	0.378
			9	0.606	0.391
MEH-PPV Doped with Gd-thd3	0.5	0.69 [149.33]	5	0.592	0.389
			7	0.633	0.412
			9	0.581	0.410
	1	0.7 [60.44]	5	0.574	0.398
			7	0.591	0.406
			9	0.586	0.409
	2	0.56 [108.44]	5	0.588	0.384
			7	0.592	0.390
			9	0.596	0.400
	3	0.63 [155.56]	6	0.558	0.389
			8	0.592	0.401
			10	0.591	0.403
	4	0.59 [201.78]	7	0.571	0.401
			9	0.585	0.410
			11	0.584	0.412

Table 8-2 Peak EQE values and sample EL CIE coordinates for all Gd-thd$_3$ PLEDs tested

8. 12 Gd-thd₃ doped PF2/6am4

Figures Figure 8-7, Figure 8-8, Figure 8-9and Figure 8-10 show the field-current, candela output, EL spectra and current density-EQE curves respectively for all PF2/6am4 PLEDs studied. A slight decrease in turn-on voltage with dopant concentration was observed(compare with other host:Dopant systems reported elsewhere[6]), with 4.05, 4.00, 3.70, 3.75, 3.25 and 3.30V required for a current of 1×10^{-5}A in the undoped, 0.5%, 1%, 2%, 3% and 4% wt. Gd-thd₃ doped PF2/6am4 PLEDs. This would suggest that there is no charge trapping at the dopant sites,which was expected given the electron affinity and ionisation potential of Gd-thd₃ and the energy levels of PF2/6am4. The decrease in turn on voltage may represent an altered film morphology in PF2/6am4 doped with Gd-thd₃ relative to that of undoped films.

The doped devices drew higher current densities for a given field strength relative to the undoped device, yet their output intensity was significantly lower, as illustrated in Figure 8-8. Referring to Figure 8-9 and Table 8-2, no significant shift in CIE coordinates for any of the doped devices relative to the undoped device was observed over all operating voltages. An increase in the height of the peak at 495nm (2.51eV) relative to the 420nm (2.95eV) peak was observed, which is usually highest for undoped PF2/6am4 PLEDs. At higher dopant concentrations the height of the lower energy peak (the excimer peak) exceeds that of the higher energy peak usually associated with pure singlet fluorescence in PF2/6am4. The EQE values of all doped PLEDs (see Table 8-2) are significantly smaller than that of the undoped device. The detrimental effect appears to have saturated by dopant concentrations of 0.5% wt., with the variation of EQE for other doped PLEDs comparable given the experimental error of the measurement system. The order of magnitude of current densities at which peak EQEs for the doped PLEDs were measured were comparable with that of the undoped PLED, unlike those for previous studies involving porphyrin doped PLEDs[2], where saturation of the dopant sites (due to the dopant phosphorescence lifetime) resulted in the EQE peaking at low current density and then falling away to low values at realistic operating current-voltage levels.

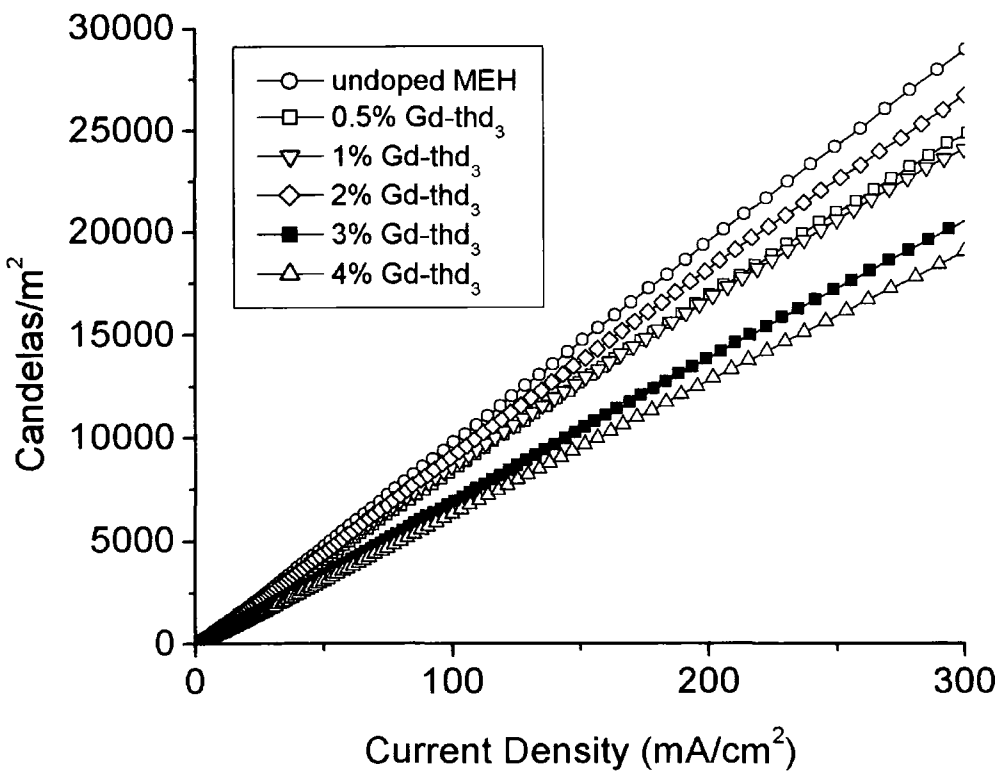**Figure 8-7** Field-Current Curves for the Gd-thd$_3$ doped PF2/6am4 devices tested

Figure 8-8 Current Density-Candela Output Curves for the Gd-thd$_3$ doped PF2/6am4

devices tested

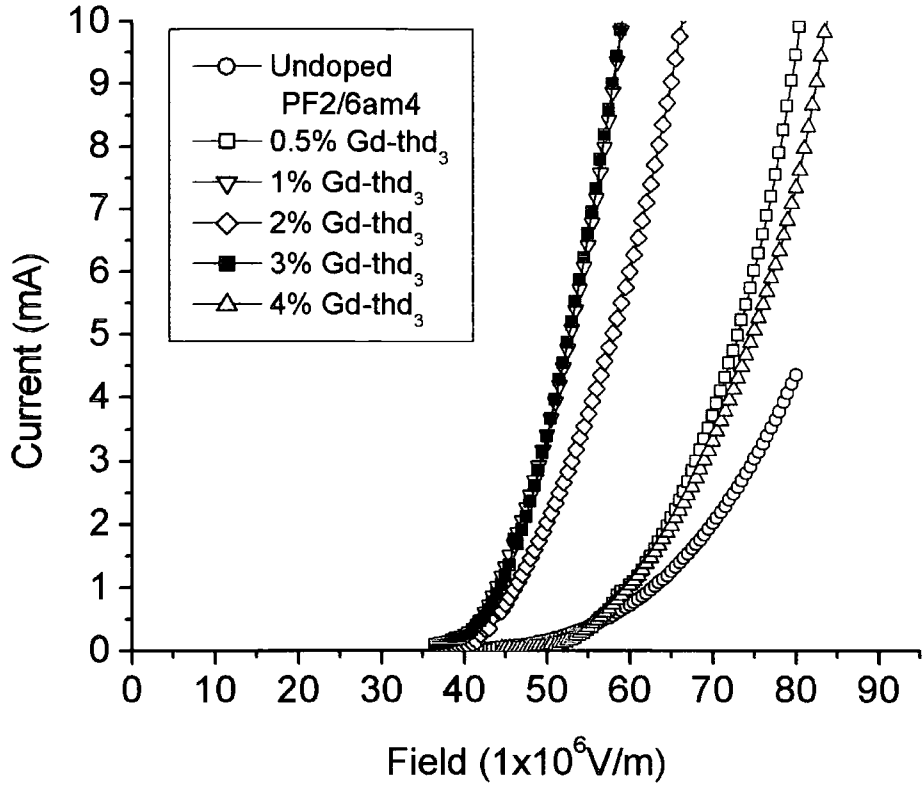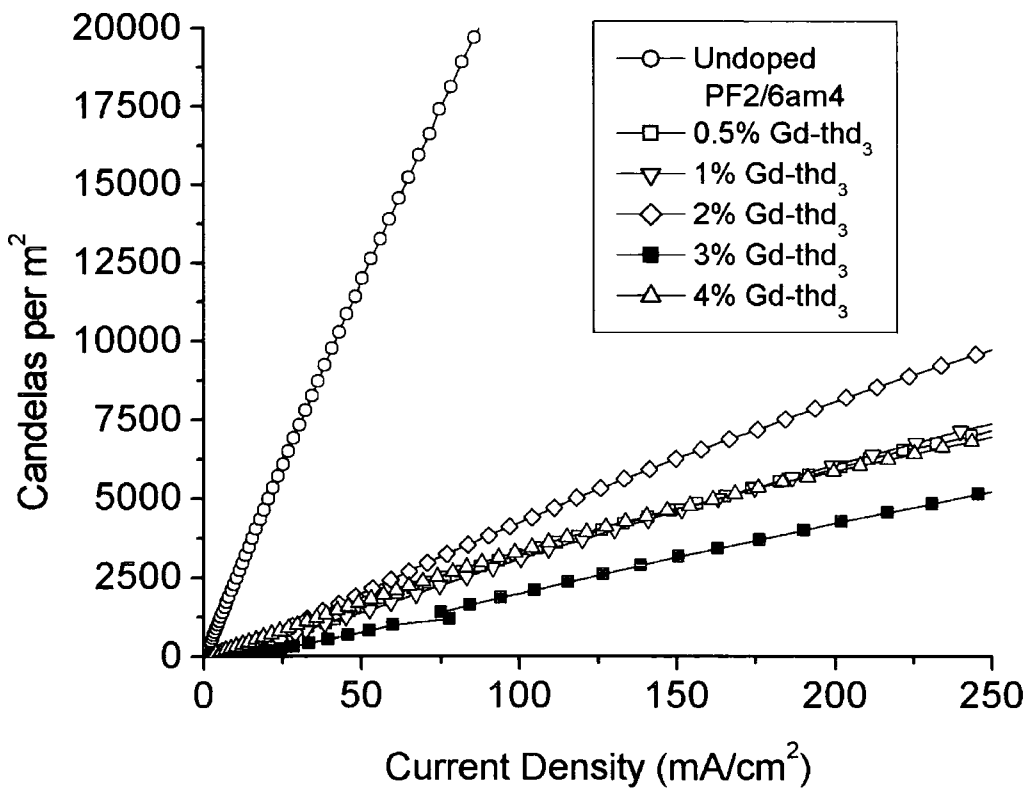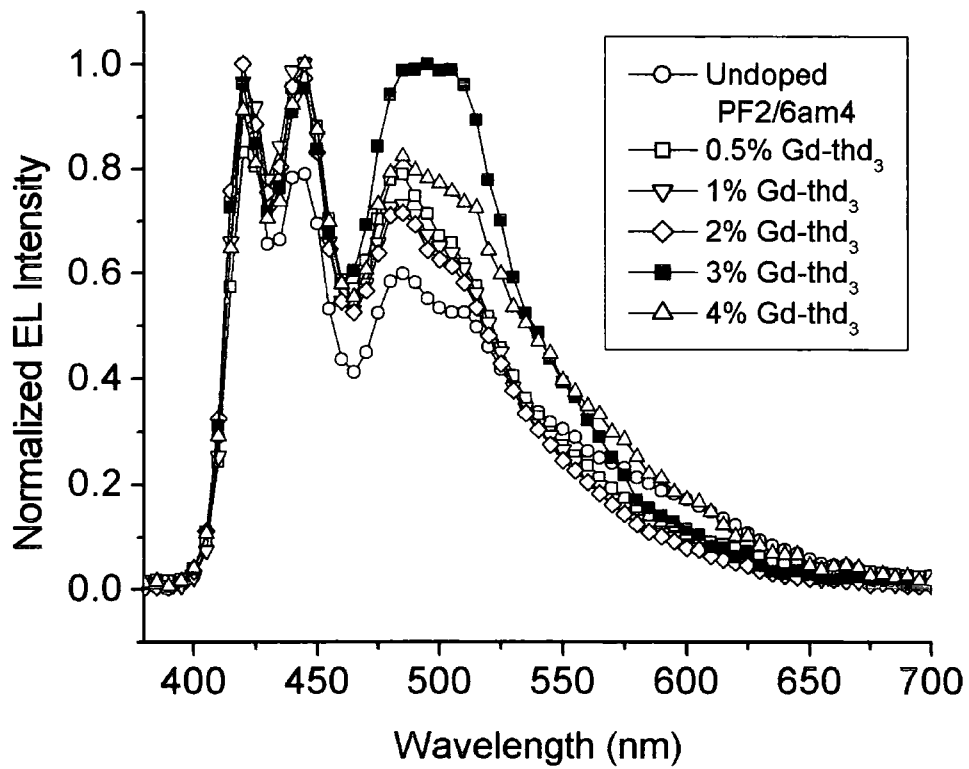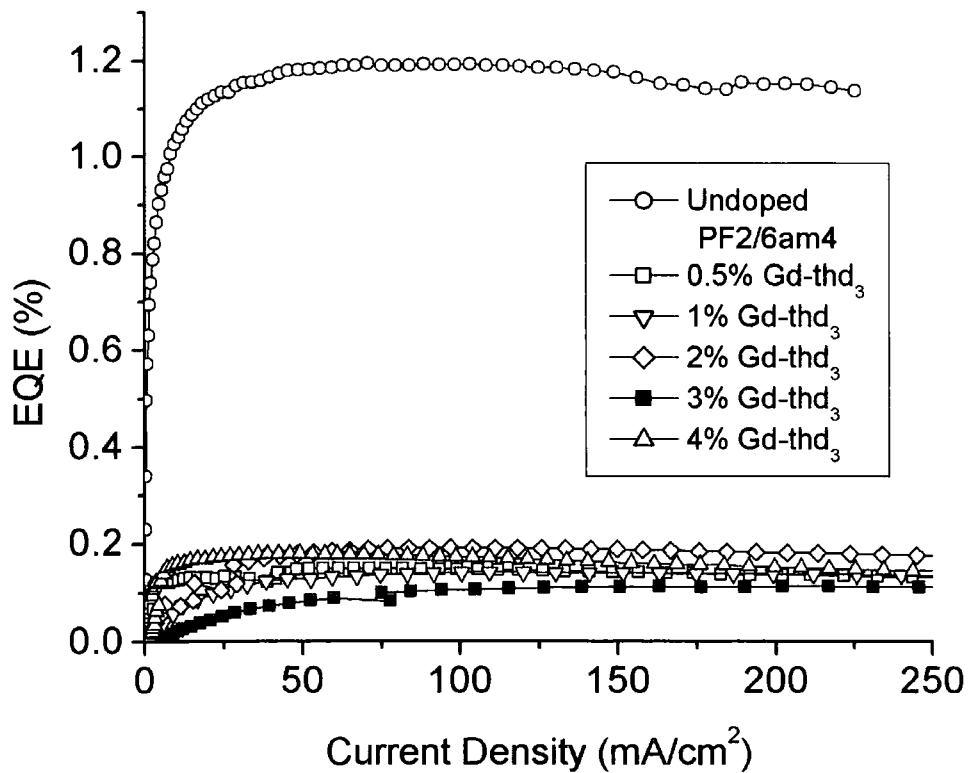**Figure 8-9** EL Spectra for the Gd-thd₃ doped PF2/6am4 devices tested

**Figure 8-10** EQE Curves for the Gd-thd₃ doped PF2/6am4 devices tested

8.13 Discussion

There appear to be two possible explanations for the observed enhancement in performance for MEH-PPV PLEDs doped with lanthanide metal complexes. The first is discussed in the classic work by Porter and Wright[7]: Triplet quenching by paramagnetic species. Porter and Wright measured the quenching ability of several metal ions on triplet naphthalene in both water and ethylene glycol. They observed quenching rates that did not relate to the magnetic susceptibility, but which crucially depended the metal ions having a degree of paramagnetism. They ascribed the variation in metal ion performance in triplet quenching effectiveness to be dependant on the overlap of wavefunctions between triplet host species and metal ion dopant.

The observed enhancment of PLED performance is likely to correlate to the triplet population within the devices. Triplets are known to be of major importance to PLED operation, with singlet-triplet annihilation within the active layer being one of the main reasons that the internal quantum efficiency of a PLED is typically well below the singlet yield measured for a given polymer in photoluminescence studies. The lanthanide complexes used are known for their parmagnetism, indeed they are used as shift reagents in Nuclear Magetic Resonance (NMR) studies. Has triplet quenching resulting in devices of higher efficiency due reduced triplet-singlet annihilation been observed? There are many reasons to discount this proposal. Firstly, looking at Table 8-1 one see that La-thd$_3$ has a negligible magnetic moment, yet it still enhances efficiency and alters EL spectra (Figure 8-6) when used as a PLED dopant. This goes against Porters' observations. Secondly, the variation in enhancement with dopant species is small compared to Porters' results. Furthermore, why would quenching the triplet concentration in MEH-PPV benefit the PLED performance whilst being detrimental to PF2/6am4?

An alternative explanation can be found in a more recent theoretical publication[3] which discusses recombination as a spin-dependant process which can be influenced by heavy atom or impurity scattering. The presence of heavy atoms results in greater mixing of triplet and singlet states i.e. higher inter-system crossing. The modeling in the literature predicts appreciable changes only for a 'spin-flip coupling constant' greater than 10^{-2}eV, which is unachievable with magnetic impurities but achievable with heavy atoms. This would explain the observed independence of performance enhancement from dopant magnetic field strength, and also the small

variation in enhancement observed with dopant species: the heavy atom effect being dominant over the paramagnetic effect. This explanation may also explain the detrimental effect of lanthanide-complex doping on PF2/6am4 PLEDs: the enhancment in the singlet yield due to intersystem crossing introduced by the presence of heavy atoms is dependant on both the twist angle of the backbone and the exchange energy (i.e. the difference in energy between the lower triplet state and the first singlet excited state; the ground state being singlet in spin). PF2/6am4 has a singlet energy of $E_S=2.79eV$ and a lower triplet energy of $E_T=2.20eV^{[5]}$ giving an exchange energy of $\Delta=0.59eV$. The literature predicts that for twist angle $\theta=0^0$ singlet yield will only be enhanced for $0.3eV<\Delta>0.7eV$, and otherwise reduced due to an enhancement of the non-radiative S_1 lifetime τ_{st1} route for non-radiative de-excitation. MEH-PPV has $E_T=1.27eV$ and $E_S=2.07eV^{[5]}$, giving $\Delta=0.79eV$. MEH-PPV is also known to have a non-zero twist angle and this gives a chance of phonon bottleneck, where loosely bound triplets relax by emitting multiple phonons and in the process flip spin, with singlet yield enhanced by increased rate of crossing from the second triplet level to singlet excited state, τ_{t2s}. This scheme is illustrated in

Figure 8-11, again modified from the literature[3,5].
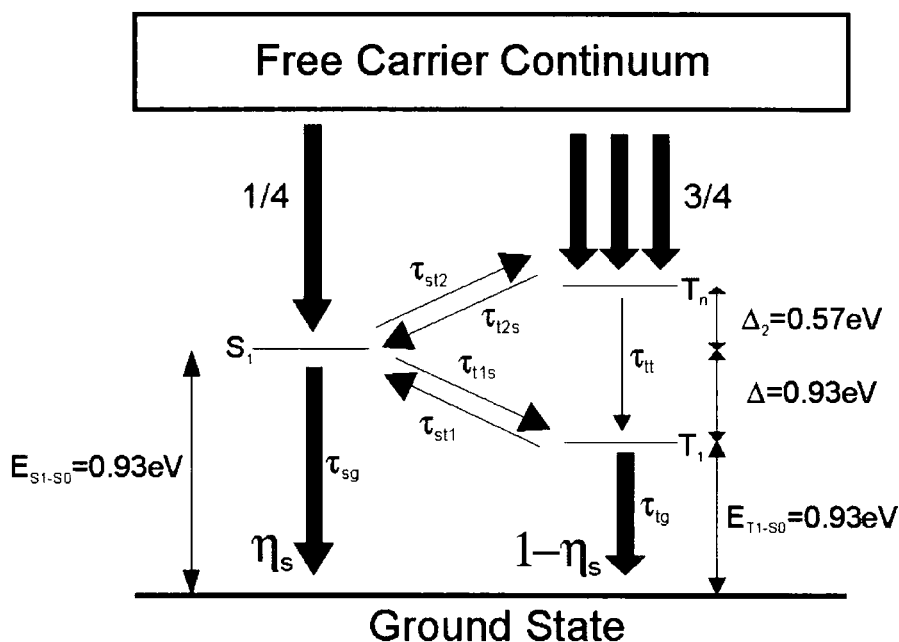
Figure 8-11 Energy level scheme proposed in the literature for MEH-PPV and used to illustrate an explanation of the results obtained in this paper

Back inter-system crossing from T_1 to S_1 is energetically highly unlikely therefore one must ascribe such back transfer to occur from an upper triplet state, T_N, to S_1. In MEH-PPV, T_N is found to be far closer to S_1 in energy ($\Delta E_{S,TN}=0.57eV$) than PF2/6am4 ($\Delta E_{S,TN}=0.73eV$) consistent with enhanced back upper excited state transfer inter-system crossing in MEH-PPV.

With either of these explanations, Porters' paramagnetic triplet quenching or intersystem crossing enhanced by the heavy atom effect, the triplet population is expected to be lower than for an undoped device in MEH-PPV active layers. The reduction of the 'excimer' peak with triplet population is worthy of note as it suggests that the formation of the lower energy excited species is facilitated by the presence of triplet excitons. Polymer triplet states readily energy transfer to oxygen to form singlet oxygen which reacts with conjugated species to form keto-type defects. This goes against current understanding of excimers, formation of which is understood to be fixed on spin casting from solution. The fact that the presence of triplets appears to be crucial to the emergence of the lower peak suggest that this peak may be due to radiative decay from an active layer species with properties distinct from those of excimers. The increase of 'excimer' or lower energy peak with Gd-thd$_3$ concentration in PF2/6am4 PLEDs is taken as further evidence in favour of the heavy atom effect; with intersystem crossing favouring triplets over singlets and casually lower energy emission.

We have demonstrated PLED performance enhancement through doping PLED active layers with lanthanide-organic complexes. The maximum factor of improvement was 1.645 for a 3% wt. Gd-thd$_3$ doped MEH-PPV PLED. The results favour the heavy atom effect as the dominant phenomena responsible for this enhancement, which is maintained over all operating voltages used and is gained without a large increase in turn-on voltage due to a lack of charge trapping, in contrast with polymer-dopant systems where energy transfer takes place. The back inter-system crossing has been shown to be dependant on the host polymer used, with the dopants proving detrimental to devices utilizing PF2/6am4 as an active layer. We have used energy level values taken from the literature in combination with another groups' theoretical findings[3] to explain the differing results for MEH-PPV and PF2/6am4.

This method of doping without energy being transferred to the dopant differs from the majority of PLED doping studies to date, and was pursued due to the lack of efficient blue-emitting dopants with which to enhance the performance of polyfluorene derivatives in PLEDs. The fact that this method has failed for PF2/6am4 emphasizes

that relative to other polymers the high singlet yield of polyfluorene and its derivatives makes it a near-optimized system which very difficult to modify without detrimentally affecting performance in PLED structures.

References

[1]   Cotton, F. A.; Wilkinson, G. The Lanthanides, Scandium and Yttrium. In *Advance Inorganic Chemistry: A Comprehensive Text*; 4th ed.; Johm Wiley and Sons, Inc.: New York, 1980; pp 982-985.

[2]   Higgins, R. W. T.; Hothofer, H. G.; Scherf, U.; Monkman, A. P. *Journal of Applied Physics* **Submitted**.

[3]   Hong, T. M.; Meng, H. F. *Physical Review B* **2001**, *6307*, 5206-+.

[4]   Jakubiak, R.; Collison, C. J.; Wan, W. C.; Rothberg, L. J.; Hsieh, B. R. *Journal of Physical Chemistry A* **1999**, *103*, 2394-2398.

[5]   Monkman, A. P.; Burrows, H. D.; Hartwell, L. J.; Horsburgh, L. E.; Hamblett, I.; Navaratnam, S. *Physical Review Letters* **2001**, *86*, 1358-1361.

[6]   O'Brien, D. F.; Giebeler, C.; Fletcher, R. B.; Cadby, A. J.; Palilis, L. C.; Lidzey, D. G.; Lane, P. A.; Bradley, D. D. C.; Blau, W. *Synthetic Metals* **2001**, *116*, 379-383.

[7]   Porter, G.; Wright, M. R. *Discussions of the Faraday society* **1959**, 18-27.

Chapter 9 Summary and Conclusions

9.1 Active Layer Doping

Work contained in this thesis has shown that there are several approaches to doping the emissive conjugated polymer. By far the most common is doping with an efficient phosphorescent emitter that harvests the excited states of the host. Other groups have reported favourable EQE values but by and large the problem of site saturation has been overlooked. Failure of the dopant to release excited energy via photon emission can lead to an enhancement in singlet-triplet annihilation over that observed for the pure undoped host. It has been shown here that the triplet excitons are the limiting factor in this process, thus a phosphorescent dopant should have a short triplet lifetime. Other groups have begun to pursue this solution, which may extend the enhancemnt factor over all operating parameters required for commercial use. Such an approach does not address the need for enhancement of blue-emitting diodes due to the need for the dopant singlet energy to be below that of the host singlet energy.

In an attempt to identify a generic enhancement for all host polymers the device physics of PLEDs with rare earth lanthanide doped active layers were investigated. The heavy atoms incorporated were expected to enhance the ISC between singlet and triplet excited states and thus provide a way of enhancing the intrinsic singlet yield over that of an undoped film. In MEH-PPV this improvement was observed for a wide range of dopants. Enhancements in EQE and power efficiency were valid over all current densities and no charge trapping at the dopant sites was observed. The presence of the dopants altered the EL spectrum of MEH-PPV, with the peak previously accounted for by excimer emission reduced proportionally with enhancement factor. The author questions the validity of ascribing this peak to excimer emission in light of these results. In combination with work by other members of this group in collaboration with the Paterson Institute for Cancer Research, which highlighted polymer triplets' ability to react with oxygen to form singlet oxygen, it favours a scenario in which during operation oxygen penetrating the active layer from the atmosphere is converted into free radicals which react with the conjugated segments to form keto-type defects.

These findings point naturally to options for further study. Firstly, the quest for an efficient phosphorescent emitter good for all current densities. Secondly, time-dependent measurements of lower energy EL peaks with time in both oxygen- and nitrogen-rich atmospheres in order to confirm that the presence of oxygen has an effect on the formation of lower energy features. In addition to providing an inert atmosphere

it is also essential to de-gas polymer solutions prior to spin coating as the mixing during dissolving is expected to diffuse considerable oxygen into the solution.

9.2 Alternative Charge Injection Layers

PANi solutions containing mobile counter-ions were shown to be bad when used as the basis for HTL layers. The mobile counter-ions appear to migrate into the active layer from I-V evidence. PANi in combination with a polymeric counter-ion was shown to produce stable PLEDs whose performance surpassed that of PEDT:PSS when used in combination with MEH-PPV. Unfortunately PANi:PSS failed to work well with MeL-PPP, presumably due to a mis-match of the formers' Fermi Level with the latters' HOMO.

Researchers in this group are now experts in PANi synthesis. Dr.Zaidi has been able to produce PANi in solution with a vast variety of counter-ions, and it is possible that one of these combinations will produce a polymer with the right energy levels for use as a HTL with polyfluorene-type backboned active layers. Thus the proposed continuation for this area of research is more combinations of active layers with novel PANi HTLs. Unfortunately this may be a process of trial and error due to the difficulty of cyclic voltametry measurements used to measure the energy levels under consideration.

Finally the author takes this opportunity to encourage more time investment on the digestion of results in this field. Whilst the pace of experimental trumpeting appear to be slowing there is still a huge gap between experimental and theoretical understanding that must be addressed in order for this area of physics to prosper long-term.

Appendices

138

APPENDIX A EFFICIENCY CALCULATIONS

1. External Quantum Efficiency

```
define qe_finder {
%volt=%1;
%curr=%2;
%index=%3;


planck=6.626076e-34; #define constants
cee=299792458;
solidang=1.374;
elec=1.60217733e-19;
pi=3.141592654;



grog=-9.17965e10; #fit response with 2nd order polynomial
hrog=7.80834e5;
irog=-0.119066;
rf=5e5; # gain of 1 (rf=5e5 when gain is unity)
resp=grog*(col(Wavelength)^2)+hrog*col(Wavelength)+irog;
cal=1.303264214;
col(3)=cal*resp;




col(4)=(col(3)*col(2))/col(1); #Calculate integral1
col(xdif)=diff(col(1));
col(ydif)=diff(col(4));
cutoff=list(0,col(xdif));
col(xdif)[cutoff-1]=0;
temp=(col(4)*col(xdif))+(0.5*col(ydif)*col(xdif));
sum(temp);
integrand=$(sum.total);



col(Integral1)[1]=integrand; #Place results in Worksheet
col(NormInt1)=(%volt/(rf*planck*cee*integrand))*col(NormInt);


xdif2=diff(col(1)); #Calculate integral2
ydif2=diff(col(NormInt1));
intgrl2=col(NormInt1)*xdif2+0.5*ydif2*xdif2;
sum(intgrl2);
int2=$(sum.total);
```

```
col(Integral2)[1]=int2; #Place results in Worksheet
Eext=(elec*pi*int2)/(%curr*solidang);
type "int1= $(integrand)";
type "int2= $(int2)";
type "Eext= $(Eext)";
col(QE)[%index]=Eext*100
};
andy=list(0,col(VoltP));
for (roger=1; roger<andy; roger+=1)
{
qe_finder col(VoltP)[roger] col(Current)[roger] roger;
};
```

2. Power Efficiency and Photometric Intensity

```
define pe_finder {
%volt=%1;
%voltd=%2;
%curr=%3;
%index=%4;


planck=6.626076e-34; #define constants
cee=299792458;
solidang=1.374;
areadi=2.25e-6;
km=683.002;
elec=1.60217733e-19;
pi=3.141592654;



fit1_dat1=1.00; #fit1 data for < 555nm (CIE Curve Data)
fit1_dat2=5.5163e-7;
fit1_dat3=3.5761e-8;
fit2_dat1=1.00; # fit2 data for > 555nm
fit2_dat2=5.5880e-7;
fit2_dat3=4.3678e-8;



grog=-9.17965e10; #fit response with 2nd order polynomial
hrog=7.80834e5;
irog=-0.119066;
rf=5e5;
resp=grog*(col(Wavelength)^2)+hrog*col(Wavelength)+irog;
cal=1.303264214;
col(3)=resp*cal;




col(4)=(col(3)*col(2))/col(1); #Calculate integral1
col(xdif)=diff(col(1));
col(ydif)=diff(col(4));
cutoff=list(0,col(xdif));
col(xdif)[cutoff-1]=0;
temp=col(4)*col(xdif)+0.5*col(ydif)*col(xdif);
sum(temp);
integrand=$(sum.total);
```

```
col(Integral1)[1]=integrand; #Place results in Worksheet
col(NormInt1)=(%volt/(rf*planck*cee*integrand))*col(NormInt);

andy=list(7.8E-7,col(Wavelength));
for (roger=1; roger<andy; roger+=1)
{
test=col(Wavelength)[roger];
if (test<555e-9)
{
xcie=test;
col(CIEdata)[roger]=fit1_dat1*exp(-0.5)*(((xcie-fit1_dat2)/fit1_dat3)^2);
}
else
{
xcie=test;
col(CIEdata)[roger]=fit2_dat1*exp(-0.5)*(((xcie-fit2_dat2)/fit2_dat3)^2);
};
};

col(SEC)=col(NormInt1)*col(CIEdata)*planck*cee/col(Wavelength);

xdif2=diff(col(1));
ydif2=diff(col(SEC));
temp=col(SEC)*xdif2+0.5*ydif2*xdif2;
sum(temp);
integrand=$(sum.total);
col(Integral2)[1]=integrand; #Place results in Worksheet
col(Cdm2)[%index]=integrand*km/(areadi*solidang);
col(LpW)[%index]=(col(Cdm2)[%index]*pi*areadi)/(%voltd*%curr);
};


dave=list(0,col(VoltP));
for (tim=1; tim<dave; tim+=1)
{
pe_finder col(VoltP)[tim] col(VoltD)[tim] col(Current)[tim] tim;
};
```

APPENDIX B CHROMATICITY CALCULATIONS

```
planck=6.626076e-34; #define constants
cee=299792458;
col(8)=col(8)*planck*cee/col(1);
col(9)=col(2)*col(8);
col(10)=col(3)*col(8);
col(11)=col(4)*col(8);


xdif=diff(col(1)); #Calculate x_el integral
ydif=diff(col(9));
temp=col(9)*xdif+0.5*ydif*xdif;
sum(temp);
int=$(sum.total);
col(12)[2]=int; #Place results in Worksheet


xdif2=diff(col(1)); #Calculate y_el integral
ydif2=diff(col(10));
temp2=col(10)*xdif2+0.5*ydif2*xdif2;
sum(temp2);
int2=$(sum.total);
col(13)[2]=int2; #Place results in Worksheet


xdif3=diff(col(1)); #Calculate z_el integral
ydif3=diff(col(11));
temp3=col(11)*xdif3+0.5*ydif3*xdif3;
sum(temp3);
int3=$(sum.total);
col(14)[2]=int3; #Place results in Worksheet

sumo=col(12)[2]+col(13)[2]+col(14)[2];
col(12)[2]=col(12)[2]/sumo;
col(13)[2]=col(13)[2]/sumo;
col(14)[2]=col(14)[2]/sumo;

x=col(12)[2];
y=col(13)[2];
z=col(14)[2];

col(12)[4]=(2.36461*x-0.89654*y-0.46807*z)/(1.85464*x+0.51546*y+0.62989*z);
col(13)[4]=(-0.51517*x+1.42641*y+0.08876*z)/(1.85464*x+0.51546*y+0.62989*z);
col(14)[4]=(0.00520*x-0.01441*y+1.00920*z)/(1.85464*x+0.51546*y+0.62989*z);
```
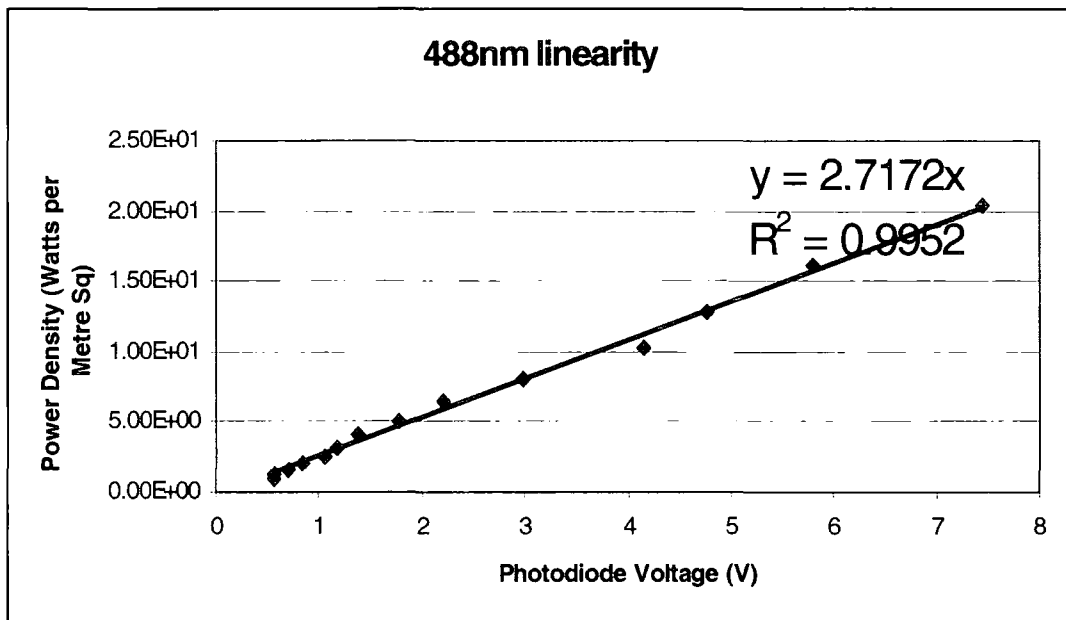
143

APPENDIX C PHOTODIODE CALIBRATION TECHNIQUE

The RS 100mm^2 large area photodiode was calibrated by contrasting its measurements of intensity at two wavelengths from an Ar$^+$ laser and comparing with the intensity measured by a NIST (National Institute of Science and Technology) calibrated power meter.
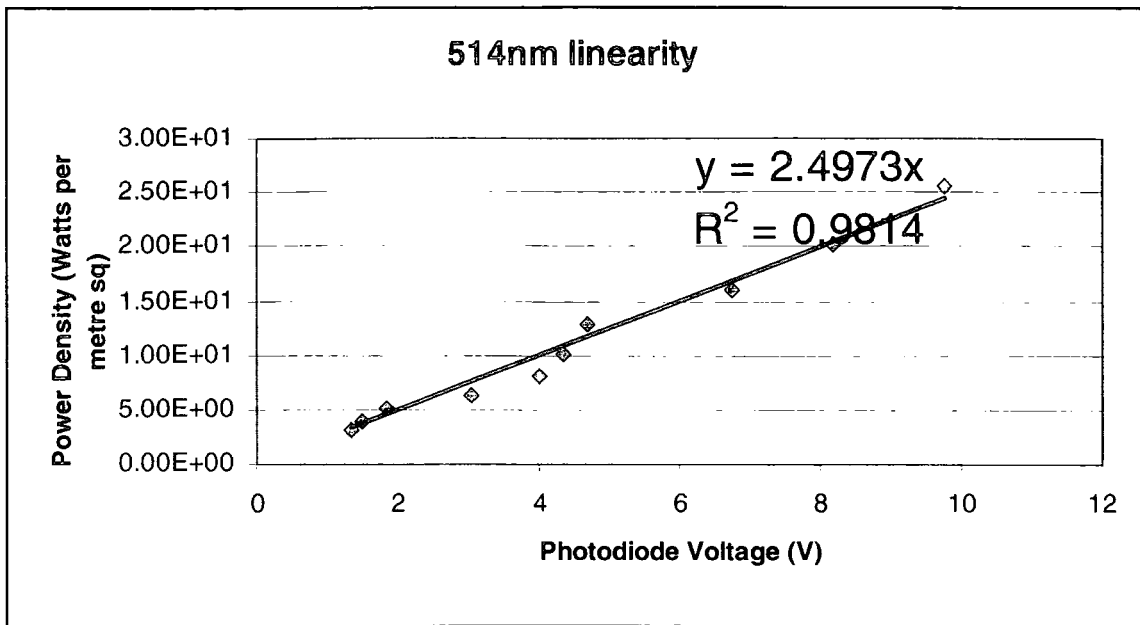
Of the lines available, two at 488nm (blue) and 514nm (green) were used. In order to vary the intensity of laser light falling on the detector at a series of neutral density filters were used. For each intensity dual measurements were taken with the photodiode circuit (connected to a Keithley 2000) and the calibrated power meter. The measured photovoltage was then converted into Watts, the internal gain of the system being known and using $P(Watts) = \dfrac{V^2}{R_T \times R_O}$ where R_T and R_O are the transimpedance and operational feedback resistances respectively, and the power measured by the photodiode was plotted against that measured by the calibrated power meter. The gradient of this graph gives us a correction factor, which corrects the height of the Silicon responsivity curve.

488nm linearity

$y = 2.7172x$

$R^2 = 0.9952$

Power Density (Watts per Metre Sq) vs Photodiode Voltage (V)

Linearity of the Photodiode Response at 488nm Excitation

514nm linearity

Linearity of the Photodiode Response at 514nm Excitation

The following is the calculation of the correction factor using the data from the 488nm excitation wavelength. From the data plotted above:

$$PowerDensity(W/m^2) = 2.7172 \times Voltage$$

$$\Rightarrow \frac{Power(W)}{Voltage} = 2.7172 \times A_{Photodiode}$$

$$= 2.7172 \times 1 \times 10^{-4}$$

$$\Rightarrow \frac{Current(A)}{Power(W)} = \frac{\left(\dfrac{\dfrac{1}{Power(W)}}{Voltage}\right)}{R_T \times R_O}$$

Using $R_T \times R_O = 5M\Omega$

$$\frac{A}{W} = 0.31294$$

Comparing with Si(λ=488nm) calculated using Equations 3-2 we calculate the correction factor

$$\Gamma_{Correction} = \frac{\left(\dfrac{A}{W}\right)_{Measured}}{Si(\lambda)}$$

$$= \frac{0.31294}{0.24012}$$

$$= 1.303264$$

The correction factor can also be calculated at other wavelengths in order to check against this value.